博 士 論 文

Leveraging Concurrent Transmission for Efficient Mesh LoRa Networks

(同時送信型フラッディングを用いた高効率メッシュ
LoRa ネットワークに関する研究)

37-176172

朱　桂兵

シュ　ケイヘイ
Guibing Zhu

Abstract

LoRa is a Low-Power Wide-Area network (LPWAN) standard and has garnered wide interests in the current Internet of Things (IoT) era. By adopting Chirp Spreading Spectrum (CSS) technology, LoRa provides a remarkably wide coverage as compared to that of the conventional standardized wireless radio frequency technologies. Recently, to further extend the coverage by utilizing multiple relays and improve the network capacity by using different Spreading Factors (SFs), a multi-hop LoRa network has become a promising technology for both academic studies and industrial applications. On the other hand, Concurrent Transmission (CT) flooding, a highly efficient multi-hop protocol which provides ultra-fast back-to-back relaying by allowing synchronized packet collision, will be a good candidate for the multi-hop LoRa network.

This thesis aims to construct an efficient mesh LoRa network by leveraging CT. Towards this, we first verify whether the LoRa receiver can endure co-technology interference (i.e., interference from LoRa packets) to realize a CT-based mesh LoRa network, namely CT-LoRa. Second, to improve the capacity of a mesh CT-LoRa network, our approach is to attempt to offload the data traffic into several subnets by utilizing the multiple-access dimension provided different SFs. Each subnet rooted at a sink node is allocated a specific SF on the basis of network clustering. This enables constructing multiple CT-LoRa subnets to transmit packets in parallel in the entire space, namely parallel CT-LoRa, to become feasible. The main contributions of this thesis are twofold.

LoRa Receiver Performance under CT: In CT-LoRa, we have evaluated the receiver performance under synchronized packet collisions from LoRa signals using the same SF (Same-SF Interference). The evaluation results show that, under identical condition, larger SFs lead to better performance under same-SF interference. Also, in practical scenarios, LoRa on each SF can benefit from the multi-hop CT flooding. On the other hand, when SFs are utilized as

a dimension for multiple access, we have evaluated LoRa receiver performance under the interference with different SFs (Different-SF interference) to verify the orthogonality between different-SF LoRa signals. The evaluation results show that the SFs are not fully orthogonal by using both simulations and real-chip experiments. Although the LoRa receiver has a tolerance in front of co-technology interference, the required signal-to-interference ratio (SIR) is different when using different SFs for the successful data transmissions. Specifically, smaller SFs (i.e., SF7 and SF8) are strongly affected by co-technology interference, while larger SFs show stronger immunity to interference and have fewer impacts on LoRa signals using different SFs.

SF Allocation for Parallel CT-LoRa: We proposed a tree-based SF clustering algorithm (TSCA) for realizing parallel transmission with a balanced SF allocation in a multi-hop CT-LoRa network. We consider the original network where all nodes keep using the fastest data rate (SF7) in the initial state. Moreover, given a well-connected tree using SF7, which is the shortest path from the relay nodes to the root node, the algorithm removes a certain number of nodes to generate spanning subtrees using larger SFs. As compared to a single-hop topology for which the connectivity check is unnecessary, the connectivity is confirmed when removing the nodes from the sub-tree that uses SF7 and inserting them into a higher SF node by node. To balance the traffic loads between all sub-trees, we employ a constraint rule with not only the data rate, but also the tree height to limit the number of nodes in each subtree. The tree height is also considered when we first estimate the capacity of each SF by using the maximum hop-count on each sub-tree. Furthermore, the TSCA is designed such that the algorithm updates the constraint rule iteratively based on the real hop count of the current topology. To reduce the hop count of each sub-tree, we attempt to remove the nodes farthest away from the root and using SF7, by inserting them into a sub-tree with a larger SF and with a lower height. Specifically, we use the Bottom-up Breadth-First-Search (BBFS) algorithm to determine the order in which extraction occurs and the Top-down Breadth- First-Search (TBFS) algorithm for the insertion. Moreover, the balance between the sub-trees is maintained by inserting the removed nodes into a sub-tree that will have Minimal Air Time (MAT) after the insertion.

Contents

List of Figures

List of Tables

Chapter 1

Introduction

In this chapter, we introduce an overview of this thesis. We first present the research background and goal of this thesis in section 1.1 and section 1.2, respectively. In section 1.3, we discuss the main contributions of this thesis. Finally, the structure of this thesis is described in section 1.4.

1.1   Research background and motivations

Wireless communications technologies enable the evolutions from *Human-to-Human (H2H)* internet to *Device-to-Device (D2D)* communications in the Internet of Things (IoT) era [1–4]. As estimated by Gartner, by 2022, the IoT market will spend \$ 2.5 million every minute and sale one million new IoT devices every hour [5]. To realize a truly connected society, the fifth generation (5G) is considered as a major driver of the growth of IoT and promises to further meet the needs of emerging IoT applications, such as network reliability, scalability, capacity, latency, and mobility [6, 7]. In the new trend of 5G, the massively interconnected devices require a more pervasive and ubiquitous network which is highly reliable to ensure end-to-end infrastructure environments and also promise the network autonomy and privacy [8, 9].

On the other hand, Low-power Wide-area Networks (LPWAN) become mainstream with various IoT deployments and industry applications [10–12]. Different from conventional cellular networks and other wireless technologies (eg., LTE, WiFi, Bluetooth, Zigbee) [13], LPWA techologies suit well with the specific needs of D2D communications, where an enormous amount of IoT devices, often driven by 3AAA batteries, require low cost, low-power long-range connectivities to grantee the longevity of the networks with a lower data rate. Thereby, in LPWAN, the limited data rate solutions provided by those cheap devices match the specific needs of massive deployments in critical scenarios, like smart meters, smart buildings, smart cities, smart agricultures and other large scale IoT deployment environments. To meet these specific needs, there are several LPWAN technologies provided by different approaches as shown in Fig 1.1. The de facto standards of LPWAN are mainly two kinds including: 1) cellular LPWAN, such as LTE-M and NB-IoT; 2) non-cellular LPWAN, such as LoRa and Sigfox [14]. We summary the technical comparisons of mian LPWAN technologies in Table 1.1.

In recent years, as a long range (LoRa) wireless communication technology against other LPWANs, LoRa has begun to attract more and more attention. The merits of
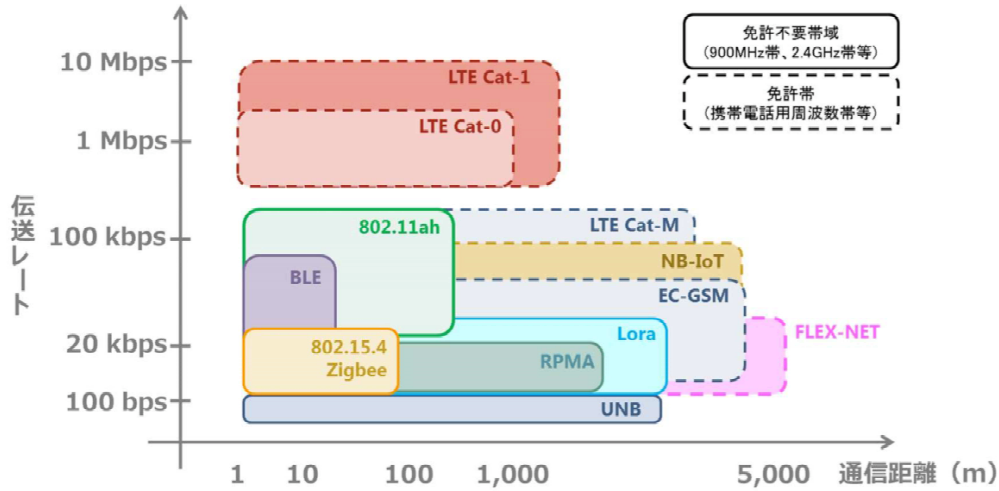
Fig. 1.1 Roadmap of wireless technologies [4].

	LoRaWAN	Sigfox	NB-IoT	LTE-M
Standardization	Proprietary	Proprietary	3 GPP	3 GPP
Spectrum	Unlicensed ISM	Unlicensed ISM	Licensed LTE	Licensed LTE
Topology	Star of stars	Star	Star	Star
Coverage	Medium/high	Medium/high	High	High
Data rate	0.3 - 37.5 kbps (LoRa) 50 kbps (FSK)	600 bps (DL) 100 bps (UL)	234.7 kbps (DL) 204.8 kbps (UL)	1 Mbps (DL) 1 Mbps (UL)
Complexity	Low	Very low	Very low	Low / medium
Longevity	Very high / high	Very high	High	Medium / high
Gateway	Yes	Yes	Optional	Optional

Table 1.1 Technical comparisons of various LPWA technologies.

LoRa include not only the wide coverage (with reported communication ranges of up to 15 km [15]) but also great flexibility to trade off sensitivity for higher throughput (100X speed up by sacrificing 20 dB sensitivity). In both academia and industry, many groups are dedicatedly developing various LoRa applications, such as a remote health and well-being monitoring system [16], long-range surveillance system [17], and object tracking and managing system [18]. LoRa also has great potentiality within fields like the smart grid or smart agriculture. Until 2017, LoRa networks have been widely deployed over 50

countries [19]. This work is mainly based on LoRa technology.

1.1.1   Problems of typical signal-hop LoRa network

The current problems of LoRa network towards academic studies and industry deployments are mainly two issues. The one is the single-hop LoRa networks have limited penetration in critical environments, such as deep indoors, undergrounds, deep mountains, density downtown, and rural areas. The second is the inefficient usage of multiple *Spreading Factors (SF)*, an important parameter in LoRa, limits the capacity of LoRa network because of the typical star topology.

In LoRa specification [20], the alliance develops the network protocol to enpower a wide-range communication by taking advantage of the physical layer design of LoRa technology. Although the goal of the LoRa physical-layer design is to provide extremely wide coverage, the single-hop star topology that current LoRa networks adopt is not necessarily the optimal design from the coverage point of view [21]. Specifically, in such a topology, all the devices communicate directly and only to a central base station. Therefore, the base stations need to be deployed in particular locations with sufficient density to ensure the coverage. Moreover, it is difficult for the single-hop star topology to provide satisfactory coverage in some indoor scenarios where the devices are deployed in highly shielded locations such as basements and pantries.

Also, the single-hop star topology prevents the LoRa network from utilizing its full capacity. Specifically, it is well known that LoRa adopts the Chirp Spreading Spectrum (CSS) technique where the most important parameter are different SFs. LoRa signals with different SF are orthogonal to each other [22], therefore SF can be used as an extra dimension for multiple access which further increases the network capacity. However, the throughput rate, receiver sensitivity, and hence the coverage are vastly different between the SFs. Specifically, the lower SF, the higher throughput and narrower coverage. Therefore, with the single-hop star-topology, only the area close to the central base station can enjoy the high capacity improvement allowed by the SF as illustrated in Fig. 1.2.

In order to slove the problems caused by the limited coverage of single-hop LoRa network and inefficient usage of multiple SFs, we have been striving to construct an highly efficient mesh LoRa network. Firstly, we envision the LoRa network as a multi-hop mesh network where the devices can autonomously relay packets to destinations that cannot be reached
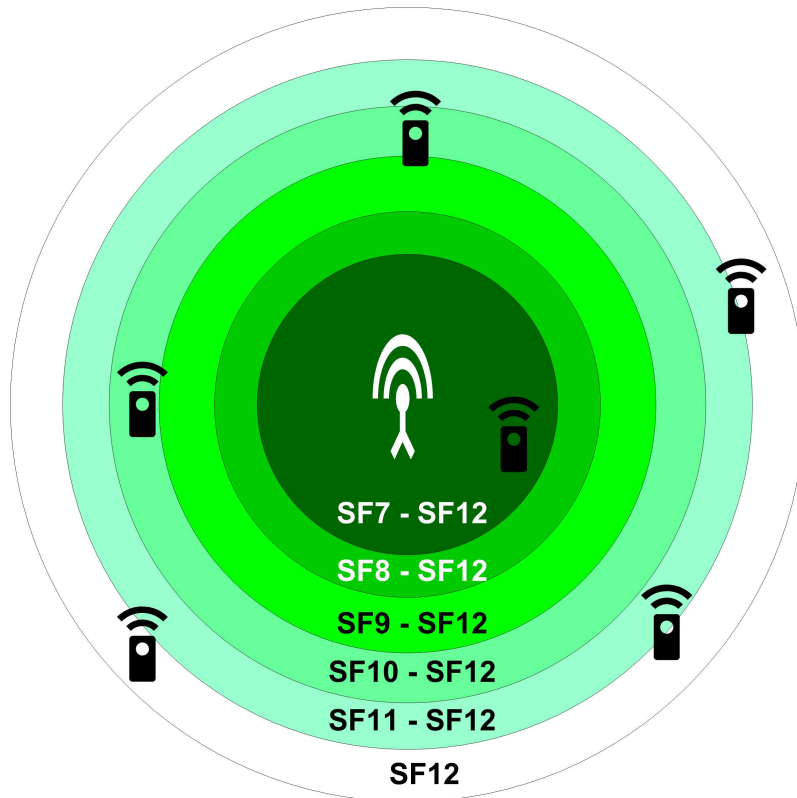
Fig. 1.2 The coverage of different SFs under single-hop topology.

via a single hop. Moreover, we also envision that the multi-hop LoRa network can smartly utilize the extra multiple access dimension provided by different SFs. For example, Fig. 1.3 (a) shows a multi-hop LoRa network providing higher network coverage by employing multiple relays. Fig. 1.3 (b) shows the use of clustering for parallel information exchange where a small SF provides higher throughput in local area and large SF allows relaying packets to distant locations.

1.2   Research goal

The research goal of this thesis is to construct an efficient mesh LoRa network by leveraging concurrent transmission. We believe that the concurrent transmission (CT) flooding [23] will be a good candidate for the multi-hop LoRa network. The CT which realizes an ultra-fast back-to-back relaying by introducing synchronized packet collision has been proven to be a more efficient multi-hop protocol. Thus, it is essential to verify

whether the LoRa receiver can endure co-technology interference (i.e., interference from LoRa packets) to realize a CT-based mesh LoRa network which exploits the capacity provided by SFs. Especially, in the CT scenario, we need to ensure that the receiver can survive synchronized collisions from LoRa packets using *identical* SF. On the other hand, when SFs are utilized as a dimension for multiplexing, the receiver suffers from an interference with *different* SFs, implying that the orthogonality between the SFs needs to be examined carefully.

To further improve the capacity of a CT-based mesh LoRa network (namely, CT-LoRa), we have been striving to realize parallel transmissions by using multiple SFs. More specifically, in a single CT-LoRa flooding, all nodes use the same SF where the multiple multiple-access dimension has not been employed. Fig. 1.4 shows a conceptual structure of parallel CT-LoRa network by conducting multiple CT-LoRa subnets to transmit packets in parallel in the entire space. By doing so, all nodes in the network need to be allocated to several subnets and each subnet uses a separated SF to communicate with the sink node independently.

1.3   Main contributions

To achieve the goal of constructing an efficient mash LoRa network by leveraging CT, in a nutshell, the main considerations of this work are as follows:

LoRa Receiver Performance under CT: We evaluated the LoRa receiver performance under co-technology interference via simulation and experiments to realize the potential of coverage extension by leveraging CT. The results show that LoRa can survive interference from time synchronized packets transmitted by multiple transmitters with an identical SF. Furthermore, to verify the possibility of realizing the parallel CT-LoRa network by exploiting the multiple-access dimension, we examined the orthogonality between different SFs by evaluating the required signal-to-interference ratio (SIR).

SF Allocation for Parallel CT-LoRa: To improve the capacity of a multi-hop CT-LoRa network, we propose to offload the data traffic into several subnets by utilizing multiple-access dimension. Each CT-LoRa subnet rooted at a sink node is allocated a specific SF on the basis of network clustering. This enables packet transmission in parallel with multiple SFs to become feasible. To allow such parallel transmissions, our considerations are: 1) ensuring the connectivity of all subnets; 2) off-loading the traffic according to
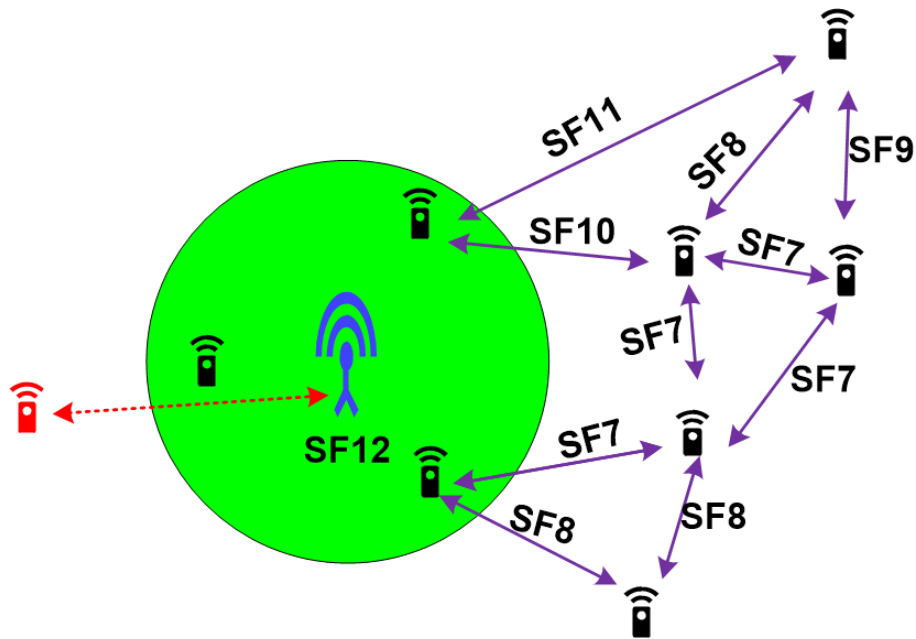
(a) Higher network coverage
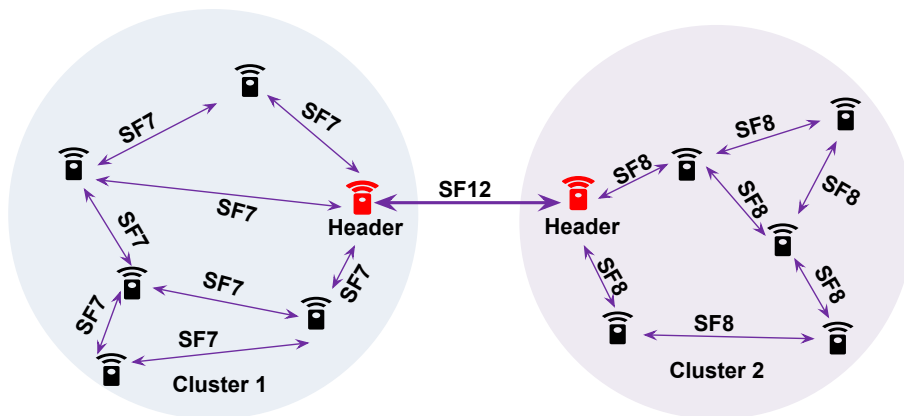
(b) Higher throughput

Fig. 1.3 Example of coverage extension and more efficient mesh LoRa network.

the number of nodes, data rates, and network topologies of each subnet; and 3) shortening the airtime of each subnet by reducing the hop count. Toward these objectives, we present a tree-based SF clustering algorithm (TSCA) to conduct SF allocation in a multihop LoRa network. The TSCA focuses on balancing the airtime between the subnets while ensuring connectivity. Furthermore, we use simulations to show that our approach can significantly increase network performance compared with other approaches. We additionally deploy a
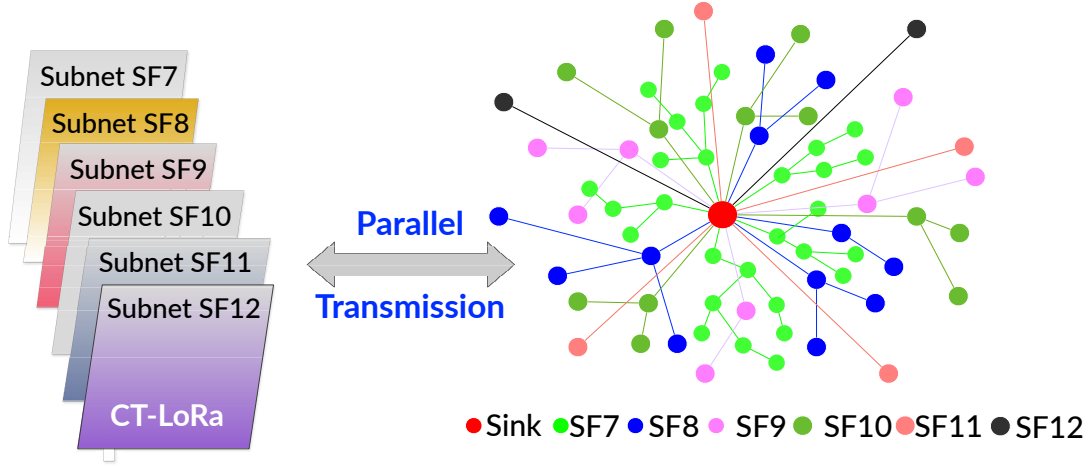
Fig. 1.4 Conceptual structure of parallel CT-LoRa.

real-chip experiment to evaluate the feasibility of parallel transmission in practice.

1.4 Thesis organization

The thesis includes five chapters which are organized as follows:

Chapter 1: In this chapter, we introduce the background and motivations of this thesis. Then, we discuss our research goal of conducting an efficient mesh LoRa network by leveraging CT and the main contributions of this study, respectively.

Chapter 2: In this chapter, we first introduce the related works of LoRa technology, including the basics of LoRa and its related work on both single-hop and multi-hop LoRa networks. Next, we discuss the related studies of CT-based protocols. Then, we introduce different approaches of realizing parallel transmission by exploiting multiple access dimension.

Chapter 3: This chapter presents the investigation of LoRa receiver performance under co-technology interference. Firstly, the possibility of conducting CT-LoRa is verified by the different level of immunity of LoRa signal facing same-SF interference. Then, we evaluate the orthogonality between SFs to show the feasibility of utilizing the multiple access in CT-LoRa.

Chapter 4: This chapter presents our proposal of realizing parallel transmission in a multi-hop CT-LoRa network to further improve network capacity by SF allocation. More

specifically, we present the design concept of SF allocation and analysis of the complexity of SF allocation problem theoretically. Finally, the performance of the proposed algorithm is evaluated by using simulations and experiments.

Chapter 5: This chapter summarizes this thesis and suggests the future work to further improve this research.

Chapter 2

Related Works

In this chapter, we first discuss the basics of LoRa standard where we focus on the physical-layer design of LoRa technology and the recent LoRa studies based on both signal-hop and multi-hop LoRa networks. Secondly, we introduce the background of CT flooding and discuss the characteristics of CT from the viewpoint of physical layer (PHY). Accordingly, we discuss the studies of CT-based protocols with different technologies. Finally, we show the different approaches to realizing parallel transmission to improve network performance. Specially, we compare the differences of conducting parallel transmission by adopting SF allocation in LoRa and that of using multiple channel assignment in the conventional wireless sensor networks (WSNs).

2.1 Basics of LoRa

This section present a brief overview of PHY design of LoRa, including the LoRa modulation and the orthogonality between SFs. Also, we review the recent LoRa-based studies categorized by single-hop LoRa network and multi-hop LoRa network.

2.1.1 LoRa overview

In this subsection, we take a close look at the LoRa modulation and dissuss the orthogonality between LoRa singals with different *Spreading Factor (SF)*, the most important parameter of LoRa technology.

(a) LoRa modulation

Long range (LoRa), is a proprietary LPWAN standard. As evident from public information and the preexisting researches [25–28], the essence of LoRa radio modulation format is a combination of CSS and high-order 2^{SF} -ary FSK modulation.

First, from the time-frequency spectrogram shown in Fig. 2.1 (modified from the figures in [24]), it can be seen that the LoRa packet consists of a series discontinuous chirp symbols. Subplot (a) shows the preamble part with several up-chirps for packet detection, gain control, and frequency recovery and down-chirps for the start of frame delimiter (SFD). Subplot (b) shows the data part consisting of several discontinuous up-chirps, where the data is modulated by the initial position of each chirp. Despite the 2 down-chirps in the end of preamble part, the other chirps are linear up-chirp that always shifts
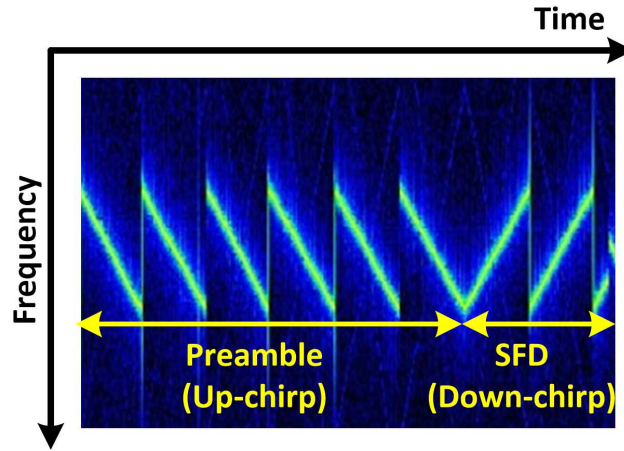
(a) Preamble part
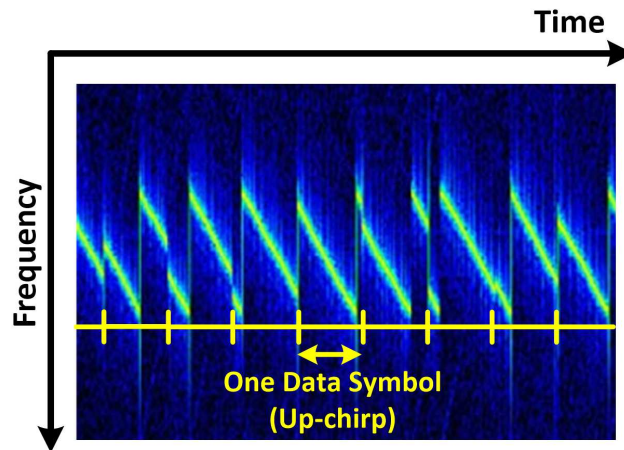
(b) Date part

Fig. 2.1 The spectrogram excerpt of the LoRa signal modified from [24].

toward the positive direction with the same slope until reaching the edge of the frequency band. This indicates that the chirp is used only for spectrum spreading and not for data modulation. Moreover, we can see that the initial positions of the chirp in the data part vary from symbol to symbol, which suggests that it is the initial point of each chirp that is used for data modulation. In other words, if removing the frequency shift caused by the chirps, the LoRa is basically an FSK modulation system.

Second, from the document of LoRa modulation spec [22], one LoRa symbol consists of 2^{SF} samples and carries SF coded bits, where SF is the spreading factor. For low-power standard like LoRa, it is very reasonable to assume that FSK and only FSK is adopted

for data modulation in order to spare the burden of coherent demodulation. Therefore, it is very likely that LoRa adopts a 2^{SF}-ary FSK modulation. This suggest that LoRa is a 2^{SF}-ary FSK system, where the frequency band is divided into 2^{SF} discrete subcarriers, and only one subcarrier per symbol would be selected for data transmission. To be more specific, it is the position of the selected subcarrier not the signal loaded on that subcarrier that represents the data. The 2^{SF}-ary FSK system is very similar to the multi-carrier OFDM system, where a time-domain symbol consists of 2^{SF} symbol and meanwhile the frequency band is divided into 2^{SF} discrete subcarriers.

Fig. 2.2 shows a possible realization of the LoRa transceiver structure. The bit stream is first interleaved and encoded. Then, every SF bits from the coded stream are then mapped to a 2^{SF} bits to the IFFT engine for the 2^{SF}-ary FSK modulation. Finally, the time-domain signal is further modulated by the chirp signal. In the receiver, the received signal is first de-chirped and passed to an FFT engine. The demodulation is done by simply selecting the subcarrier with maximum power at the FFT output.

(a) Transmitter

(b) Receiver
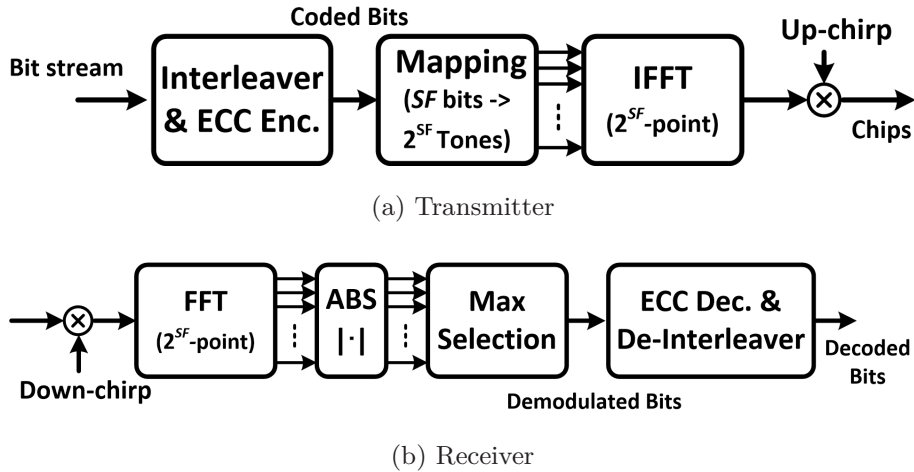
Fig. 2.2   One possible realization of the LoRa transceiver.

(b)   The orthogonality between SFs

In LoRa, one LoRa chirp symbol contains 2^{SF} samples and has a symbol length in time of $2^{SF}/BW$, as revealed in LoRa modulation basic [22]. The more the samples in one symbol, e.g., 4096 samples with the maximum SF12 and 128 samples with the minimum SF7, yield better sensitivity gain within a fixed bandwidth as shown in Fig 2.3, . Thus, the attractive sensitivity gain is actually provided by a tradeoff of the sampling length.
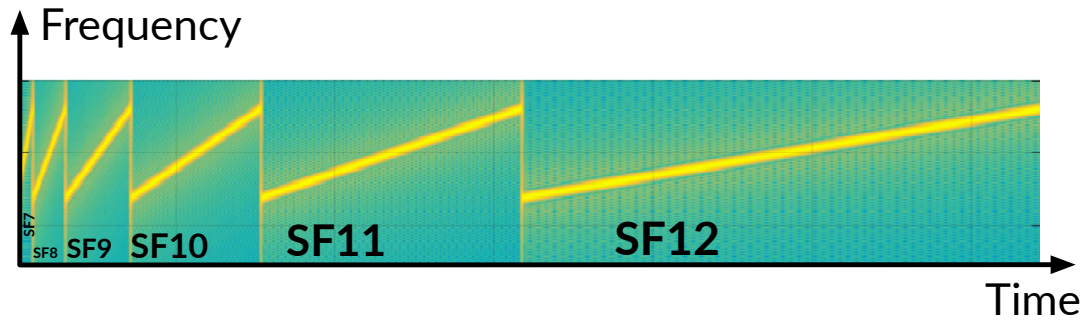
Fig. 2.3 Comparasion of spectrogram of LoRa sepreading factors modified from [29].

Different SFs result in different chirp spreading owing to the CSS. During interference with different SFs, the energy of interference itself will be averaged and the power density will decrease as the interference will spread out over a wide bandwidth. However, the desired signal is still focused in a narrow band after decoding, implying that CSS greatly reduces the effect of different SFs.

2.1.2   Single-hop LoRa networks

LoRaWAN [30], which typically adopts a single-hop topology, implements an ALOHA or a slotted ALOHA mechanism on the Medium Access Control (MAC) layer with the physical design of LoRa technology [31]. LoRaWAN ensures connectivity by standardizing the Adaptive Data Rate (ADR) mechanism to allow the node to step down its data rate. However, the ADR, which is based on the number of received acknowledgement (ACK) messages from gateways, is a basic method. These methods are inaccurate for assessing the highly-varying wireless environment, and render data transmission inefficient [32].

Subsequent research [33–36] considered an SF distribution scheme based only on the distance from the node to gateways. Adelantado et al. [33] showed that an excessive number of nodes (28 % of the network) should use the largest SF (SF12) to ensure the coverage of urban cells. This approach only considered the path loss and ignored the airtime when using SF12. Reynders et al. [35] provided SF distribution scheme to balance the packet error rate [34] and lightweight scheduling to group the nodes into different power level and selected SFs to improve the reliability and scalability of the LoRaWAN network. Slabicki et al. [36] showed that a network-aware approach can further improve the delivery ratio of dense networks by using global knowledge of the node locations.

However, the proposed algorithms based on ADR are not considered in the same way as for parallel transmission. Cuomo et al. [37] extended the work on parallel transmission in a single-hop LoRa network. Specifically, these authors proposed to use the airtime to balance the nodes of each group with a specific SF and to attempt to use a high data rate to offload the traffic to less congested larger SFs.

These strategies cannot be easily applied to a multi-hop LoRa network because of their lack of consideration in regards to multi-hop relays. In contrast to a single-hop network in which the airtime of different groups is only decided by the number of nodes and their data rates, the airtime in a multi-hop network is also determined by the hop count of each subnet. Moreover, the connectivity between multiple relays is still not considered when conducting SF allocation in a single-hop LoRa network.

2.1.3   Multi-hop LoRa networks

As compared to single-hop LoRa networks, multi-hop networks are more flexible to extend the coverage and more efficient to improve the data transmission without increasing the number of gateways. A practical strategy that transforms the topology from star to mesh when the coverage range exceeds $3.2km$ was proposed [38]. Moreover, it was shown [39] that constructing a mesh LoRa network is a good solution to solve the coverage problem in extensively shadowed urban areas. However, few reports that discuss the SF allocation in a mesh LoRa network have been published.

2.2   Basics of CT

In this section, we first present an overview of CT technology. Next, we analyze the CT characteristics form PHY viewpoint, and also discuss CT-based studies on different technologies.

2.2.1   CT overview

Concurrent transmission (CT), which realizes an ultra-fast back-to-back relaying by allowing synchronized packet collision, has been proven to be a highly efficient network protocol in wireless sensor networks (WSNs). As shown in Fig. 2.4, the basic process of
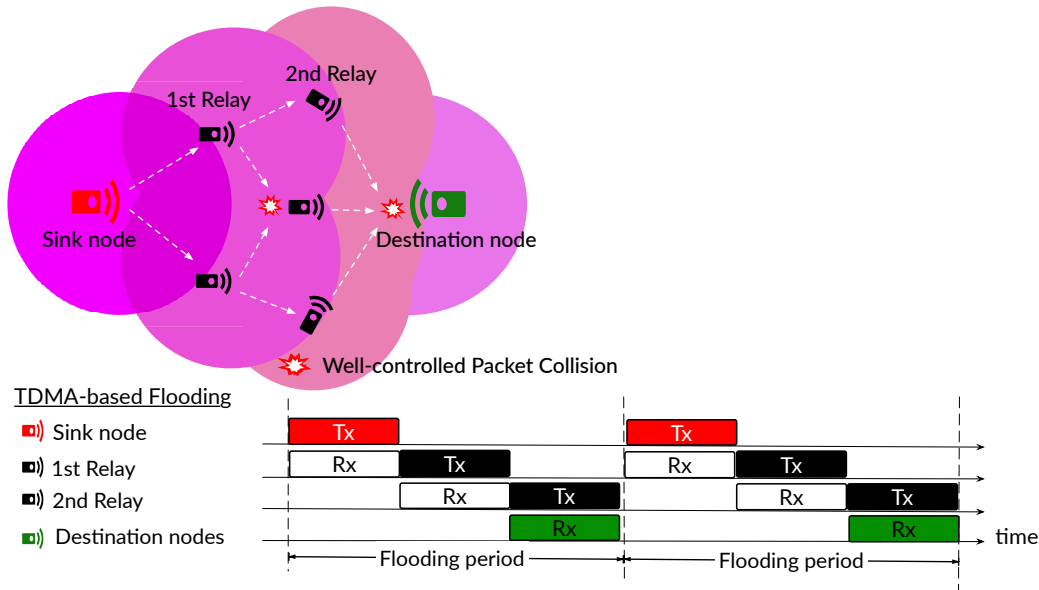
Fig. 2.4 Illustration of TDMA-based CT flooding.

CT flooding is to allow multiple transmitters to join the automatic relaying behavior of the same-content packages concurrently and immediately, right after the package on the air has been received. By doing this, CT-based protocols can enjoy both of the low latency of data transmission under back-to-back realying in the MAC layer and the high efficiency of ultra-fast infrastructure-free flooding in the network layer.

In each CT flooding, there would be one and only one node serving as the initiator. The initiator broadcast the first packet to trigger the flooding. Every node who successfully receives the packet for the first time shall then perform immediate retransmission as another broadcast. The same procedure carries on until the packet floods over the whole network.

The essential difference between CT and the conventional link-layer protocol (e.g. CSMA/CA adopted in IEEE 802.15.4 [40]) is the view toward packet collisions. While the conventional ones strive to avoid packet collisions, CT embraces the synchronized packet collisions that happen when multiple relays perform immediate retransmissions at the same time. By removing the overhead of the collision avoidance mechanism, the packet can flood through the network very quickly through the seamless relays. This property is particularly important when constructing a LoRa multi-hop network since the LoRa packets tend to be long (an order of hundred milliseconds to even seconds) and the conventional

collision avoidance mechanism could easily result in very long latency and wake-up time.

To accommodate packet transmissions from different initiators, a super scheduler is needed to coordinate the transmission order in a Time-Division-Multiple-Access (TDMA) manner. Note that, the TDMA-based coordination can be easily implemented in the CT-based network since the nodes are naturally synchronized by each flooding. To be specific, since each node performs immediate retransmission, the node can accurately estimate the absolute transmission timing of the initiator by subtracting the receiving time by multiplication of the packet length and the hop count. Therefore, all the nodes can perform the synchronization once whenever the super scheduler starts flooding.

The super scheduler assigns dedicated timing slots for the nodes that want to transmit packets. The nodes serve as an initiator in its own slot and transmit a packet using CT flooding while serving as a relay in others' slots. The duration of the slot is set to be just long enough so that a packet flooding can finish within one slot. Specifically, the duration of a packet flooding is as long as the product of the packet length times and the diameter of a network in terms of hop count. Using the interpretation in [41], the CT flooding network acts like a bus connecting all the nodes. Only one node can access the bus at a time, but each access is very short. In [41, 42], schedulers for the CT flooding that can dynamically arrange the transmission order according to the real-time traffic demands are proposed.

The superiority of CT against the state-of-the-art network and link-layer protocols has been verified in [41, 42]. When comparing to other multi-hop protocols, CT achieves a much lower energy consumption due to the accurate duty cycling enabled by the well-scheduled TDMA mechanism. Moreover, since the packet could be heard several times in one flooding, CT also enjoys higher reliability. In addition, although every node in CT needs to dedicate to the current flooding so that the parallel transmissions are prohibited, the short flooding duration in CT compensates the loss in the network utility. Finally, CT does not require any knowledge about the topology and maintains no routing table, which makes CT very lightweight and robust to mobile scenarios.

2.2.2   PHY viewpoint of CT

To better understand CT, we discuss the CT behavior from PHY viewpoint in this subsection. In spite that the network efficiency can be highly improved by constructing synchronized package collision, the destructive package collision is considered to be

harmful to the receiver and naive CT will degrade the network performance inversely. To verify the prerequisites of conducting synchronized package collision successfully, many studies examine the imperfect effects of CT from the theoretical analysis to experimental evaluations.

Unlike the conventional multi-hop protocols that try to prevent packet collisions, CT exposes the physical-layer receivers under synchronized packet collisions to exchange for higher efficiency in the upper layers. Therefore, the essential prerequisite for CT to be effective is to nd the sufficient conditions for receivers to survive such synchronized collisions.

First of all, many success receptions under CT can be attributed to the capture effect [43], which originally refers to a phenomenon in the FM system that only the strongest signal of multiple co-channel ones would be demodulated. In the CT researches, it has been widely adopted to describe the successful receptions of the strongest packet when its power is large enough comparing to the others'. The receiver that can survive CT should have a low Signal-to-Interference-plus-Noise Ratio (SINR) requirement to allow the capture effect to happen easily. On the other hand, for the cases that the reception is not captured by a single packet, the inevitable timing offset and CFO between the packets could affect the reception. Specifically, the timing offset between packets results in an effect similar to the multi-path channel, which leads to inter-symbol interference (ISI) and frequency-selective fading effect. Similarly, the CFO results in an effect that similar to the mobile channel, which leads to inter-carrier interference (ICI) and a fast-fading-like effect more often called beating. The receiver behavior should be carefully investigated to identify the surviving condition against these offsets.

In the context of IEEE 802.15.4 system, there have been many studies trying to conduct the aforementioned investigations. Specifically, many experimental results [44–46] have verified that a 3 dB power difference is sufficient for the packets to be captured. Moreover, for the non-capture cases, the accuracy of the timing synchronization has been proven to be critical to the reliability of packet reception, and the synchronization accuracy needs to be within 0.5 s [23]. Finally, [47] demonstrates that it is the direct sequence spread spectrum (DSSS) adopted in the IEEE 802.15.4 standard that allows the receiver to survive the beating effect.
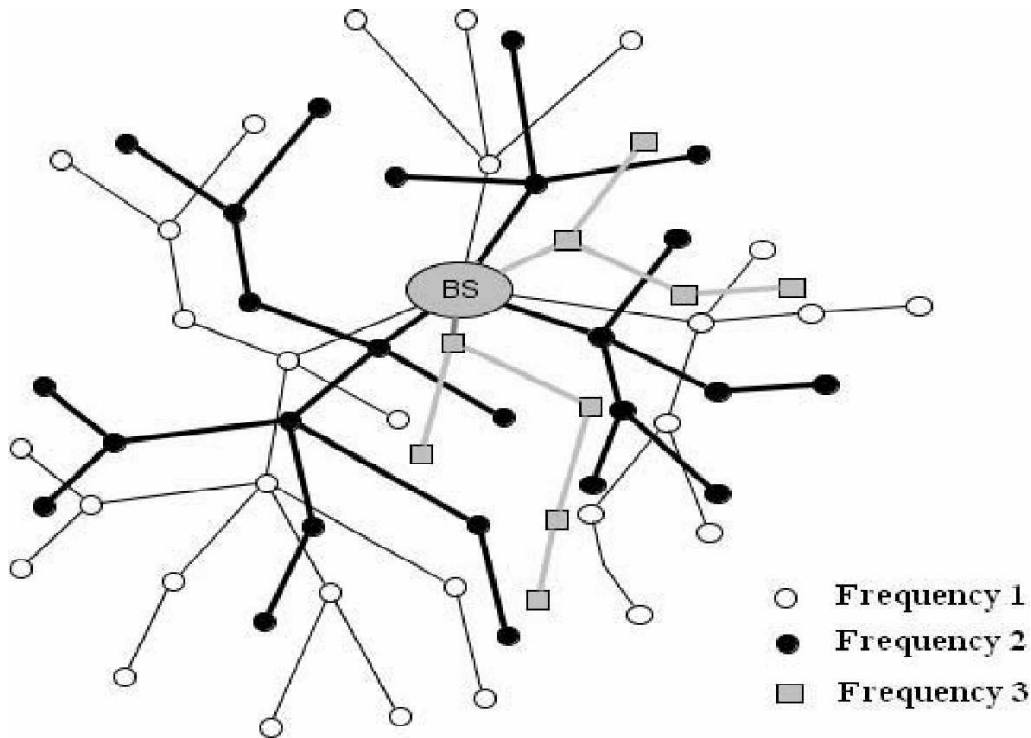
Fig. 2.5 The concept design of TMCP. [48]

2.3   Parallel transmission for multiple access

In this section, we discuss the conventional methods of improving the capacity of a multi-hop ad-hoc wireless network by adopting multiple-channel parallel transmissions.

Similar to SF allocation in a mesh LoRa network, the adoption of parallel transmission by using multiple channels has already been implemented in conventional multi-hop single-root data collection networks. In data collection networks, the proposed protocols [48, 49] usually construct a static channel assignment approach to maintain the simplicity of channel coordination.

Wu et al. [48] have already proven multi-channel assignment as an NP-complete problem by reducing the k-coloring problem to assign a node to different channels.They presented a Tree-based Multichannel Protocol (TMCP) in which a Breadth-First Searching (BFS) algorithm was adopted to construct a fat tree rooted at the sink node and then assigned the channel from the top layer to the bottom layer according the topology and operate

parallel transmissions among sub-trees for data collection as shown in Fig 2.5. However, the paper does not discuss the balance between different sub-trees.

A more recent proposal [49] involved a multi-channel multi-path data collection protocol based on Basketball Net Topology (BNT), which maintains not only a tree-based topology but also the connectivities between peer nodes located at the same height in the tree. This protocol enables child nodes to rejoin the network, even when their parent node disappeared from the original tree structure, by using peer links to communicate with other nodes and employed the first available channel algorithm that adopts BFS to assign a channel to a node after the frist available channel is determined. However, the connectivities of peers extend the hop counts to the sink node, which inversely increases the airtime of the entire network. These approaches ignored the balance between different subnets. In terms of channels, the coverage range they achieved was consistent, whereas the coverage was attenuated by using a smaller SF with a higher data rate.

The use of LoRa enables the coverage range to be extended when a lower data rate with a larger SF is chosen. As compared to multi-channel assignment algorithms, we needed to consider an approach that would decrease the hop count of each sub-tree using a different SF while ensuring that the airtime between different sub-trees remains balanced.

2.4   Summary

This chapter presents the related works of LoRa and CT, respectively. In LoRa, we overview the basics of LoRa technology and recent studies based on single-hop LoRa networks and multi-hop LoRa networks. To leverage CT technology on mesh LoRa networks, we first introduce the basics of CT flooding and the related CT-based protocols. Then, we focus on the non-ideal effects (CFO, PO, TO) of CT from PHY viewpoint and its previous works. Moreover, we also describe the convention approaches of realizing multiple access by using multiple channels as compared to realize parallel transmission in CT-LoRa by conducting SF allocation.

Chapter 3

Receiver Performance under CT

In this chapter, we present our investigation on LoRe receiver performance under co-technology interference. We first analyze the characteristics of CT-LoRa from physical layer viewpoint. Accordingly, we introduce our evaluation methodology which includes the evaluation modeling, evaluation metrics, and our platform as a matter of considerations. Then, we present our evaluation of LoRa receiver performance under identical-SF interference and different-SF interference, respectively. More specifically, in the identical-SF interference scenario, we evaluate whether CT will be effective in the LoRa network for all SFs. For each SF, we observe the possible performance degradation caused by imperfect CT effects under the same condition. The receiver performance under each SF is evaluated by repeated simulations and real-chip experiments. In the different-SF interference scenario, we measure the required signal-to-interference ratio (SIR) of each pair of two SFs where the one is served as a victim and the other is served as an interference.

3.1   PHY viewpoint of CT-LoRa

This section introduces the characteristics of LoRa physical layer which leads to LoRa receiver behavior under CT is quite different from other wireless technology. More importantly, the difference between LoRa signals with different SFs varies the receiver performance under CT flooding.

The first feature is its long symbol time which is aiming to trade for good sensitivity performance. Specifically, when the LoRa is configured at the lowest rate mode (with SF and the bandwidth being 12 and 125 KHz, respectively), one data symbol consist of 4096 samples, which is as long as 32.7 ms. In CT scenario, the long symbol makes LoRa immune to the beating effect caused by CFO. As we mentioned in the previous section, beating is fading-like effect, which results in bursty demodulation error when deep fading occurs. We have shown that the effect of beating is negligible if the fading duration of the beating is narrower than the symbol time. Moreover, we showed that the beating caused by CFO typically has a fading duration of the order of several μs. Since the LoRa has a ms-order symbol time, it is very unlikely for the beating to deeply fade a whole LoRa symbol.

The second feature of LoRa, which is also empowered by the long symbol length, is that LoRa adopts a very high-order M-ary FSK modulation in order to increase the spectral efficiency. As a result, the frequency deviation of M-ary FSK modulation is extremely

small compared to CFO. Specifically, when LoRa is configured as the lowest-rate mode, the FSK is in 4096-ary, and the frequency deviation is only 30.5 Hz, while the CFO between the transmitters typical has a standard deviation of several KHz. In the CT scenario, even though that the concurrently transmitted packets all carry the same payload, the CFO could easily bias the FSK modulation and distort the packet as if they are carrying independent payloads. To illustrate, Fig. 3.1 shows an example of LoRa demodulation under a CT scenario of two transmitters. The stronger packet (blue arrow) is treated as the wanted signal by the receiver, while the weaker one (red arrow) becomes the interference. Since the CFO biases the interference to another subcarrier, the wanted packet could only be successfully decoded when the power offset is large enough. Subplot (a) illustrates a case without energy spreading effect, where the CFO and the timing offset are the integer times of f_{dev} and t_S, respectively. When the CFO is not the integer of f_{dev} (Subplot (b)), or the timing offset is not the integer times of t_S (Subplot (c)), the energy of the interference is spread on multiple subcarriers and results in larger power offset.

Under such independent packet collisions, the capture effect (the presence of a significantly strong packet) is obviously the only reason that the packet reception could succeed, and this seems to make LoRa incompatible with CT. However, also thanks to the high-order M-ary FSK modulation property, there are two effects that allow an extra margin for the capture effect, and hence significantly increase the probability of surviving. We refer to these two effects as the *frequency-domain* and *time-domain energy spreading* effect.

- **Frequency-domain energy spreading effect**: Since the CFO is a continuous random value that is typically larger than the frequency deviation, it is very likely that the interference tone locates between two subcarriers. In such cases, the energy of the interference tone would spread among the adjacent subcarriers as shown in Fig. 3.1 (b), and hence results in an extra power offset between the strongest tone and interference tone. We refer to this effect as the frequency-domain energy spreading effect. The maximum frequency-domain energy spreading happens when the interference locates exactly in the middle of two subcarriers so that the energy spread out on that two adjacent are equal. In such cases, there would be at least an extra 3 dB power margin, which is large enough to allow LoRa receiver to survive the non-capture scenario.

- **Time-domain energy spreading effect**: The other energy spreading effect happens when there is timing offset between the received packets. We use the example

(a) No energy spreading effect

(b) Frequency-domain energy spreading effect

(c) Time-domain energy spreading effect

Fig. 3.1 An example of the LoRa demodulation under a two-transmitter CT scenario.

in Fig. 3.1 (c) to illustrate. When there is timing offset, each symbol of the wanted packet would be affected by two adjacent symbols of the interference packet, and each interfering symbol contributes only part of its power. Since each LoRa symbol carries independent SF bits, the probability for the adjacent symbols to be different is $(2^{SF} - 1)/2^{SF}$, which is very close to 1 since SF is large in LoRa. Therefore, the partial power of interference would be very likely to locate on independent tone, which also results in more power margin for demodulation. Moreover, we expect that the optimum timing offset would be half of the symbol time, and the resulted power margin is also larger than 3 dB.

Due to these two energy spreading effects, the LoRa receiver could have a high probability of surviving the CT scenario even without the capture effect. However, the carrier space of LoRa symbol and its symbol time are also changed by different SFs. Then, we analyze the power margin obtained by the two energy spreading effects. Before the chirp modulation, the baseband signal of an M-ary FSK LoRa symbol using the kth subcarrier can be represented as

$$s_k(t) = e^{j2\pi k f_d t}, (t \in [0, t_s]) \tag{3.1}$$

where t_s and f_d are the symbol time and frequency deviation, respectively Therefore, a de-chirped LoRa symbol using the kth subcarrier ($k \in [-\frac{M}{2}, \frac{M}{2} - 1]$) and being affected by a CFO αf_d and a timing offset βt_s can be represented as

$$s'_k(t) = e^{j2\pi(k+\alpha)f_d(t-\beta t_s)}, (t \in [\beta t_s, \beta t_s + t_s]), \tag{3.2}$$

where α and β are factors for normalizing the CFO and timing offset, respectively. Without losing of generality, we assume both α and β are in the range of $(0, \frac{1}{2}]$.

As shown in the Fig. 2.2 (b), after the de-chirp operation, the non-coherent matched filter receiver estimates the transmitted FSK symbol by selecting the subcarrier with maximum magnitude from the outputs of the M matched filters as

$$\hat{m} = \operatorname*{arg\,max}_{m \in [-\frac{M}{2}, \frac{M}{2} - 1]} | \sum_{n=0}^{M-1} (r(nT_c)e^{-j2\pi m f_d nT_c})|, \tag{3.3}$$

where $\hat{m}$ is the estimated subcarrier number, T_c is the chip time, and $r(t)$ is the received signal. Note that, in the LoRa system, the symbol time t_s, chip time T_c, frequency deviation f_d, and system bandwidth W satisfy the following equations.

$$t_s = MT_c = \frac{1}{f_d} = \frac{M}{W}. \tag{3.4}$$

Assuming that the $s_k(t)$ is transmitted and there is no CFO and timing offset, it is straightforward to show that only the kth matched filter would have the maximal value, and the other matched filter would output zero due to the orthogonality between the subcarriers. By substituting $s_k(t)$ for $r(t)$ in (3.3), the maximal value can be simply calculated as M.

On the other hand, with the presence of CFO and timing offset, the orthogonality is corrupted and the energy would be spread around multiple subcarriers. Since most of the energy would still concentrate on the subcarriers near to the kth one, we substituting the offset LoRa symbol $s'_k(t)$ for $r(t)$ in (3.3) and calculate the corresponding output magnitude of the $(k + \Delta)^{\text{th}}$ matched filter output as

$$
\begin{aligned}
A(\Delta, \alpha, \beta) &= |\sum_{n=0}^{M-1} (s'_k(nT_c) \times e^{-j2\pi(k+\Delta)f_d nT_c})| \\
&= |\sum_{n=\lceil \beta M \rceil}^{M-1} (e^{j2\pi \frac{(\alpha-\Delta)n}{M}})| \\
&= |\frac{1 - e^{j2\pi \frac{(\alpha-\Delta)(M-\lceil \beta M \rceil)}{M}}}{1 - e^{j2\pi \frac{(\alpha-\Delta)}{M}}}|,
\end{aligned}
\tag{3.5}
$$

where $\lceil \cdot \rceil$ is the ceiling function.

Finally, the power margin can be evaluated by calculating the ratio between the magnitude $A(\Delta, \alpha, \beta)$ with the maximal value M of the non-offset case, or specifically

$$
\rho(\Delta, \alpha, \beta) = 20 \times \log_{10}(A(\Delta, \alpha, \beta)/M).
\tag{3.6}
$$

Fig. 3.2 illustrates the numerical results of the ρ value for different Δ, α, and β. Specifically, Subplot (a) to (d) correspond to the case with Δ equal to -1, 0, 1, and 2, respectively. These are the three nearest subcarriers to the kth one. The X- and Y-axis in each subplot correspond to the value of α and β, respectively.

From the numerical results, the following observations can be made

- Most of the energy concentrates on the nearest two subcarriers, and the maximal value appears on the nearest subcarrier with $\Delta = 0$. Therefore the receiver performance would be dominated by the case with $\Delta = 0$.

- The results show that the timing offset and CFO help to increase the power margin. In the the case where $\Delta = 0$ in Fig. 3.2 (b), a more than 6 dB power margin can be obtained by the two energy spreading effects if both α and β are both 0.5.

(a) $\Delta = -1$

(b) $\Delta = 0$

(c) $\Delta = 1$

(d) $\Delta = 2$
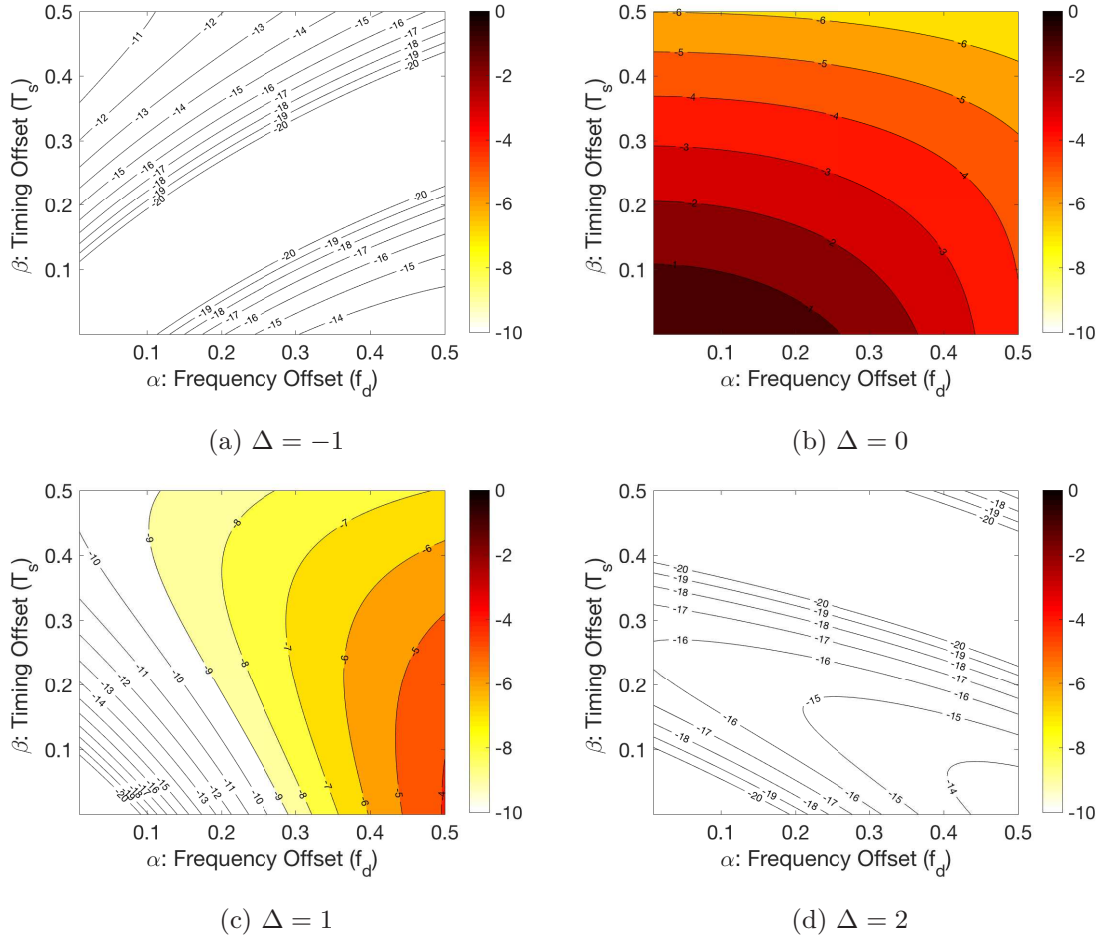
Fig. 3.2 The power margin obtained by the two energy spreading effects.

- The power margin resulting from the time-domain energy spreading effect is more significant than that from the frequency-domain one.

3.2 Receiver performance under identical-SF interference

In this section, we present the evaluation of LoRa receiver performance under identical-SF interference based on each SF. First, we introduce evaluation modeling, metric, and scenario, respectively. Next, we present the simulation results LoRa reiceiver performance from SF7 to SF12. Then, we describe several experiments conducted in the real environment to support our simulation results.
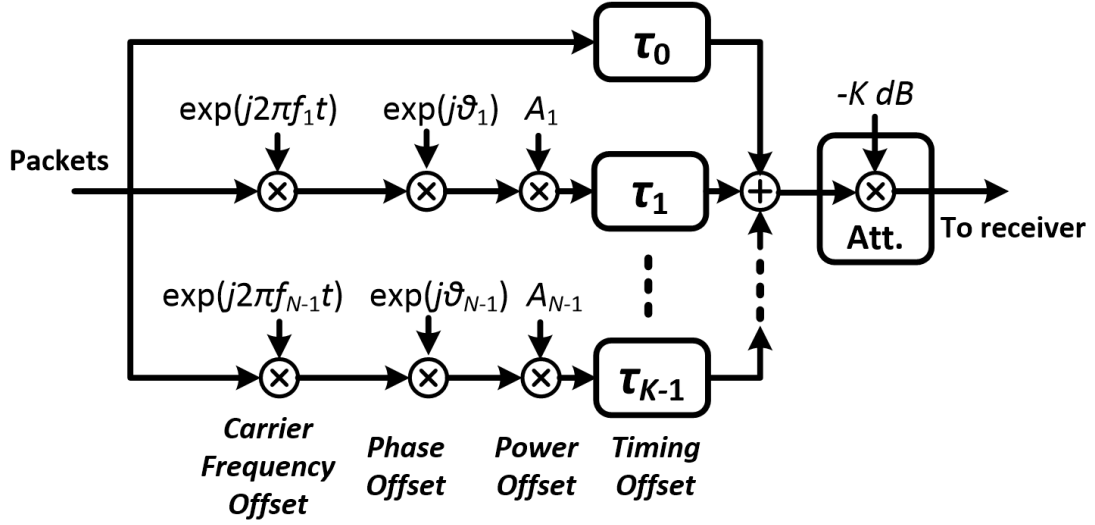
Fig. 3.3 The equivalent one-hop channel model of CT.

3.2.1 Evaluation methodology

This subsection describes the methodology for LoRa receiver performance under CT includes the evaluation model, evaluation metric and evaluation scenario, respectively.

(a) Evaluation model

In our simulation evaluation, we evaluate LoRa receiver performance by the typical one-hop transmitter-channel-receiver model. Specifically, LoRa packets are first generated according to the transmitter block diagram as shown in Fig. 2.1 (a), and then passed through a CT equivalent channel model, and demodulated by the receiver as shown in Fig. 2.1 (b). The CT equivalent channel model is a one-hop additive composite channel as shown in Fig. 3.3 [47]. In this model, a packet is transmitted by multiple transmitters and each of the transmitters has independent power, phase, timing offset, and CFO. The signals from each transmitter are then combined additively. Our simulation randomly generated 15-byte packets with a specific SF (from SF7 to SF12) and BW-125KHz mode are used.

(b) Evaluation metric

In CT, only adopting the packet reception rate (PRR) as the evaluation metric usually made some groundless remarks, assessing the receiver performance over-optimistically. To

faithfully react the loss resulting from the CT, we evaluate the receiver performance in terms of the sensitivity gain, defined as the difference of sensitivity performance between CT reception and conventional collision free reception [47]. To calculate the sensitivity gain, we assume that the first transmitter is the strongest and with a unitary power and zero offsets, while the power of the other ones is always smaller without losing the generality. After the combination, the signal is first attenuated by K dB before fed to the receiver. We also assume that the receiver achieves perfectly timing and frequency synchronization to the stronger transmitter. In our evaluation, we gradually increase the attenuation K until the packet error rate (PER) reaches 1 %, and record the K value as the maximum allowable attenuation. As the final metric, we calculate the difference of K value between the CT and collision-free reception and refer to this difference as the sensitivity gain. Note that, since LoRa is a proprietary standard, the adopted interleaving and error correcting code scheme are not open to the public. Therefore, our evaluation is based on uncoded PER.

(c) Evaluation senario

The simulation in this chapter is to evaluate the receiver performance under CT effects with all SFs. In the evaluation, we adopt a 2-Tx scenario with two transmitters using the same SF. One Tx is set as a stronger one with zero dB and no offsets. Then, we carefully sweep the TO and CFO of the other Tx under the larger/small PO with the first transmitter. Additionally, the phase offset is set as (0 - 2 π) with a random uniform distribution.

3.2.2 Simulation evaluation

In our simulation, we generated a one-hop transmitter-channel-receiver channel based on 2^{SF}-ary FSK modulation, further spread by the LoRa chirp signal. The sensitivity gain or loss between two transmitters was determined to evaluate the LoRa receiver performance under CT. The parameter space and specific setup are listed in the Table 3.1 and Table 3.2. Depending on the chosen SF in LoRa network, the *symbol time (T_s)* and the *frequency deviation (f_{dev})* can be calculated in a simple manner using the Eq. (3.7) and Eq. (3.8) respectively, as described in [20].

SF Para.	SF12	SF11	SF10	SF9	SF8	SF7
T_s (ms)	32.8	16.4	8.2	4.1	2.05	1.02
f_{dev} (Hz)	30.5	61	122	244	488	976

Table 3.1 Parameters for different SFs.

$$symbol\ time = 2^{SF} * chip\ time = \frac{2^{SF}}{BW} \tag{3.7}$$

$$subcarrier\ space = \frac{BW}{2^{SF}} \tag{3.8}$$

where SF is the spreading factor, and BW is the signal bandwidth.

Timing offset (TO)	0 to 4 T_s
Carrier frequency offset (CFO)	0 to 4 f_{dev}
Power offset	0 dB, 1 dB, 2 dB, 3dB
Phase offset	Random (0 to 2π)
Bandwidth	125 KHz
Error correcting code (ECC)	Unused

Table 3.2 Simulation setup.

The results for SF7 - SF12 are shown in Fig. 3.4, 3.5, 3.6, 3.7, 3.8, and 3.9, respectively. Each subfigure (a), (b), (c), and (d) corresponds to a special power offset (0-3 dB) and the X and Y axes represents CFO and TO, respectively. The X and Y axes represent the CFO (0 - 4 f_{dev}) and timing offset (0 - 4 T_s). The degree of sensitivity loss or gain is indicated by a (2-D) contour map where the darkest areas are the areas which are most affected by sensitivity loss. Several observations can be made from these results which are described as follows.

(a) Power effect

In Fig. 3.4 (a), the surviving zone of SF7 is limited. SF7 CT could barely survive in the LoRa network with zero power offset. When the power offset was increased by 1 dB, the receiver performance improved as per our expectation. Under 2-dB power offset, as

(a) Power offset: 0 dB

(b) Power offset: 1 dB

(c) Power offset: 2 dB

(d) Power offset: 3 dB
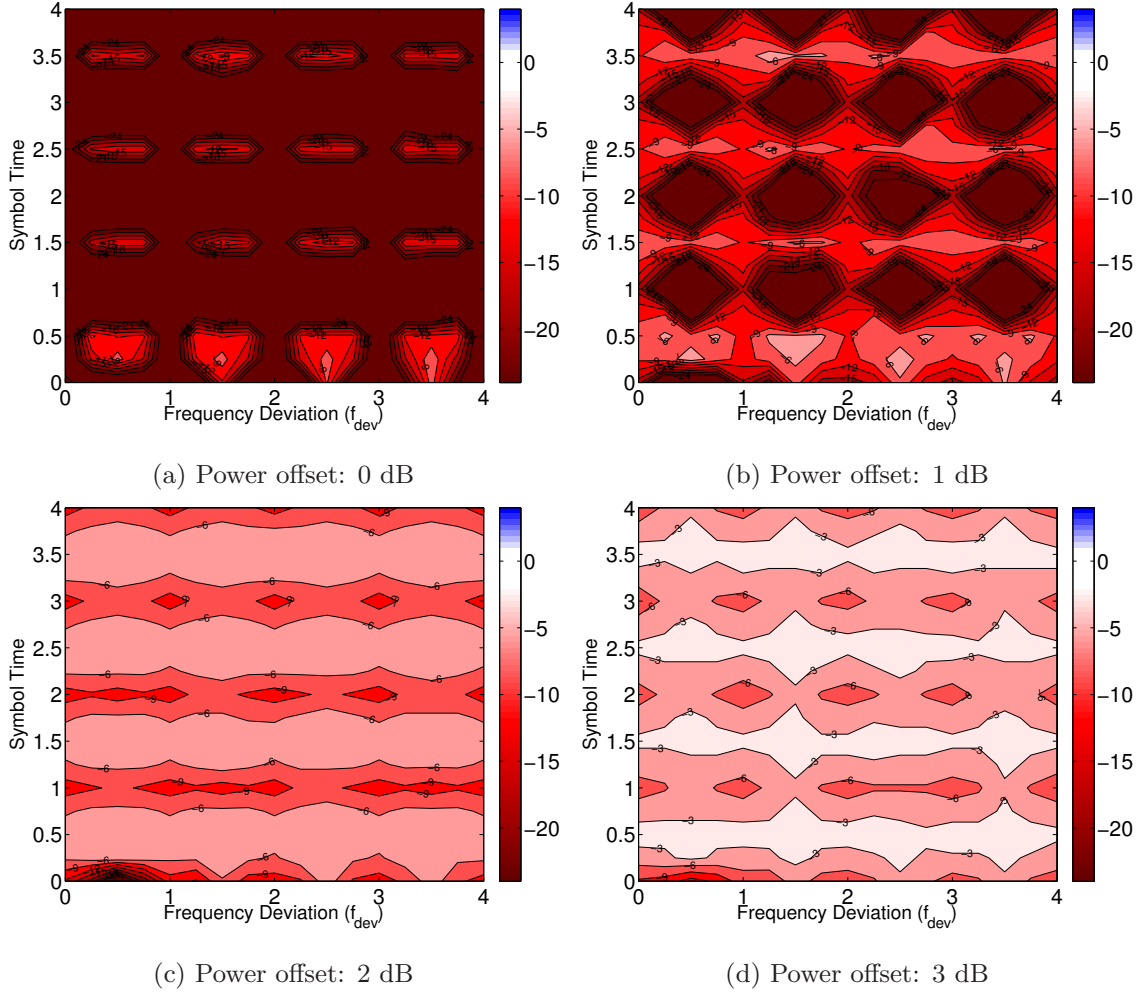
Fig. 3.4 Simulation results for SF7.

shown in Fig. 3.4 (c), the sensitivity loss was roughly 10 dB lower in SF7, indicating the high potential of application of CT to LoRa network for all SFs in a real environment.

The simulation results show the required power offset that ensures the capture effect for LoRa. Also, if there is at least 3 dB power offset between that two packets, the receiver can enjoy a comparable performance as the collision-free links regardless of the value of the timing offset and the CFO.

(b)   Frequency-domain energy spreading effect

For the non-capture effect shown in each of subfigure (a) and (b) of Fig. 3.4 - Fig. 3.9, we can see that the CFO value affects the receiver performance significantly, where each figure

(a) Power offset: 0 dB

(b) Power offset: 1 dB

(c) Power offset: 2 dB

(d) Power offset: 3 dB
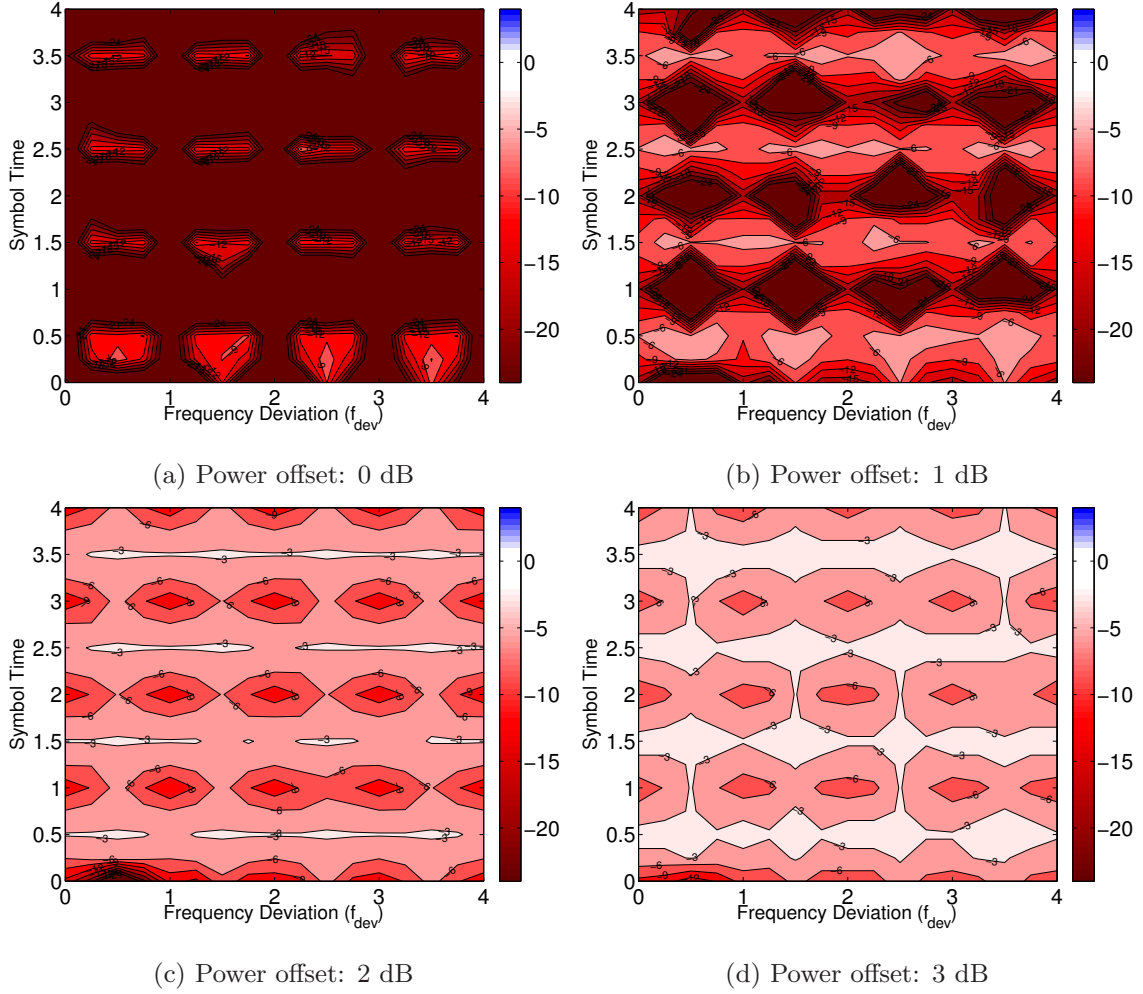
Fig. 3.5 Simulation results for SF8.

shows consistent results that the best receptions always appear under the CFO that are half-integers of frequency deviation. Particularly, there is a clear periodicity of the receiver performance that varies according to the CFO value (the horizontal direction). When the CFO value is the integration times of the f_{dev}, the sensitivity suffers significantly. On the other hand, the sensitivity performance improves greatly while the CFO is not an integer times of f_{dev}. This verifies our previous analysis of the frequency-domain energy spreading effect.

(c)   Time-domain energy spreading effect

Similar periodicity can also be observed in the time-domain (the vertical direction). The sensitivity suffers the most when the timing offset is the integration times of the symbol

(a) Power offset: 0 dB

(b) Power offset: 1 dB

(c) Power offset: 2 dB

(d) Power offset: 3 dB
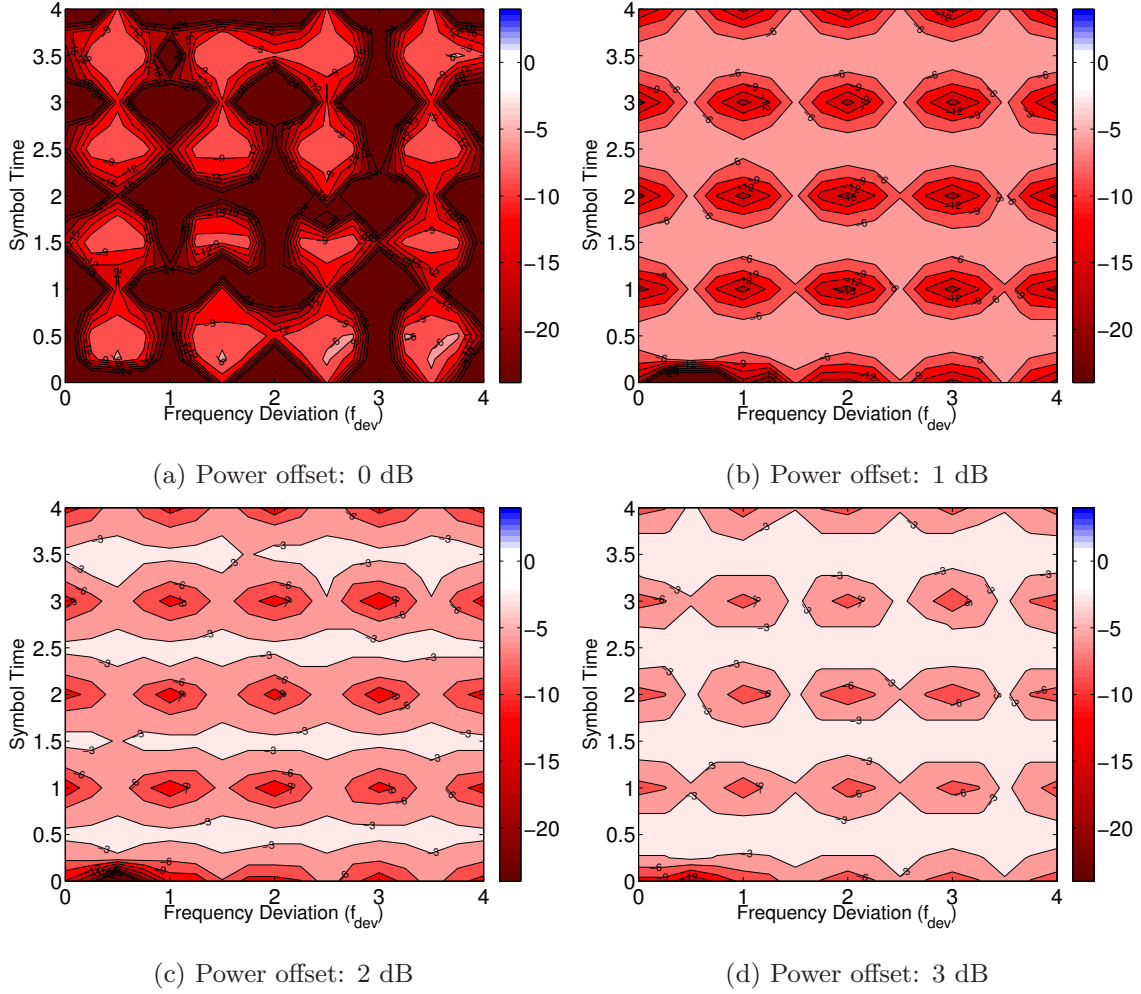
Fig. 3.6 Simulation results for SF9.

time, while the sensitivity performance is comparable to the collision-free case when the timing offset is 0.5 times offset from the integer symbol time. This verifies our analysis of the time-domain energy spreading effect.

(d)   The slow beating area

In each of subfigure of Fig. 3.5 - Fig. 3.9, we observe an exceptional bad-performance area between when the CFO is between 0 and 1 f_{dev}. This is the slow beating region where the fading duration of beating is wider than the symbol. In this region, some symbols could be totally deeply faded and failed to be demodulated. However,the probability for the CFO to full in this region is negligible due to the very small f_{dev} of LoRa modulation.

(a) Power offset: 0 dB

(b) Power offset: 1 dB

(c) Power offset: 2 dB

(d) Power offset: 3 dB
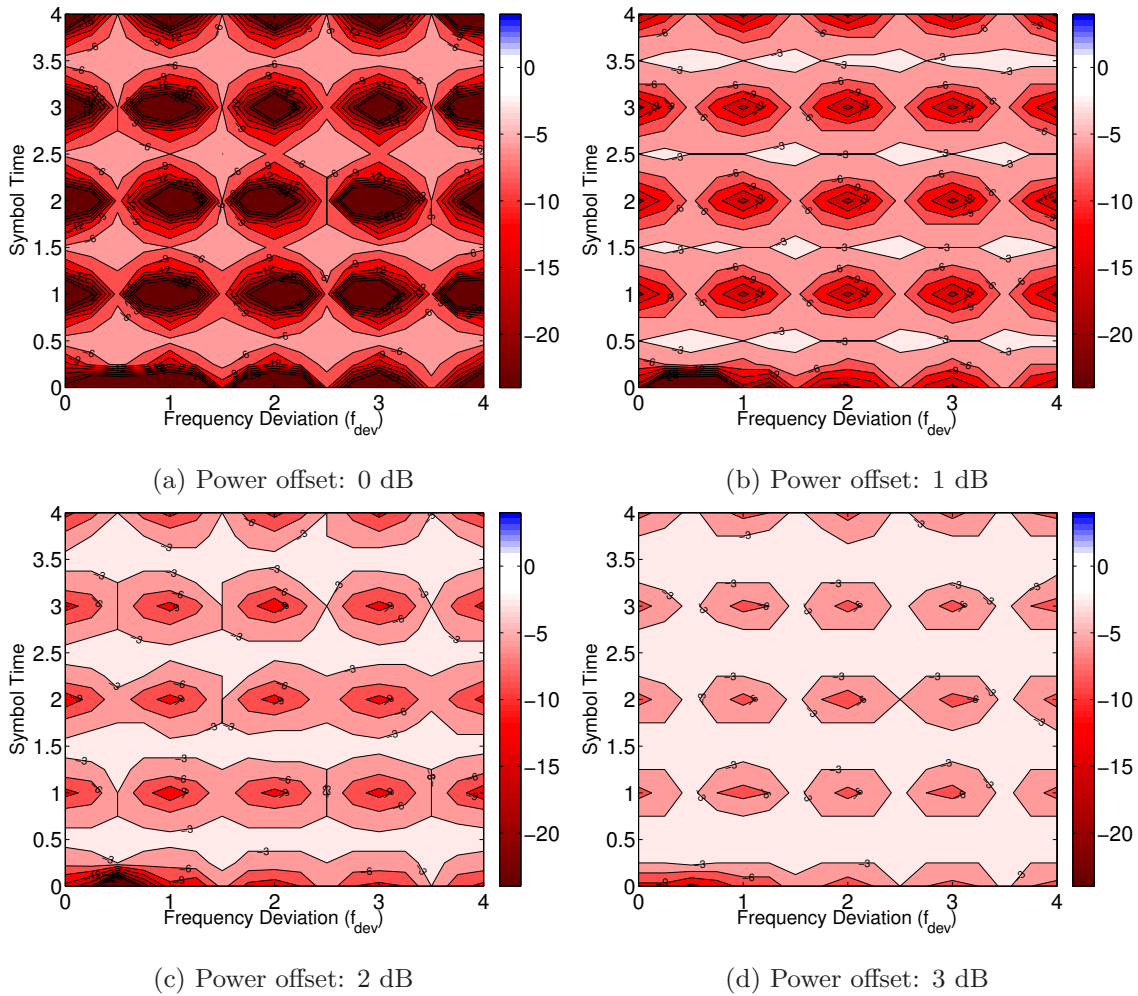
Fig. 3.7   Simulation results for SF10.

Note that, if the CFO is larger than fdev, the relation between the sensitivity performance and the CFO can be estimated by calculating the remainder after dividing the CFO by f_{dev}. Moreover, since the standard deviation of CFO in practical systems is a random variable whose standard deviation is typically much larger than the fdev, the remainder can be regarded as a random variable uniformly distributed between 0 and fdev.

(e)   SF difference

Larger SFs yield a clearly better performance under identical conditions as compared with smaller SFs. Even without the power offset, using SF > 9 yields the best performance, with approximately 5 dB sensitivity loss as presented in subplot (a) of each figure. When the power exceeds 3 dB, as shown in each subfigure (d) of Fig. 3.6 - Fig. 3.9 (d), the receiver

(a) Power offset: 0 dB

(b) Power offset: 1 dB

(c) Power offset: 2 dB

(d) Power offset: 3 dB
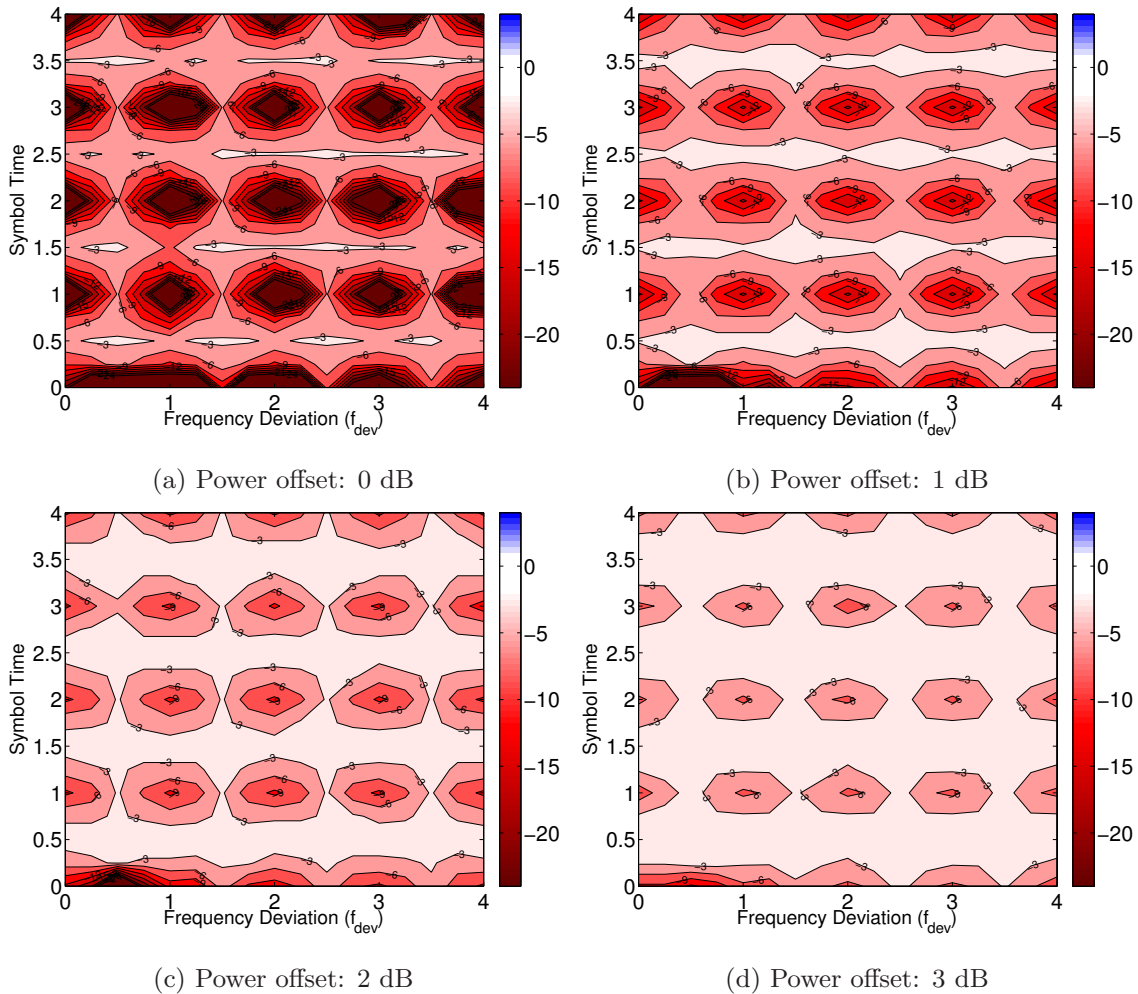
Fig. 3.8 Simulation results for SF11.

performance is comparable to that in a collision-free case. More specifically, closer SFs present similar results under CT-LoRa, where the smallest value that is SF7 presents the worst results for identical-SF interference, and SF9 and SF11 are similar to each other. The largest of the values, SF12, yields the highest immunity against interference for different SFs.

3.2.3   Real-chip experiments

We conducted real-chip experiments for all SF in two-building and four-building scenarios in a practical environment to evaluate the efficiency and robustness of CT-LoRa. Specifically, we used 18 LoRa RF modules equipped with Semtech SX1272 [50] and

(a) Power offset: 0 dB

(b) Power offset: 1 dB

(c) Power offset: 2 dB

(d) Power offset: 3 dB
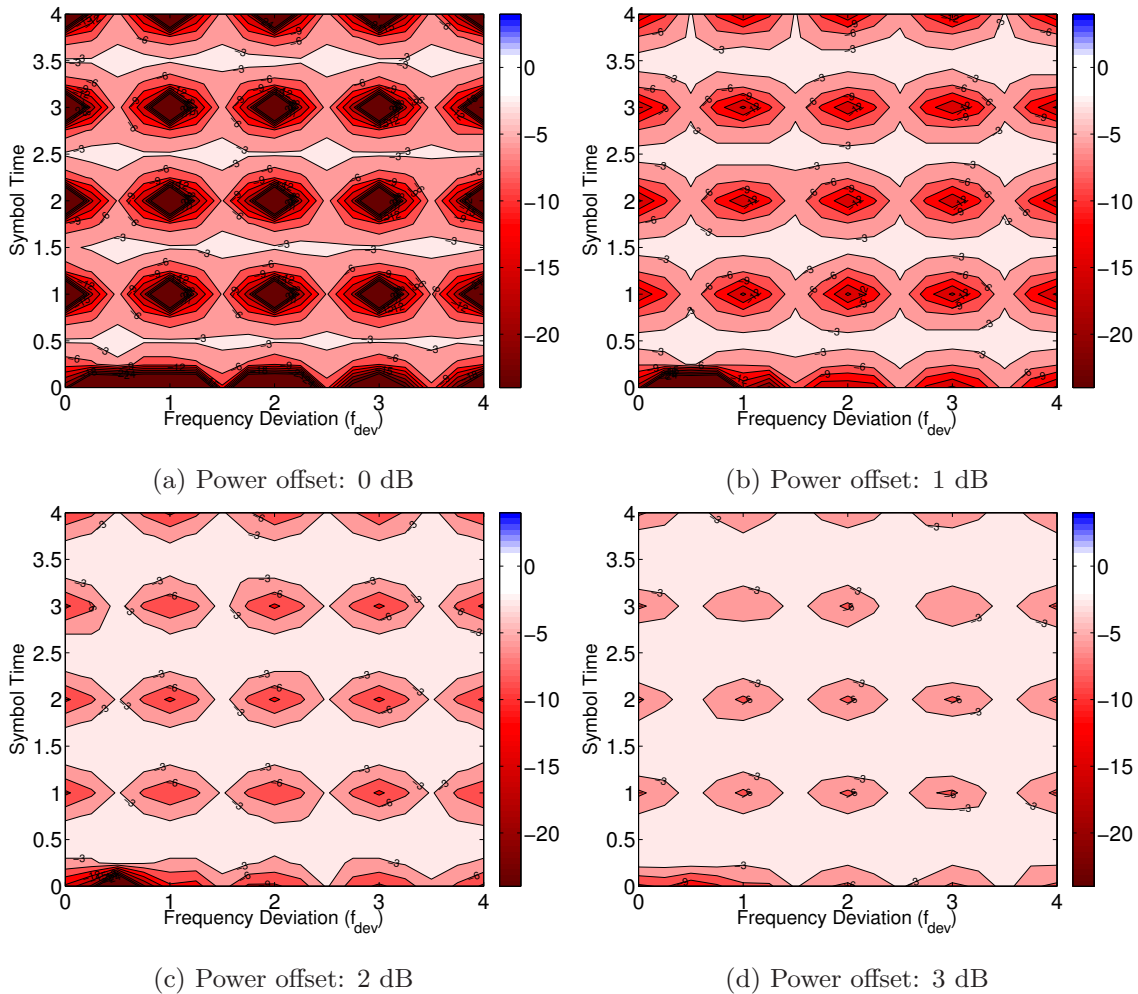
Fig. 3.9　Simulation results for SF12.

STM32L151 [51] microprocessors to cover the buildings. Each node acts as an initiator in a round-robin manner and the others as relays. In each experiment round, the initiator transmits 100 packets with a 15-byte packet length to trigger CT flooding 100 times for each SF and the correctness of packet reception is determined by the CRC check. Finally, the experiment is conducted on the 920.6 MHz band, with SF, bandwidth, and code rate being 12, 125 KHz, and 4/5, respectively. We show the detailed deployment map in Fig. 3.10 (a) and (b). Note that, different with simulation, CRC check is adopted for the correctness of packet reception.

Fig. 3.11 shows the experiment results under the two scenarios, including the worst and average network PRR and the maximum and average hop count between any two nodes according to each SF. From the experiments, the following observations were made.
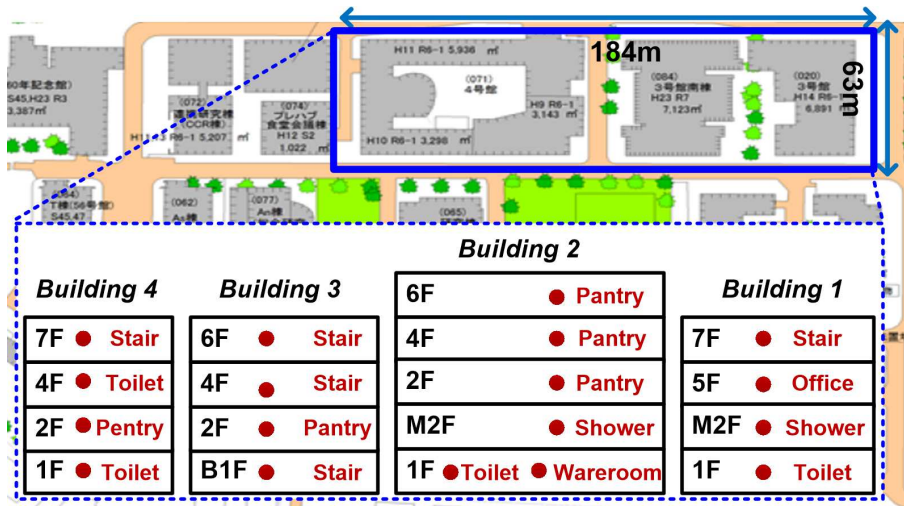
(a) Four-building deployment map
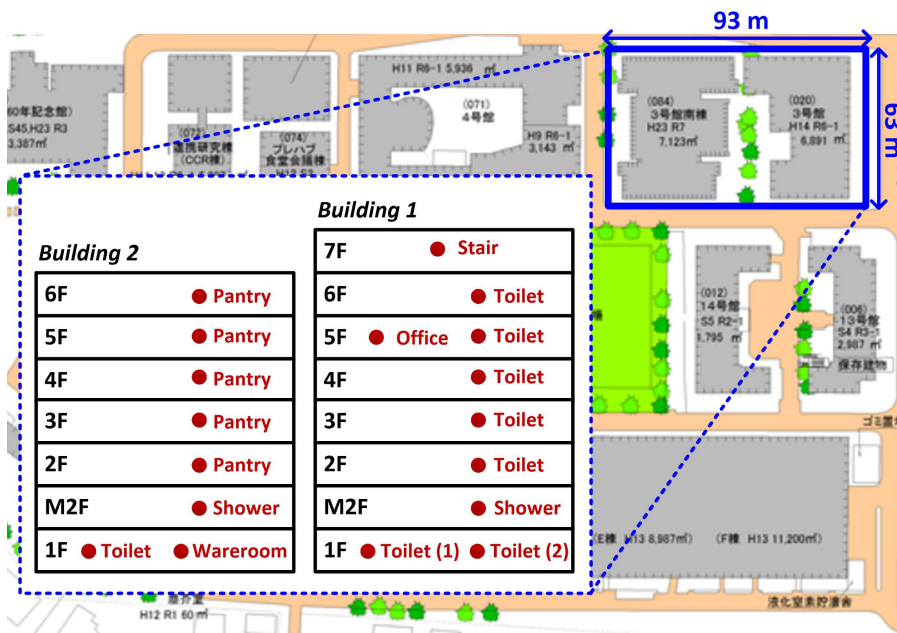
(b) Two-building deployment map

Fig. 3.10 Experimental deployment of two scenarios.
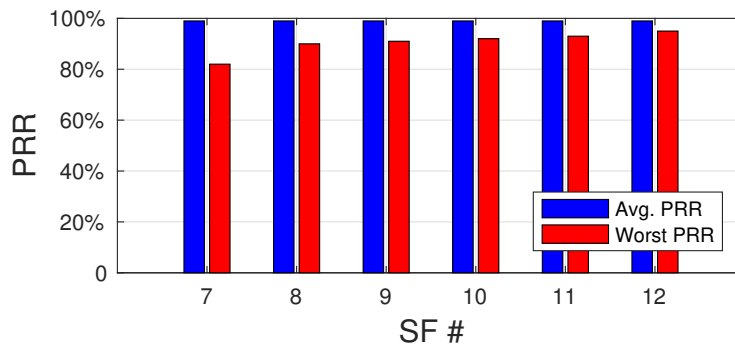
(a) PRR in the two-building scenario
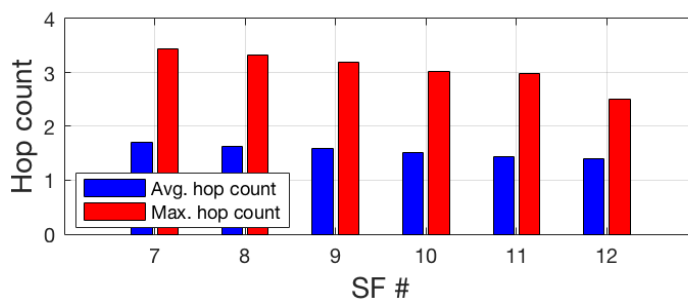
(b) Hop count in the two-building scenario
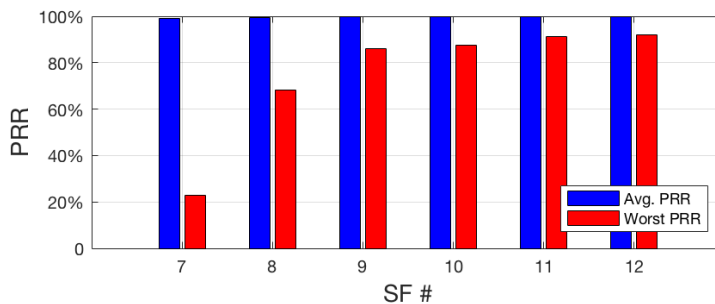
(c) PRR in the four-building scenario
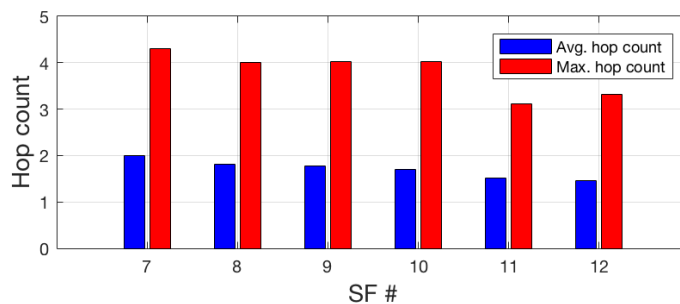
(d) Hop count in the four-building scenario

Fig. 3.11 Experimental results for two scenarios.

(a) Immunity against identical-SF interference

As seen in the simulation analysis results, Fig. 3.11 shows that the larger SF provides stronger immunity against identical-SF interference. In Fig. 3.11 (a) and (c), all SFs shows an average network PRR exceeding 99 % for both two scenarios under CT-LoRa. The results show that the performance of CT-LoRa using all SFs is still robust to destructive packet collisions. On the other hand, smaller SFs present worse network PRR as compared to the larger SFs. For SF7, PRR was approximately 80 % PRR, while for others, it was close to 90 % in the two-building experiment.

(b) Coverage of different SFs

Fig 3.11 (b) and (d) proves that even LoRa has a notable coverage range under each SF. In the indoor environment where some nodes may be considerably shielded, a multi-hop LoRa network is much more flexible and necessary to guarantee coverage. In our experiment, to cover two buildings, the maximum hop count while using SF12 was three hops and four hops for SF7, as shown in Fig. 3.11 (b). Moreover, the hop count results for both scenarios show differences in coverage between SFs, corresponding to our previous analysis results. Even the network performance is similar to others; Fig 3.11 (c) shows a 22 % and 68 % worst PRR between two nodes under SF7 and SF8, respectively, when covering four buildings. This result shows that the higher efficiency presented by the smaller SF is obtained by sacrificing the sensitivity of LoRa signal. Additionally, the use of a single SF has limitations and is inefficient to guarantee the robustness of a multi-hop CT-LoRa network.

3.3 Receiver performance under different-SF interference

In order to verify the orthogonality between different SFs, we evaluated the required minimum SIR at which LoRa still can survive different-SF interference. We first verified the orthogonality between different SFs by using the simulation platform. Additionally, we conducted a series of experiments to verify our simulation observations.
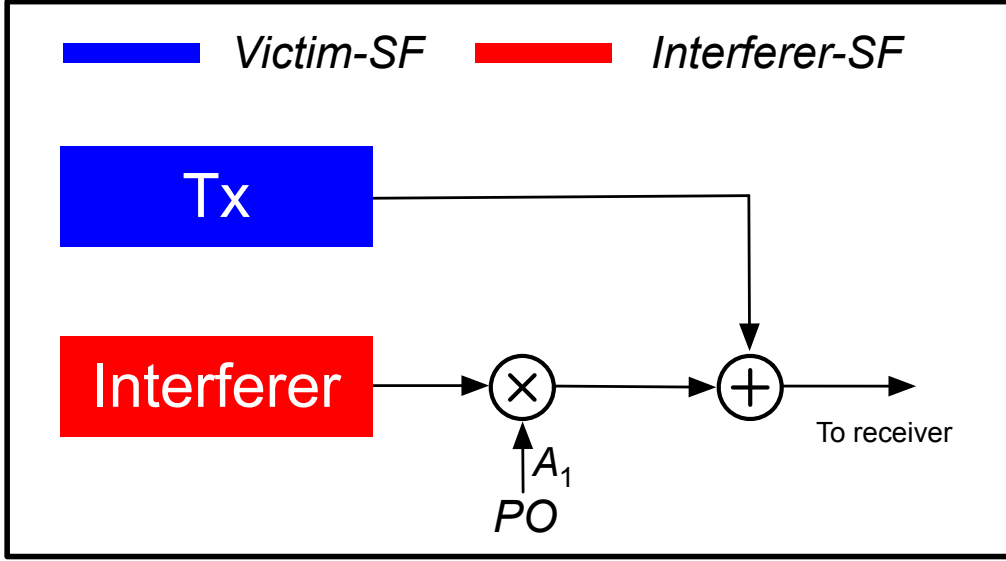
Fig. 3.12 Evaluation model of LoRa recevier facing different-SF interfrence.

3.3.1   Evaluation methodology

In this subsection, we discuss our methodology for the evaluation of the receiver performance under different-SF interference. As shown in Fig. 3.12, we considered the single hop scenario with one transmitter and receiver in the evaluation. The transmitter and receiver with the same SF are referred to as the victim. Another signal with an SF different from the transmitter is considered the interferer. We tested all possible combinations of *victim SF* and *interferer SF*.

To evaluate the mutual-immunity in front of different-SF interference, we define the metric as the required signal-to-interference ratio (SIR) when the receiver can successfully decode the packet using each SF in the evaluation. In the simulation, we fixed the stronger Tx as 0 dB without thermal noise. And we carefully change the power of interferer to find the threshold when PRR is larger than 90%. The required SIR can be represented as

$$SIR_{dB} = P_{signal,dB} - P_{noise,dB} \tag{3.9}$$

where $P_{signal,dB}$ and $P_{noise,dB}$ represents the power of transceiver and the interferer, respectively.

On the other hand, it is difficult to control the power offset precisely. In order to model the behavior of practical receivers, we conduct repeatable experiments where we inten-

tionally fixed the location of the transceiver and receiver. Then, we carefully adjust the location of the interferer and record the difference of *Received Signal Strength Indication* (RSSI) form the receiver's side. The required SIR can be calculated as

$$SIR_{dB} = RSSI_{w/ \, interfrence,dB} - RSSI_{w/o \, interfrence,dB} \tag{3.10}$$

where $RSSI_{w/ \, interfrence,dB}$ and $RSSI_{w/o \, interfrence,dB}$ is the RSSI of received signal under the scenario that the interfrence of different-SF LoRa packet exists or not exsits, respectively. Not that, we assume that the effects of environmental change are negligible during the short period of the experiment.
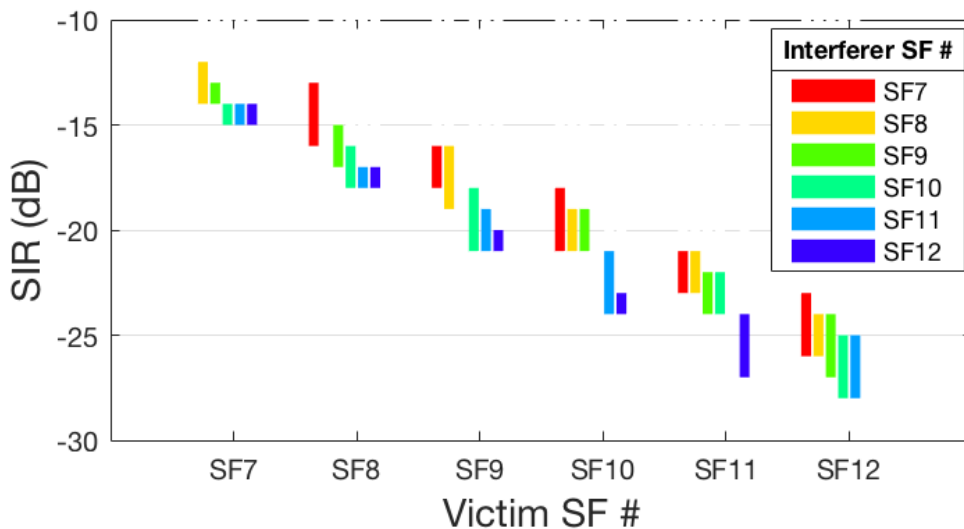
Fig. 3.13 SIR statistics of each SF with different-SF interference.

3.3.2   Simulation of orthogonality between SFs

In the simulation, we set the wanted signal as 0 dB while changing the power level of the interferer. We recorded the required SIR corresponding to 10 % PRR and 90 % PRR. The thermal noise is set zero.

We present the simulation results in Fig. 3.13. The figure shows six groups that represent the victim SF on the X-axis, and the colors listed in the legend correspond to different interferer SFs in each group. The Y-axis represents the PRR of each bar between 90 %
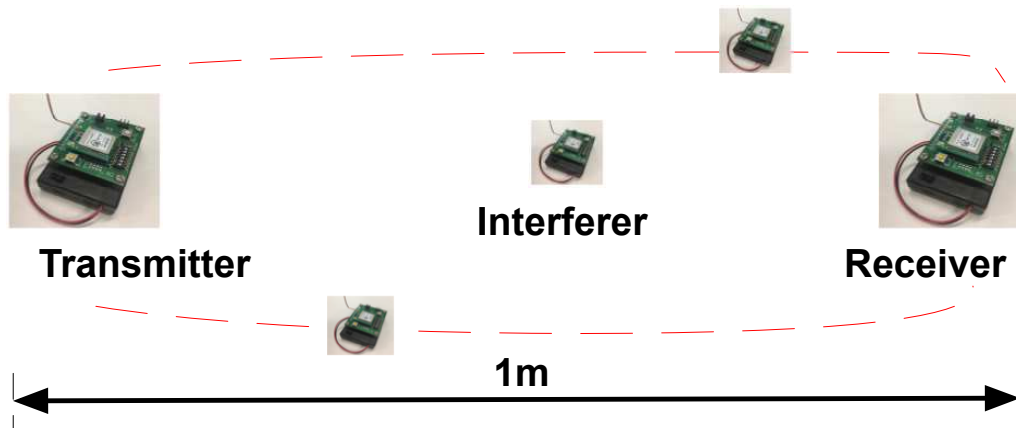
Fig. 3.14 Different-SF interference experiment setup.
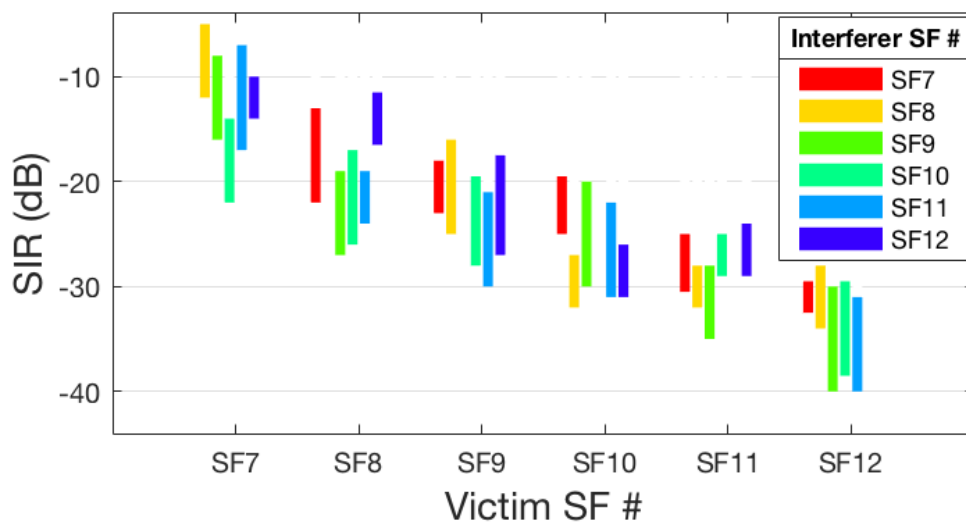
Fig. 3.15 Experiment results of different-SF interference.

and 10 %. The case in which the victim and interferer use identical SF is not considered and is not plotted in this figure.

The results show that different SFs provide different tolerances to interference as the SFs are not orthogonal. From the viewpoint of the victim, larger SFs always provide better immunity to interference than the smaller ones. On the X-axis, the results show a clearly decreasing trend as SF increases. In the bar set of SF12, the SIR is roughly -25 dB, while for SF7, it is approximately -12 dB. From the viewpoint of the interferer, in each group,

the interference with smaller SF affects the transmission to a greater extent than when using larger SF. As a given example, in the bar set of SF10, with interference with SF7, the gap of PRR changes from -17 dB to -21 dB, while the value ranges from -23 dB to -24 dB for interference with SF12.

3.3.3   Real-chip experiments of different-SF interference

To further confirm our analysis about the LoRa receiver performance under different-SF interference, we conducted real-chip experiments to determine the required minimum SIR in a real environment.

(a)   Experiment setup and procedure

We used the three LoRa modules described in the previous subsection. The experimental setup is shown in Fig. 3.14. The interferer broadcasted continuously and uninterruptedly with a specified SF to occupy the whole frequency band during the experiment period. The transmitter sent 100 packets using different SFs in one experiment period, while the receiver recorded the number of packets received successfully. The parameter settings for the experiment were identical to the ones for the simulation, unless specifically mentioned. Note that with the interference with an identical SF, the transmission always fails and dies. During the experiment, the initiator used all SFs, except the same one, for interference. Also, the experiments are conducted repeated under each parameter setting. The parameter settings are same with simulation setting if it is not specially mentioned.

Initially, we set the transmitter and the receiver at two fixed positions at a distance of 1 m from each other to determine the receiver performance under different SIRs, as shown in Fig. 3.14. By adjusting the location of the interferer manually within the area between the transceiver and receiver, we recorded the RSSI corresponding to the transmitter and the interferer in the view of the receiver. Finally, we determined the boundary value of average RSSI when PRR was slightly larger than 90 % or less than 10 %.

(b)   Results and discussions

The experimental are shown in Fig. 3.15. The trend is the same as that observed in the simulation analysis. Larger SFs always yielded better performance than smaller ones for different SF interference. We have no knowledge of the LoRa module and the kind of

PRR(%) Inter. Victim	SF7	SF8	SF9	SF10	SF11	SF12
SF7	N/A	98	100	100	100	100
SF8	100	N/A	100	100	100	100
SF9	100	97	N/A	100	100	100
SF10	100	100	100	N/A	100	100
SF11	100	98	98	98	N/A	100
SF12	100	100	100	100	100	N/A

Table 3.3 Experiment results in high SIR scenario.

PRR(%) Inter. Victim	SF7	SF8	SF9	SF10	SF11	SF12
SF7	N/A	0	99	99	99	99
SF8	0	N/A	100	100	100	100
SF9	<10	<10	N/A	100	100	100
SF10	<10	<10	100	N/A	100	100
SF11	<10	<10	99	100	N/A	100
SF12	55	100	100	100	100	N/A

Table 3.4 Experiment results in low SIR scenario.

error correcting code (ECC) chosen for LoRa decoding; we expect that the ECC might improve the receiver performance in our real-chip experiment. Specifically, the SIR values in each bar set present approximately 5 dB gain as compared to the simulation results. Furthermore, in the bar set of SF12, SIR ranges from -30 dB to -40 dB and the average SIR of bar SF7 is approximately -15 dB.

Precise control of RSSI and measurement of SIR are difficult in the practical environment. In Fig. 3.15, each bar set does not show a clear trend for different SF interference. In agreement with the simulation analysis results, the experiment results also present that the smaller SFs are much more sensitive to mutual SF interference.

To further evaluate the orthogonality between SFs, we considered two extreme experimental cases based on the setup environment. The results are shown in Table 3.3 and

Table 4.3. In the first case, the interferer is set close to the transmitter deliberately, providing a high SIR from the viewpoint of the receiver. Table 3.3 shows that the PRR when using each SF is almost 100 % with a high SIR. However, in some cases, for instance, when the transmission uses SF11 and is under interference from SF8, SF9, and SF10, packet loss occurs because of the possibility that interfering signals collide with the packets.

In another case, the interferer is set close to the receiver to ensure the power of the interfering signal is larger than that of the data packet. As shown in Tab. 4.3, when the SF value of interference exceeds eight, transmission using all SFs have good performance, achieving almost 100 % PRR. However, when the transmission uses the smallest SF7 and SF8 (shown in the first two columns) and the interference arises from SF7 to SF11, the network almost crashes with a PRR less than 10 %. On the other hand, when interferer uses SF12, the PRR becomes 55 % and 100 %, respectively, clarifying that larger SFs provide better receiver performance. Additionally, when the transmission is subjected to identical-SF interference, the results are not applicable (N/A) in both two tables.

3.4   Summary

In this chapter, we present a complete evaluation of LoRa receiver performance under identical-SFs interference and the orthogonality of the LoRa signal using different SFs.

With power offset larger than 3 dB, LoRa receiver exhibited good performance under packet collision with identical SFs where the capture effect occurs and it is highly possible for LoRa receiver to decode the packets successfully. Performance with smaller SFs was more sensitive to power offset and interference while the lager SF has stronger immunity facing the identical-SF interference. Also, the energy spreading effect in both viewpoint of frequency-domain and time-domain increase the possibility of the survival of LoRa technology when conduction concurrent transmission. By conducting real-chip experiments, we present the CT-LoRa performance on each SF in practical. The experimental result shows consistent results with the simulation which confirm our analysis and further prove the necessity of deploy mesh topology to ensure the indoor coverage.

On the other hand, to evaluate the feasibility of utilizing multiple access dimension in LoRa provided by different SFs, we evaluated the orthogonality between mutual SFs, owing to which different SIRs are required to transmit the packets successfully using different

SFs. With the Error correcting code, the real-chip experiments show even better results as compared to that from the simulation.

Chapter 4

SF Allocation for Parallel CT-LoRa
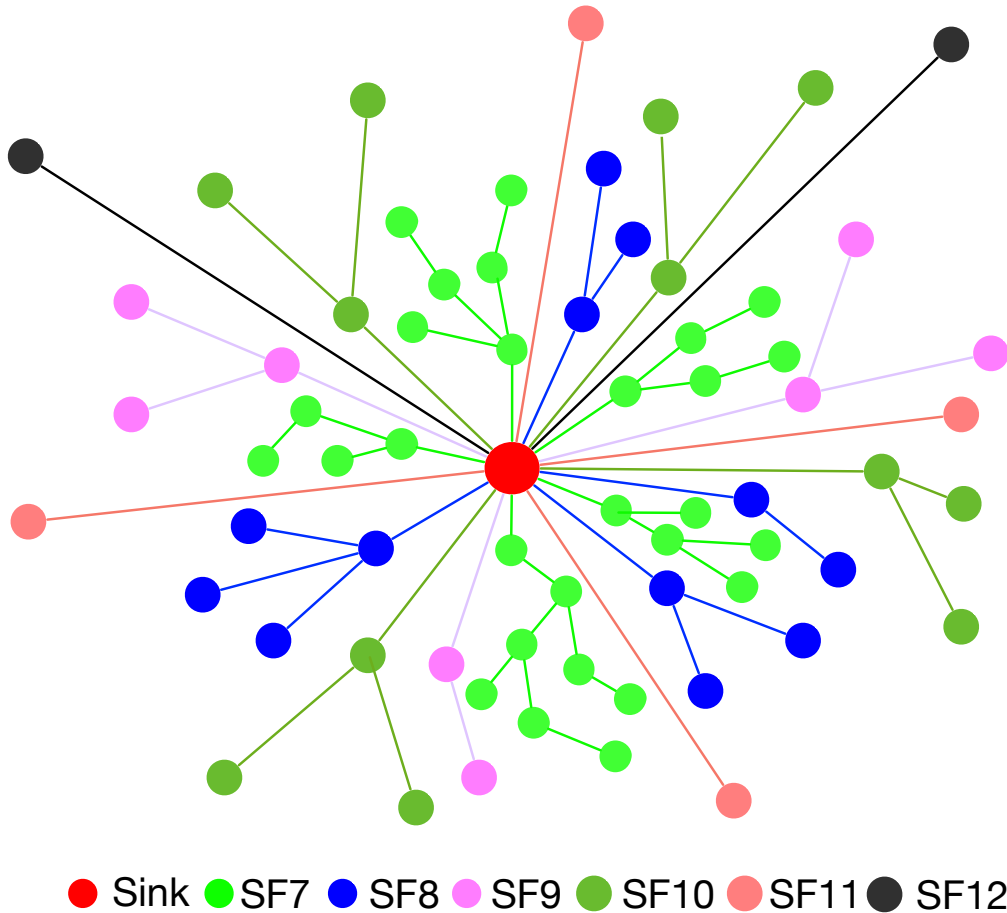
Fig. 4.1 Conceptual topology of SF allocation with multiple subnets.

In this chapter, we introduce how to further enhance the performance of CT-LoRa network by leveraging multiple Spreading factors (SFs), where the SF not only serves the purpose of airtime-range tradeoff (similar to the MCS index in LTE or WiFi) but also provides an additional dimension for multiple access protocols such as CDMA. Specifically, the network performance can be significantly enhanced by allocating different SFs to the nodes and by transmitting packets in parallel. Firstly, we overview the concept of performance improvement of realizing parallel transmission in CT-LoRa. Then, we formulate the SF allocation problem and analysis the complexity of the problem. To address the problem, we proposed a tree-based SF clustering algorithm (TSCA) for realizing parallel transmission with a balanced SF allocation in a multi-hop CT-LoRa network and we discuss the details of TSCA in the sequential subsection. Finally, the efficiency of conducting parallel transmission by adopting TSCA is evaluated by using simulations and real-chip

experiments.
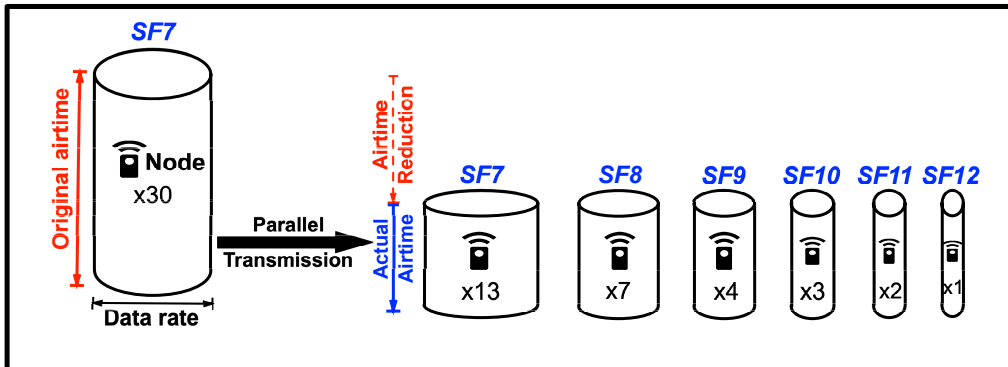
Fig. 4.2 Example of well-balanced parallel transmission.

4.1   Overview of parallel CT-LoRa

In a single-SF CT-LoRa network, the nodes directly perform Device-to-Device (D2D) communications to relay the packets to the sink nodes by fast flooding. Adopting a mesh topology not only allows us to extend the coverage by multiple relays, but more importantly provides the possibility to enhance network efficiency [38, 52]. However, researchers [27, 53–55] also suggested that a performance enhancement such as this would require a proper allocation algorithm regarding the most important parameter in LoRa namely the SFs.

In contrast to a single-hop network, SF allocation in a multi-hop LoRa network not only affects the network connectivity but also influences the flexibility in terms of the coverage, airtime, and latency. Specifically, the airtime of each SF in a single-hop network is determined only by the number of nodes and its data rate [37]. However, in a multihop LoRa network, the airtime of each subnet depends on the particular topology and this dependency has not yet been considered in previous research.

4.1.1   airtime improvement by parallel transmission

The technique overview of LoRa and LoRaWAN reports that [30], in LoRaWAN, the network airtime is determined by the number of SFs, data rate of each SF, the packet length, and also how frequently the data will be transmitted by the nodes. Also, many
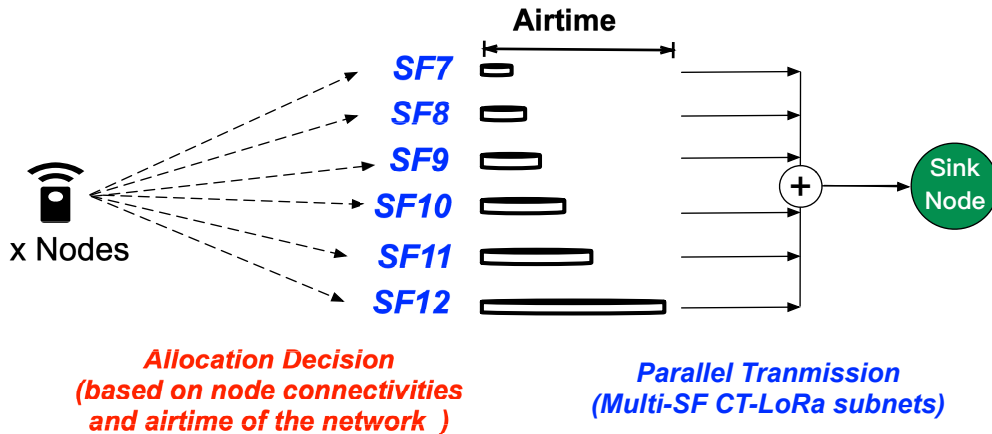
Fig. 4.3 Illustration of decision making of SF allocation.

following studies discussed the different approaches to further improving the airtime of LoRWAN [28, 37, 56]. However, the definition of airtime is still ambiguous and may not be suitable for the scenario of multi-hop LoRa networks. To clarify the so-called airtime of the network, we define the network airtime of mesh LoRa networks noted by the following definition.

Definition 4.1.1. During a given transmission period with optimal scheduling of the nodes which are synchronized ideally, the airtime of a mesh LoRa network is quantified as the theoretical minimal airtime of the entire network, where the maximum quantity of data can be received by the base station simultaneously by utilizing multi-rate SF channels.

Based on this definition, the approach we followed to realize parallel transmissions in a multi-hop CT-LoRa network, was to develop a conceptual structure of SF allocation, shown in Fig. 4.1, where all nodes in the network need to be allocated to several subnets and each subnet uses a separated SF. Nodes marked with the same color use one specific SF to transmit packets. In each subnet, the connectivity of each of the nodes is well confirmed and enables the node to communicate with the sink node using the shortest path and the number of nodes is well balanced according to the airtime of each subnet. In addition, it was necessary to take the following considerations into account:

（1） The connectivity of each subnet would have to be guaranteed after SF allocation.
（2） The traffic load of each subnet would have to remain balanced because of the asymmetry of SFs (the data rate of SF7 is 18.6 times the data rate of SF12).

（3） The hop count of the multi-hop network would have to be minimized to decrease the airtime of each transmission which is equivalent to the reciprocal of parallel transmission.

Finally, as comparded to all nodes using the fastest SF7 shown in Fig 4.2, a proper SF allocation method which exploits the orthogonality between different SFs enables packet transmission in parallel with multiple SFs to become feasible. To allow such parallel transmissions, our considerations are: 1) ensuring the connectivity of all subnets; 2) offloading the traffic according to the number of nodes, data rates, and network topologies of each subnet; and 3) shortening the airtime of each subnet by reducing the hop count.

4.1.2   The complexity of SF allocation problem

We formulate the SF problem and analysis the complexity of the problem in this subsection. To realize the well-balanced parallel transmission by SF allocation, the SF allocation can be defined as a decision-making problem as shown in Fig. 4.3. By allocating all nodes into different-SF disjoint subnets based on the connectivities and the airtime of the network, each node allocation gives a *YES* or *No* answer corresponding to a specific SF subnet. And, the final decision can minimize the airtime of the subnets which have a mesh topology.

To ease of understanding, we clarify the definition and list the notations in Table 4.1. As described in the aforementioned section, the theoretical achievable airtime of LoRa network requires an optimal data transmission scheduling in which the nodes are synchronized ideally. In a TDMA-based CT flooding scenario, as shown in Fig 4.4, the maximum airtime of each subnet is the largest data rates to transmit a quantity of data generated the nodes. To simplify the analysis, we assume the amount of data load generated by M_s nodes is a determined value of α and needs to be transmitted in the fixed transmission period. Note that, when the generated data is not equalized, α is a variable correlated to differnet nodes and the discussion of different types of data collection is out of the scoop of this study. Thus, the total amount of generated data can be represented as $\alpha \times M_s$. For a specific subnet SF_s, the data rate is R_s. In every single flooding, all nodes join the packet relaying initiated by node n_i with a maximum $H_{max,s}$ times relays where $H_{max,s}$ is the maximum hop count of the subnet. Then, the airtime of CT flooding can be written as $R_s/H_{max,s}$. Also, the maximum airtime of a subnet can be defined as, to transmit a

TDMA-Based data collection in CT-LoRa
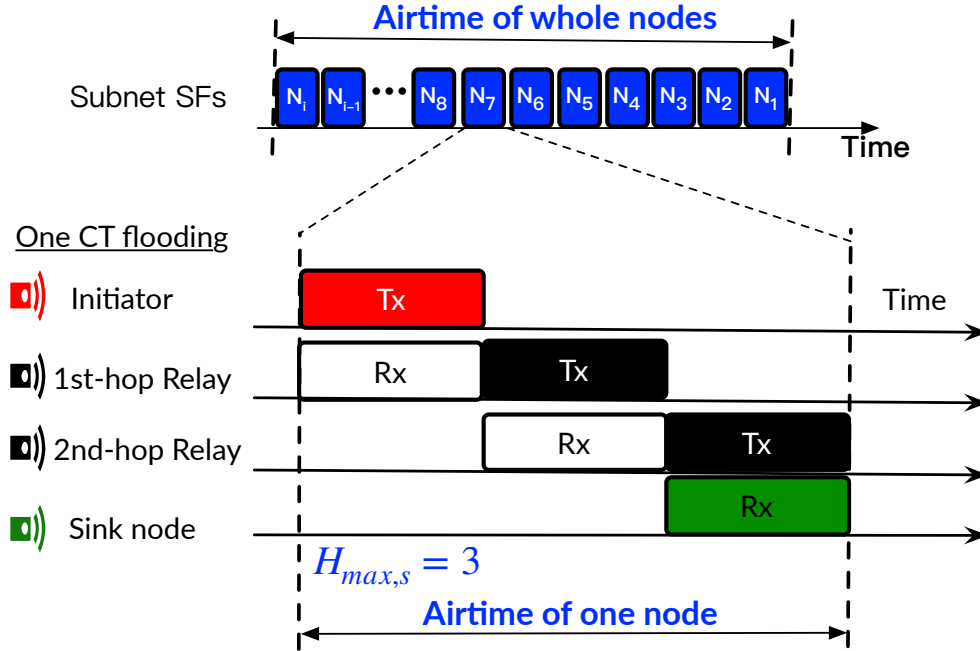
Fig. 4.4 TDMA-based data collection in CT-LoRa subnets.

quantity of data generated by the nodes, the required transmission period with a TDMA-based CT flooding scheduling and described as $T_s = (\alpha \times M_s \times H_{max,s})/R_s$. In front of the amount of data generated by all nodes, our goal is offloading the data traffic into multiple subnets with different SFs and the SF allocation can make the data traffic in each sunset keep a good balance of an optimal parallel transmission. The objective is to minimize the maximum airtime of the subnets which has a maximum value as compared to all subnets. Then, the overall problem can be formulated as

Table 4.1 List of Notations.

Notation	Definition
S	Index of Spreading Factors, $S \in \{7 \sim 12\}$
T_s	Airtime of the subnet SF_s
M	Number of nodes in total
M_s	Number of nodes in subnet SFs
α	Generated data size in each node within a given period
A_s	Set of nodes exist in subnet SF_s
$H_{max,s}$	The maximum hop count of subnet SFs
R_s	Data rate of SF_s
n_i	The node of index i, $1 < i < M$
$\Psi_s(n_i)$	Set of one-hop neighbor nodes of node n_i with SF_s
$\Theta_{h,s}$	Set of nodes of height h of the subnet with SF_s
$\Pi_i(n_j)$	Set of parent nodes of node n_i with SF_s
$\Phi_i(n_j)$	Set of child nodes of node n_i with SF_s
BW	Bandwidth

$$\text{Minimize} \quad \max_{s \in \{7 \sim 12\}} T_s \tag{4.1}$$

$$\text{subject to} \quad T_s = \frac{R_s}{\alpha \times M_s \times H_{max,s}} \tag{4.2}$$

$$R_s = SF_s \times \frac{BW}{2^{SF_s}} \tag{4.3}$$

$$\sum_{s=7}^{12} M_s = M \tag{4.4}$$

$$\bigcap_{s=7}^{12} A_s = \varnothing \tag{4.5}$$

$$\Theta_s(n_i) \cap A_s \neq \varnothing, \quad \forall n_i \in A_s, \quad 1 < i < M \tag{4.6}$$

Check: Eq. (4.1) with Eq. (4.2), Eq. (4.3), Eq. (4.4), Eq. (4.5) and Eq. (4.6). More specifically, Eq. (4.3) is the calculation of the data rate of SF_s. Eq. (4.4) describes that all nodes need to be allocated to a specific SF. Eq. (4.5) shows the uniqueness of SF allocation where a node cannot be assigned to more than one SF simultaneously. And,

Eq. (4.6) ensures the full connectivities of the network where a node can noly be allowed to assign to the subnets that at least have one parent node to communicate with.

To analysis the optimization of SF allocation problem, we discuss the complexity of the problem which is similar to the well-known partition problem in computer science [57]. Different from the two sets of partition which is usually considered as the easiest NP-hard problem [58], the SF allocation has SF_s sets and, without prior information, there are exponential possible partitions $(SF_s)^M$ with M nodes in total.

In the lecture presented by MIT open course [59], the lecturer shows that the 2-set partition problem is a weakly NP-complete problem while 4-Partition is a strongly NP-complete problem. By following the method, the SF allocation problem can be also proven as NP-complete by reducing the partition problem. For the NP-complete, SF allocation problem can not be solved in a polynomial time that can always provide the optimal solution of the subset sum. From the viewpoint of CT-LoRa, we propose a tree-based SF allocation algorithm for the SF allocation in practice and examine the effectiveness of the algorithm in the next subsection.

4.2   Tree-based SF clustering algorithm (TSCA)

4.2.1   Design concepts of SF allocation in CT-LoRa

In this section, we introduce the design concept of SF allocation in a mesh LoRa network. We describe the overall considerations in section (a) and discuss each of these considerations in the following subsections.

(a)   Overall considerations

To achieve performance improvement by parallel transmission, we aim to separate one full-connected network into several disjointed subnets with different SFs. Specifically, each node is allocated with a single SF and the nodes using the same SF forms a multi-hop sub-network that operates independently with the others. Under such a scenario, three aspects need to take into consideration to minimize the airtime of the whole network: 1) The traffic needs to be offloaded to each subnet in a balanced way to prevent any subnet becoming the bottleneck; 2) Each subnet needs to be well-connected without any

unreachable nodes; 3) With a proper SF allocation, the diameter (network height) of each subnet can also potentially be reduced so that the airtime is further improved. In the following subsections, we discuss how the proposed TSCA achieve the aforementioned three aspects.

(b) Balancing the airtime with each SF

To protect a subnet from being allocated with too many nodes, we determine the number of nodes in each subnet according to their airtime. The number of nodes in each subnet M_i can be given by

$$M_i = M \times \frac{T_i}{\sum\limits_{j=7}^{12} T_j}, \ i \in \{7 \sim 12\}, \tag{4.7}$$

where M is the total number of nodes in the network and T_i is the airtime of a subnet with SF i.

One straightforward way to estimate the airtime is to use the data rate of each SF, namely

$$T_i' = R_i, \tag{4.8}$$

where R_i is the data rate of the subnet with SF i. This estimation has been adopted to the single-hop scenario, such as LoRaWAN [37]. Therefore, in this work, we refer to this method as the Single-hop Estimation (SHE).

Different from adopting SHE in a multi-hop LoRa network, the airtime of each subnet can maintain a more acceptable balance when taking the height of the subnet into consideration. Accordingly, we propose to use the Maximum-hop Estimation (MHE) to estimate the airtime of each subnet where C_i can be written as

$$T_i'' = \frac{R_i}{H_{max,i}}, \tag{4.9}$$

and $H_{max,i}$ is the maximum hop count of the subnet with SF i and determines the worst case of data transmission. Note that, Eq. (4.8) is a subset of Eq. (4.9) where the value of $H_{max,i}$ is always one. Contrary to SHE, MHE estimates each $H_{max,i}$ by allocating a specific SF i to all nodes, respectively. Moreover, the algorithm conducts the SF allocation

iteratively where MHE will be executed in the first iterative cycle. In subsequent cycles, the algorithm calculates the resultant $H_{max,i}$ based on the previous cycle to further balancing each C_i.

Using Eq. (4.9), we adopt a constraint rule to limit each M_i and rewrite Eq. (4.7) as

$$M_i < M \times \frac{R_i}{H_{max,i} \times \sum_{j=7}^{12} R_j/H_{max,j}}, \ i \in \{7 \sim 12\}. \tag{4.10}$$

To simplify the analysis, we assume a common data collection scenario where each node generates an equal amount of data periodically and those data need to be transmitted to the sink node within a given period of time. When inserting too many nodes into a subnet, the airtime of finishing the transmission in this subnet will be longer than the others and becomes the bottleneck of data collection. .

Therefore, in this work, the proposed algorithm aims to minimize the maximum airtime of each subnet. After SF allocation, the transmission time of each node is a product of the airtime of the data transmitted per bit and the actual $H_{max,i}$. Then, the definition of the airtime of each subnet can be rewritten as

$$T_i = M_i \times \frac{H_{max,i}}{R_i}, \ i \in \{7 \sim 12\}, \tag{4.11}$$

where T_i is the airtime of the subnet using SF i. Accordingly, to evaluate the performance of conducting parallel transmission, the airtime of the entire network is defined as

$$T = \max_{i \in \{7 \sim 12\}} (\frac{1}{T_i}), \tag{4.12}$$

where T is the maximum airtime between the subnets. Furthermore, during the node insertion and extraction process, we also calculate the dynamic T_i and assign the extracted node to the emptiest subnet with the MAT to maintain the balance among the subnets.

(c)   Ensuring connectivity

Another important aspect of SF allocation is to ensure the connectivity of each subnet. For every process that determines a node needs to be extracted from the original network and then inserted into a subnet with a larger SF, the algorithm guarantees connectivity. More specifically, we assume that, initially, the network is well connected with SF7. The node extraction process checks whether all child nodes of the current determining node have at least one remaining parent node after the current one is extracted from the original network. After the node is earmarked for extraction from the subnet with SF7, the insertion process would also need to ensure that the extracted node has an available parent node in a spanning subnet with a larger SF with which to communicate, otherwise, the node would remain with SF7 to ensure connectivity.

(d)   Reducing the height of subnets

In order to minimize T, the algorithm is necessary to reduce each $H_{max,i}$ which is strongly affected by the order in which nodes are extracted and inserted during SF allocation. An effective order of extraction allows $H_{max,7}$ to be reduced whereas an effective order of insertion ensures that the height of the other subnets remains small.

When reducing $H_{max,7}$, it is beneficial to extract more nodes from the bottom layer of the tree. Further, it is preferable to insert the extracted node by starting from the upper layer to prevent the height from becoming excessive. Consequently, we use the BBFS algorithm to determine the order of extraction from SF7 and the conventional TBFS algorithm to ensure the extracted node is inserted into a sub-tree with a larger SF, which is the shortest path to the root node. Moreover, the subnets identified for accepting the extracted nodes need to be prioritized.

4.2.2   Framework of TSCA

This subsection describes the framework of the proposed TSCA. The flowchart of the proposed TSCA is shown in Fig. 4.5. After initialization, the algorithm changes the iterative conditions according to the airtime of each SF in every iterative cycle. The termination condition manages the node extraction, connectivity check, and node insertion processes in each iterative step. The algorithm outputs the topology of each subnet after all nodes are allocated to a specific SF. The corresponding pseudocode is presented in Algorithm 1. As shown in the figure, the main parts are as follows:
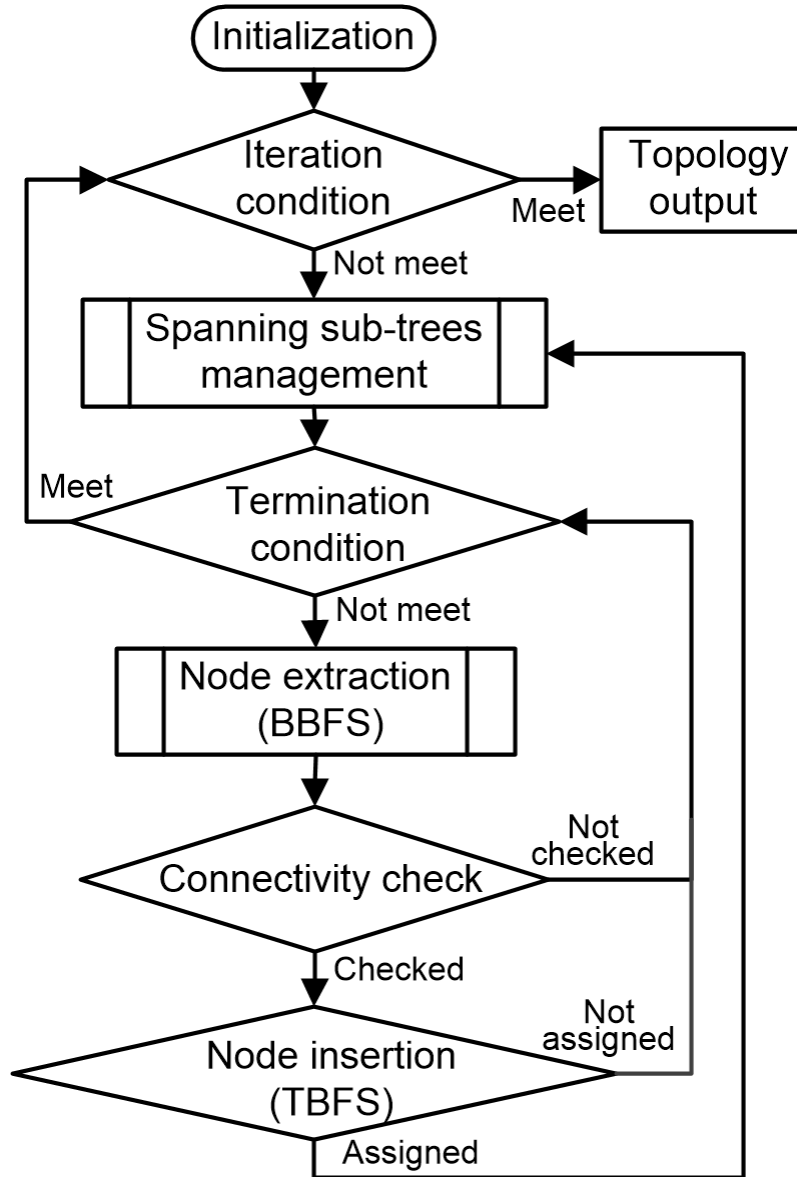
Fig. 4.5 Flowchart showing the scheme of the TSCA.

(a)   Initialization

After the algorithm builds a well-connected network with SF7 in the initial phase, the root node retains the one-hop knowledge for all relay nodes and records their hop counts of all the existing shortest paths from each relay node to the root node. We define the topology of a sub-tree with SF i as a set $\Theta_{h,i}$, where h is the hop count to the sink node. For every node n_j, the parent set and child set are $\Pi_s(n_j)$ and $\Phi_s(n_j)$, respectively.

Algorithm 1 TSCA: Tree-based SF Clustering Algorithm (To be continued)

Input: $\Theta_{h,7}$; $\Theta_{h,s \neq 7}$ $\begin{cases} \{root\} & h = 1 \\ \emptyset & h > 1 \end{cases}$; $\Pi_i(n_j)$ and $\Phi_i(n_j)$ set of every node n_j.

Output: $\Theta_{h,s}$

1: **START**

2: // Constraint rule changed with iterations

3: **while** Iteration condition not met **do**

4:     **while** Termination condition not met **do**

5:         $\{n_j\} \leftarrow$ NODEEXTRACT$(\Theta_{h,7})$

6:         **for** $j = 1 : end$ **do**

7:             $Checked \leftarrow$ CONCHECK(Θ_7, n_j)

8:             **if** Checked **then**

9:                 $Agn \leftarrow$ NODEASSIGN$(\Theta_{h,8\sim12}, n_j)$

10:                **if** Assigned **then**

11:                    //Spanning Sub-tree Management

12:                    $\Theta_{h,i} \leftarrow$ TREEMGN$(\Theta_{h,i}, n_j, Agn)$

13:                    $break$;

14: **return** $\Theta_{h,i}$

The simulation assumes the root node is able to communicate with its first-hop relay nodes by using all SFs in parallel. Moreover, according to the coverage of each SF, the algorithm builds the topologies under all SFs where all nodes use a specific SF from 7 to 12 in one subnet.

(b)   Iterative condition

The TSCA is designed to estimate the airtime of each subnet by using the constraint rule (Eq. 4.7). In step 3 of Algorithm 1, the iterative condition is set to limit the number of nodes in each sub-tree according to the estimation of MHE, which is the maximum hop count of each subnet we calculated from the initialization phase in the first iterative cycle. After the first cycle, the algorithm calculates the current topology information and then renews the iterative condition according to the actual hop count of each sub-tree.

Every iterative cycle is terminated when the number of nodes in each subnet meets the iterative condition or when this cycle has no more nodes that can actually be extracted

from the original network after the algorithm searched all nodes with SF7. If no additional nodes are extracted in the next iterative cycle as compared to the previous one, the simulation is terminated as the final iterative cycle.

(c)   Termination condition:

The termination condition is determined according to every iterative condition. In step 4 of Algorithm 1, the termination condition takes charge of every node assignment process in an iterative step, which includes a successful assignment, the connectivity check being false, and the insertion being false. When the constraint is met in this iterative cycle or the algorithm searches all nodes in the original network with SF7, the termination condition terminates the iteration and outputs the topology information to renew the next iterative condition.

(d)   Spanning sub-trees management:

We show the function for the management of spanning sub-trees in step 22 of Algorithm 1. This function generates five empty sub-trees rooted at the sink node in the initial phase, where $\Theta_{h,i}$ is $\emptyset$ when $i \neq 7$ and $h > 1$. For every successful node assignment, the management process deletes node n_j from sub-tree $\Theta_{h,7}$ and spans the sub-tree $\Theta_{h,Agn}$ into which node n_j is inserted.

(e)   Node extraction process:

In order to determine the order in which to extract the nodes from the original subnet, the BBFS first searches the nodes in the bottom layer where h is equal to $H_{max,i}$ and then proceeds to a higher layer as shown in step 1. After an identified node is assigned to a larger SF successfully, BBFS runs the search from the bottom layer again in an attempt to extract additional nodes from the lower layers. After the algorithm searches all nodes with SF7, the algorithm terminates the current iteration.

An example of SF allocation is shown in Fig. 4.6, where we illustrate the conceptual process of node extraction that consists of two rounds in one iterative cycle. The subnet of SF8 and SF9 is two nodes and one node, respectively. The small numbers beneath the nodes in the sub-tree using SF7 indicate the order of extraction. The red relay node is an example of a failed extraction because of the connectivity check whereas the blue node indicates successful SF allocation to join a subnet with a larger SF. In the first round,

BBFS determines the extraction order from 1 to 6 and checks the connectivity from node F. The first extracted node is node C, which can communicate with the root node by using SF8. Then, the algorithm starts to search the extraction sequence from the bottom layer again in round 2. Because node C is assigned to SF8, node F can communicate with the root node in two hops by using SF8. The algorithm continues to search for a possible node that can be assigned to SF9 until the end of this round.

On the other hand, we compare BBFS with the Breadth-First-Searching algorithm (BFS) [48, 49] and the Depth-First-Searching algorithm (DFS) which show different strategies to perform the node extraction process. As a reference, we present the pseudocode of the BFS and DFS functions in Algorithm 3. In the case of BFS, the algorithm starts to traverse the tree at the sink node and checks all of the neighboring nodes at the current height. After all nodes are explored, the algorithm moves on to the nodes at the next height. Using Fig. 4.6 as an example, the visiting order is A, B, C, D, E, F where node A and node E can be extracted to subnet SF8. However, because of the connectivity problem, the extracting node F cannot be assigned to subnet SF9 even though SF9 is not filled to maximum allowed number of nodes. As opposed to BFS, DFS traverses the tree from the sink node and explores each branch of the tree as far as possible by recursively calling the pre-order function. In Fig. 4.6, the visiting order is A, B, C, F, D, E when using DFS and the extracted nodes are A, C, F, E in the first round. Node A and node C are inserted into subnet SF8 and node F still faces a connectivity problem with regard to being inserted into SF9.
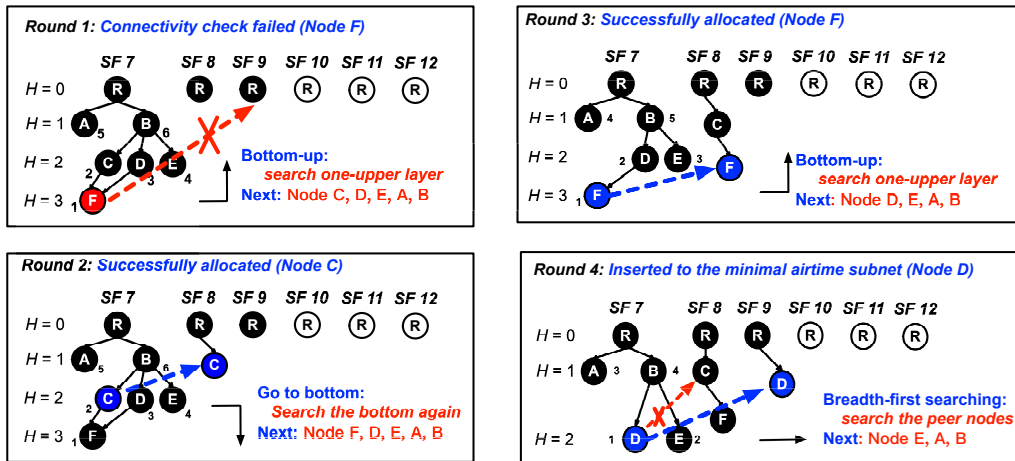

Fig. 4.6 Conceptual procedure of the TSCA with six child nodes in total.

(f)   Node insertion process:

The node insertion function, in step 12 of Algorithm 1, adopts TBFS to search all sub-trees for which SF is larger than 7 and the search proceeds from the top layer to the bottom layer until the first possible parent node n'_x is found for node n_i. The algorithm records all possible SF s to insert the node. The algorithm maintains the height of the spanning sub-trees at the lowest possible level by selecting a sub-tree into which to insert the nodes based on the computation of MAT.

Moreover, we compared the insertion priorities with the first-available channel algorithm [49], in which we present the LFS and SFS as different strategies of the node insertion process. After a node was extracted from subnet SF7, LFS chooses the first-available largest SF and SFS chooses that of the smallest SF to assign the node.

(g)   Connectivity check

For any child node n_x of extracted node n_j, the connectivity check confirms whether more than one parent node with SF 7 exists. Then the algorithm sets the flag *Checked* to 1 if all child nodes have at least one other parent node with which to communicate.

Lastly, we present an example of SF allocation with 200 nodes in Fig. 4.7. As shown in the figure, The sink node is marked with red color. Nodes marked with the same color are allocated to one subnet with a specific SF. First, the nodes are allocated to different SFs in a balanced manner - about half of the nodes are distributed to SF7, half of the remainder to SF8, and so forth. Second, the nodes near the sink node are allocated to smaller SFs, whereas those far away from the sink are assigned to larger SFs. This allocation helps to reduce the hop count of packet relays. The nodes located close to the sink node are assigned a smaller SF and the nodes farther from the sink node are assigned a larger SF. The nodes in the subnets with different SFs are well balanced with a declining trend of the number of nodes using a larger SF. In addition, the nodes using a larger SF stay further from the sink node, which maintains the hop count of each subnet small.

4.2.3   Time complexity of TSCA

In this subsection, we discuss the time complexity of proposed TSCA. Particularly, we describe the time complexity of advance preparation, and discuss the run-time complexity of the algorithm, respectively.
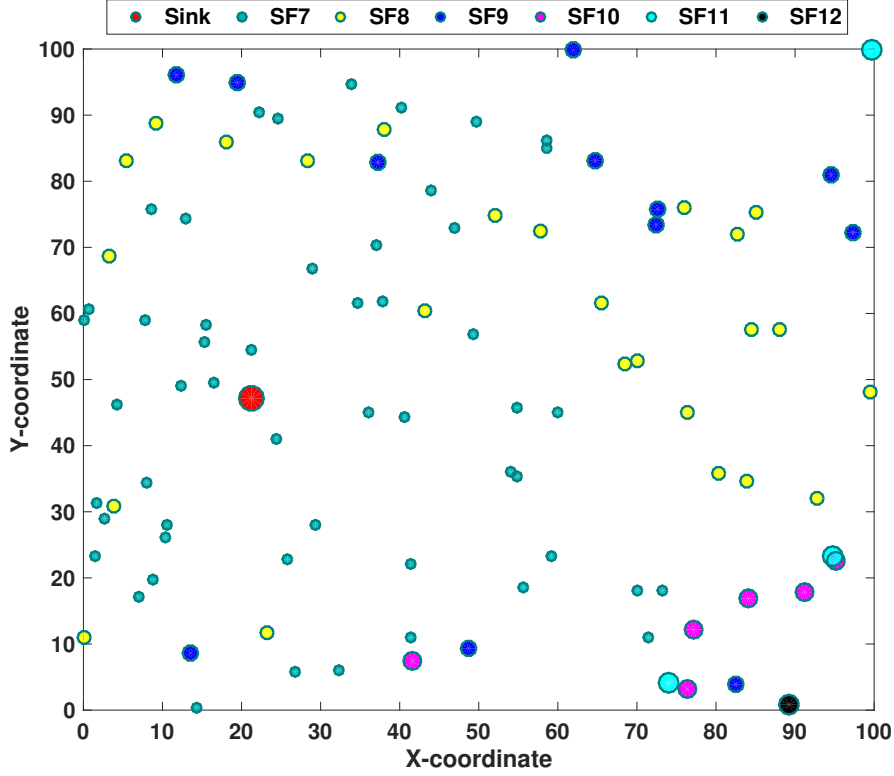
Fig. 4.7 Example of spatial distribution with 200 nodes in 2-D space.

(a)   Advance preparation

To conduct SF allocation in CT-LoRa, the prior information of TSCA is the one-hop neighbor link between any pair of the nodes with all SFs. Given a graph $G(V, E)$, where V is the set of nodes and E represents the one-hop link between any two nodes, the link connectivity can be described as if $e_s(n_i, n_j) \in E$, then $n_j \in \Theta_s(n_i)$, for $\forall n_i \in V, \forall n_j \in V$. Note that, in practice, the link connectivity can be evaluated as the Packet Reception Rate (PRR) with an average of k attempts between every two nodes.

Using node-by-node collecting, the time complexity is $\mathcal{O}(s \cdot m^2)$ with m number of nodes and s number of channels. In this study, we collect collectivity information by using CT flooding. All nodes in the network play the role of initiator in turns and pass through all SFs. Within one flooding, the initiator collects the one-hop link information with all other nodes. The time complexity of the collecting is $\mathcal{O}(s \cdot m)$.

(b)   Run-time complexity of TSCA

To construct a well-connected tree which is the shortest path to sink node by using SF7, the time complexity of the quicksort algorithm is $\mathcal{O}(m \log m)$. In TSCA, an intermediate stage is there are x number of nodes in subnet SF7 and $m - x$ number of nodes are assigned to other subnets using other nodes. Note that, we consider the complexity of confirming the link connectivities for extracting or inserting a specific node is consider as $\mathcal{O}(1)$. Then, the worst case of each extracting and insertion need m times of searching and the time complexity of the allocation is $\mathcal{O}(m)$. After a node is assigned to a larger SF subnet successfully, the algorithm starts to search the subtree from the bottom side again, where the number of bottom-up cycles is $\mathcal{O}(m)$ in a worst case and $\mathcal{O}(1)$ in a best case, respectively. In total, the time complexity of TSCA is $\mathcal{O}(m^2)$ with the worst case.

4.3   Simulation evaluations

In this section, we evaluate the performance of the proposed TSCA by simulations. We describe the simulation setup in section 4.3.1. Before presenting the detail, we first show that the TSCA can achieve a more optimal balance as compared to other approaches in section 4.3.2.In each subplot, the x-axis shows the two airtime estimation methods, MHE and SHE, respectively, and the y-axis shows the airtime of a subnet with a value normalized to that of all nodes using only SF7. For each set of bars, the subnets with different SFs are distinguished by different colors and patching objects according to the legend. Moreover, in each subplot, we identify the maximum airtime of subnets with an arrow pointing to the particular subnet. In section (a), we further discuss the performance of different airtime estimation methods, tree-searching algorithms for the node extraction process, and assignment order for the node insertion process. We also discuss the effect of the number of iterative cycles.

4.3.1   Simulation methodology

In the simulation, we assume the nodes are uniformly and randomly distributed on a rectangular space related to the length (L units) and width (W units) of its sides. We also assume that one unit is equal to the coverage of SF7 and increasing SF by 1 extends the coverage range by a factor of $\sqrt{2}$ based on the free space model. We assume that

(a) DFS-LFS   (b) DFS-SFS   (c) DFS-MAT

(d) BFS-LFS   (e) BFS-SFS   (f) BFS-MAT

(g) BBFS-LFS   (h) BBFS-SFS   (i) BBFS-MAT
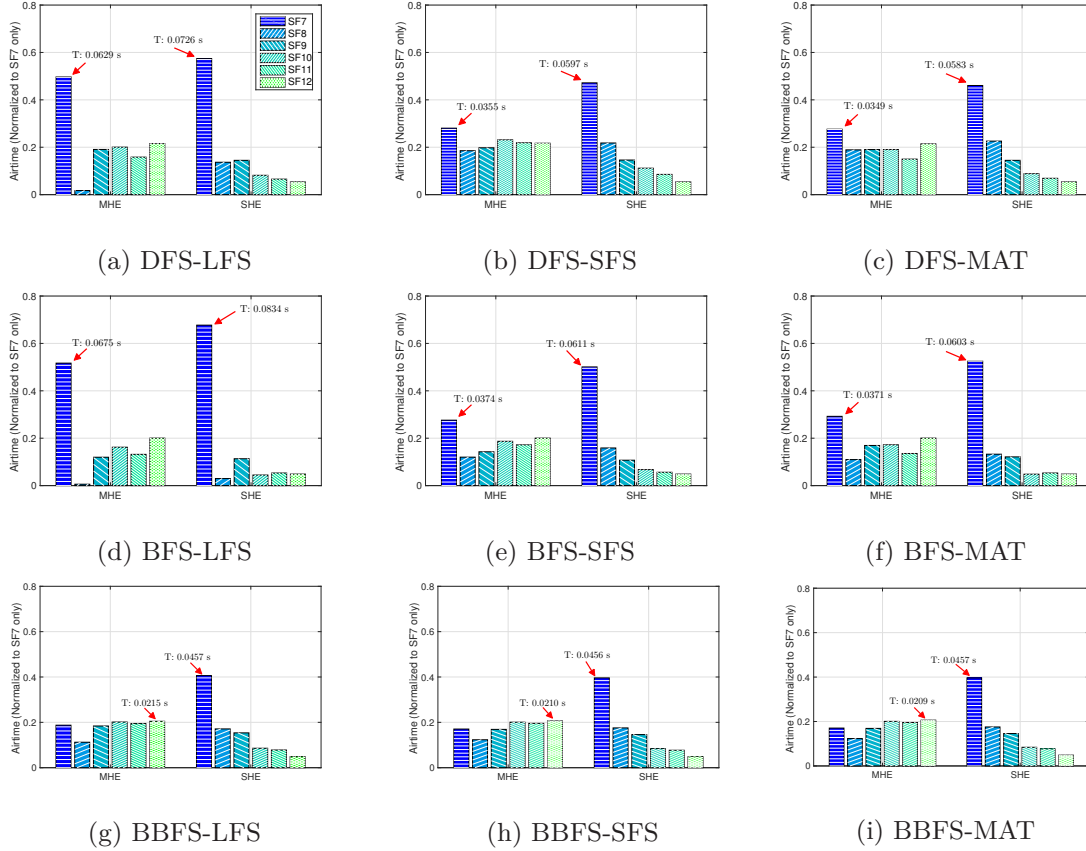
Fig. 4.8 Balance of the airtime of each subnet with the different comparisons.

connectivity between two nodes exists only if one node is within the coverage of another node and all nodes are well connected by using SF7.

We simulate two scenarios. The first involves a square space (L =5, W=5) as the normal scenario. We additionally consider another scenario with long length and narrow width (L =25, W=1), which creates a linear topology with a large hop count. The number of nodes is increased from 20 to 200. For each number of nodes and each topology, we run the simulations up to 10,000 times. According to previous research [12], the coverage of SF7 is roughly 1 km in an urban area and the simulated scenario covers areas of approximately 25 km^2.

4.3.2   Evaluation of the degree of balance between each SF

In this subsection, we describe the evaluation of the balance of each SF by using TSCA. In Fig. 4.8, we compare the different strategies of SF allocation by simulating each T_i with

SF i. The rate at which the airtime decreases is shown by normalizing each T_i to that of the network using only SF7. In an effective balanced scenario between the subnets, the airtime of all subnets should be as close as possible such that the airtime of the network becomes the smallest by adopting parallel transmission. The number of nodes in the network can be assumed to be 100 in the following discussions unless otherwise stated.

In each subplot in the figure, the results show that MHE outperforms SHE, with MHE capable of offloading more traffic into the larger SFs and balancing the airtime of each subnet. As compared to each column of the plot, the proposed BBFS, which is designed to extract more nodes from the bottom side of the original network, decreases the airtime of subnet SF7 most effectively compared to BFS and DFS. As compared to each row of the plot, the proposed MAT minimizes the airtime of the network as opposed to when using LFS and SFS. Fig. 4.8 (a) suggests the allocation loses the balance of subnet SF8 where the airtime is largely less than that of the other subnets. Furthermore, in Fig 4.8 (d), the large amount of airtime for subnet SF7 indicates the failure to insert nodes into subnets with larger SFs. As shown in Fig. 4.8 (i), the airtime of the network reduces to roughly 20% of that of using SF7 only by running TSCA.

4.3.3   Evaluation of the effect of each strategy of TSCA

(a)   airtime estimation methods

In this subsection, we further discuss the effect of the SF allocation based on each strategy of TSCA. To make the comparison fair, the proposed MHE, BBFS, and MAT are set as default when one of the three have been chosen for comparison with other approaches and the other two are not mentioned.

The effect of airtime estimation methods is investigated by evaluating the extent to which MHE can outperform SHE. Fig. 4.9 shows the estimated number and the actual allocated number of nodes in each subnet by using two methods, respectively. Subplot (a) scenario in which nodes are distributed in a $5 \times 5 \ m^2$ square space, and subplot (b) scenario in which nodes are distributed in a $1 \times 25 \ m^2$ rectangular space. The x-axis shows the subnets of each SF and the y-axis the percentage of nodes distributed. The asterisk and plus signs represent the estimated number of nodes of each subnet by using MHE and SHE, respectively. The blue and green bars are the actual number of nodes assigned to each subnet after the first iterative cycle, respectively.

The results in Fig. 6 (a) show that the allocated number of nodes can achieve the estimated airtime of each subnet by using both MHE and SHE in the area defined as a square. MHE outperforms SHE by extracting more nodes from SF7 and allows the insertion of more nodes into subnets with larger SFs in a balanced way.

On the other hand, in the long and narrow rectangular area, the results in Fig. 6 (b) suggest that MHE and SHE did not achieve the estimated airtime of the subnets with smaller SFs (SF8, SF9). Specifically, the limited coverage prevents the insertion of nodes that are difficult to insert into subnets because of their connectivity. Because of this, MHE can allocate additional airtime to the larger SFs and still outperforms SHE with more nodes inserted to the subnets.

(b)   Order of node extraction:

To demonstrate the importance of determining the node extraction order, we compare the performance of different tree searching algorithms including BBFS, BFS, and DFS. Our evaluation shows that BBFS can effectively lower the tree height (maximum hop count) of subnet SF7 as compared to the other two methods.

The results in Fig. 4.10 show the probability of the hop count decreasing and the averaged decrease in the hop counts by adopting different tree searching algorithms.Subplot (a) square space distribution and subpolt (b) rectangular space distribution. The x-axis represents the different searching algorithms. The y-axis on the left shows the percentage reduction of the distribution of the hop count where the legend distinguishes the number whereby the hop count was decreased for each bar. The y-axis on the right indicates the ratio of the average decreased hop count as compared to the original maximum hop count of the network. The square and rectangular spaces achieve an average maximum hop count of 7 and 24 hops by using SF7, respectively. Fig. 4.10 (a) shows that, in the square space, BBFS outperforms BFS and DFS with the most simulation rounds that can decrease the number of hops of a subnet by a larger percentage.

An average 84 % of simulation rounds cannot reduce the height of subnet when using BFS, and the maximum hop count is only decreased one hop with 50 % of simulation rounds when using DFS. The result shows that the use of BBFS can reduce the height of the original network by an average of 41 % in the square space.

Fig. 4.10 (b) shows, in the rectangular space, the searching algorithms undergo a performance degradation with no significant decrease in the hop counts. In this scenario,
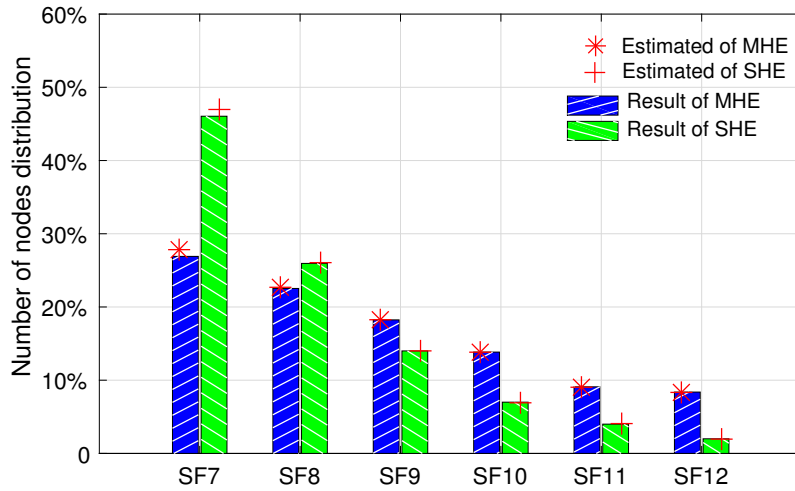
(a) Square space distribution
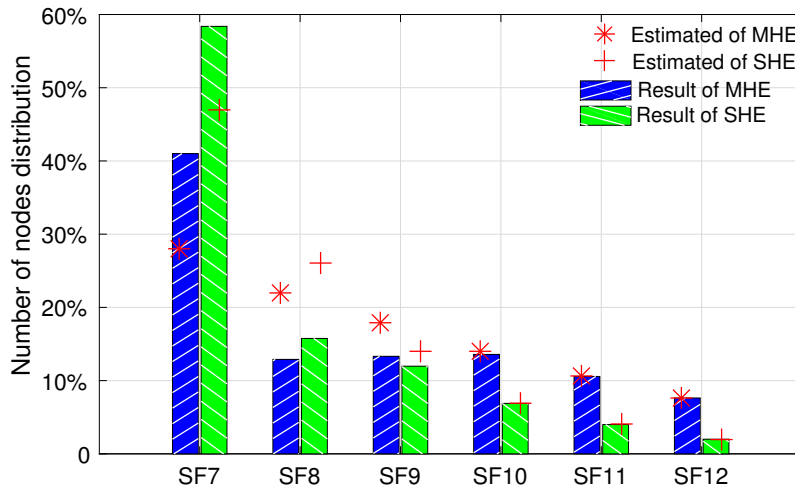
(b) Rectangular space distribution

Fig. 4.9 Number of nodes distributed for each subnet.

BFS and DFS can barely reduce the height. In this space, the performance of the pro-
posed BBFS is weaker as compared to the square space and the result shows that the tree
height can be reduced by an average of 12 % when the maximum hop count is significantly
increased.

Further, we evaluate the airtime of the network by increasing the number of nodes

in the square space. Fig. 4.11 shows parallel transmission to be an effective approach as compared to the network without parallel transmission. Nodes are distributed in the same square space. The x-axis shows the number of nodes in the network. The y-axis on the left represents the airtime of the network. The red dashed line shows the airtime in the absence of parallel transmission. The blue lines with different markers show different extraction orders by using different searching algorithms. Note that MHE and MAT were adopted and the results are based on the first iterative cycle.

The result demonstrates that BBFS is more effective to decrease the airtime of the network as compared to the other two algorithms.

(c)   Order of node insertion:

We also evaluate the performance of using different strategies to determine the node insertion order including MAT, LFS, and SFS. In Fig. 4.8 (a-f), the results show, when adopting BFS and DFS, that MAT performs the best by achieving the lowest airtime of the network. Moreover, Fig. 4.8 (g-i) shows, when BBFS is adopted, the performance of different insertion strategies is similar. The airtime of each subnet is more balanced and the difference in the airtime required by the network is small when MHE and BBFS are adopted.

(d)   Iterative cycles:

We evaluated the effect of balancing the airtime of the network by running additional iterative cycles. The ratio of the airtime of the network between parallel transmission and the network using only SF7 is shown. The comparison is between conducting SF allocation without iteration and that of conducting SF allocation iteratively by using MHE and SHE.

The results in Fig 4.12 show that running the allocation iteratively can further decrease the airtime of the network. The red and blue lines represent the results of SHE and MHE, respectively. The triangular and square markers represent the results obtained without iteration and those obtained iteratively, respectively. The x-axis is the number of nodes and the y-axis shows the ratio of airtime of the network as compared to all nodes using SF7. The extraction and insertion were performed with BBFS and MAT. When using SHE, the airtime of the network decreased largely by running iterative cycles. When using MHE, the performance of running more iterative cycles is only improved with a low-density scenario where the number of nodes is small.
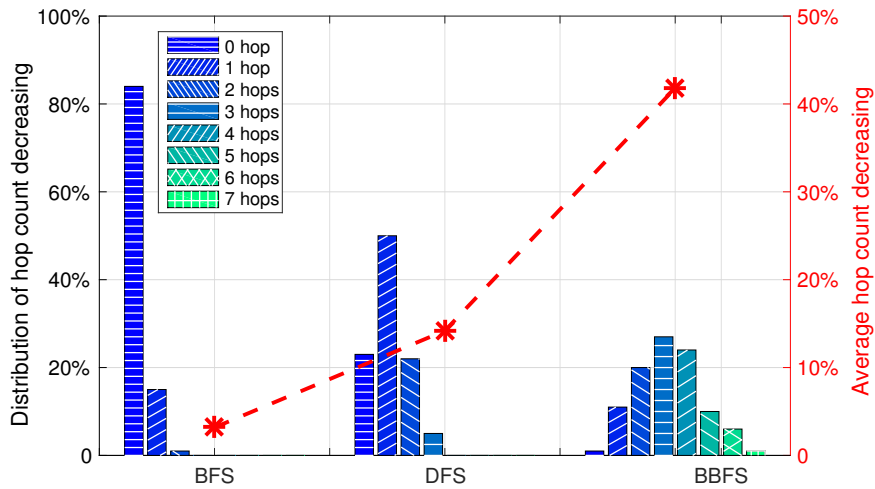
(a) Square space distribution
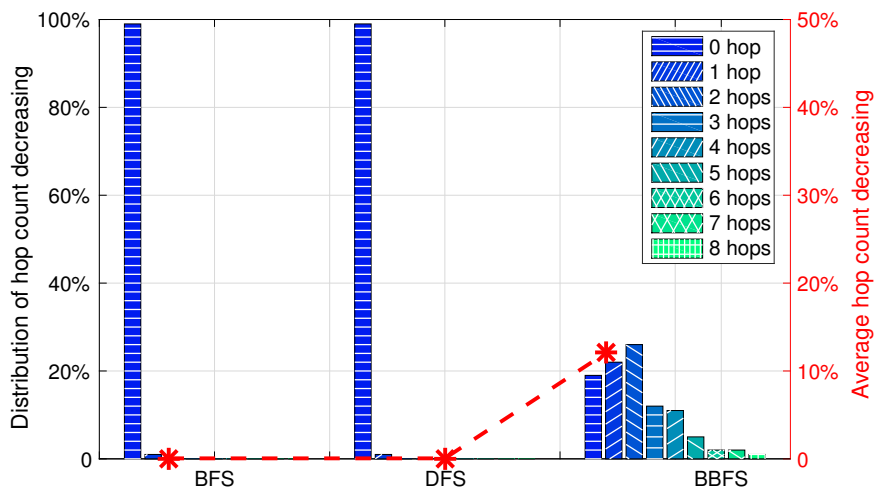
(b) Rectangular space distribution

Fig. 4.10 Decrease in the hop count of the original network.

On the other hand, in order to evaluate the rate of convergence of using MHE and SHE, we show the necessary number of iterative cycles. As shown in Table 4.2, the number of nodes is 50 in a low-density scenario and 100 in a high-density scenario. The results show that, in both low-density and high-density scenarios, SHE needs a larger number of iterative cycles than MHE. Moreover, the number of iterative cycles increases with an
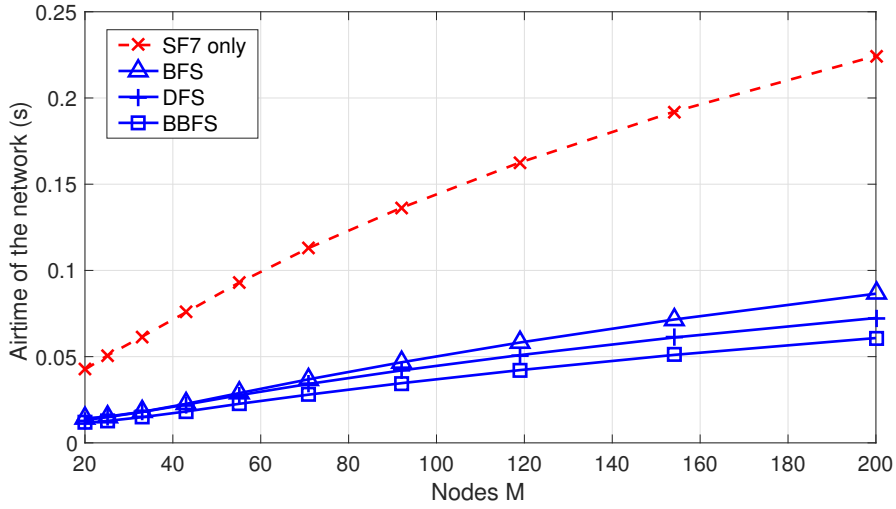
Fig. 4.11 Decrease in the airtime of the network.

increase in the number of nodes.

To analyze the overall performance of the iteration, we discuss the performance loss when using SHE as compared to MHE. The one reason is the difficulty of balancing the airtime among the subnets. In the low-density scenario, a slight difference in the number of nodes in the subnets is not expected to change the calculated airtime of the largest SFs (SF11, SF12). However, the rounding errors of the number of nodes in the subnets vary the airtime of the network considerably whereas MHE allows more nodes to be inserted into the largest SFs.

Moreover, although BBFS decreased the height of subnet SF7 substantially, the nodes extracted from the bottom of the subnet have a lower possibility to be inserted into the subnet with smaller SFs (SF8, SF9) when considering the coverage. This complicates the achievement of the calculated airtime of the subnets (SF8, SF9) as shown in Fig. 4.9. On the other hand, in the high-density scenario, SHE outperforms MHE slightly. This is because the increased connectivity allows the use of SHE to more effectively balance the subnets by running additional iterative cycles.

4.4   Experimental evaluations

This section describes the feasibility of parallel transmission in a mesh LoRa network by using multiple SFs. The efficiency of the proposed TSCA was further evaluated by
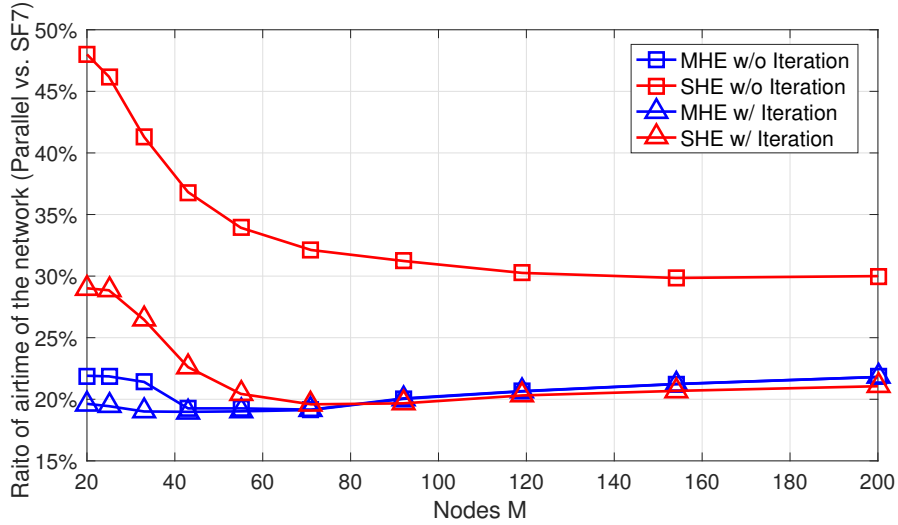
Fig. 4.12   Effect of using iteration.

Table 4.2   Necessary number of iterative cycles.

	Low density (M=50)		High density (M=100)	
	SHE	MHE	SHE	MHE
Probability of 1 cycle	0	41.1%	0	8.1%
Probability of 2 cycles	95.6%	57.6%	22.4%	71.2%
Probability of 3 cycles	4.4%	1.3%	70.4%	19.5%
Probability of 4 cycles	0	0	7.2%	1.2%
Average iterative cycles	2.04	1.60	2.85	2.14

additionally conducting real-chip experiments in a practical environment.

4.4.1   Experimental scenario and setup

In the evaluation, we used 36 LoRa RF modules fitted with a Semtech SX1276 and STM32L0 microprocessor to cover two main buildings on the campus. Because the LoRa end-point devices cannot normally communicate with multiple SFs simultaneously, six nodes were assigned to act as the sink node with one specific SF and remain close to each other to emulate the parallel transceiving function of LoRa gateway. We show the distribution of all the nodes deployed in the experiment in Fig. 4.13. Most of the nodes are located in Building 1 and three nodes are deployed in Building 2 with three other nodes
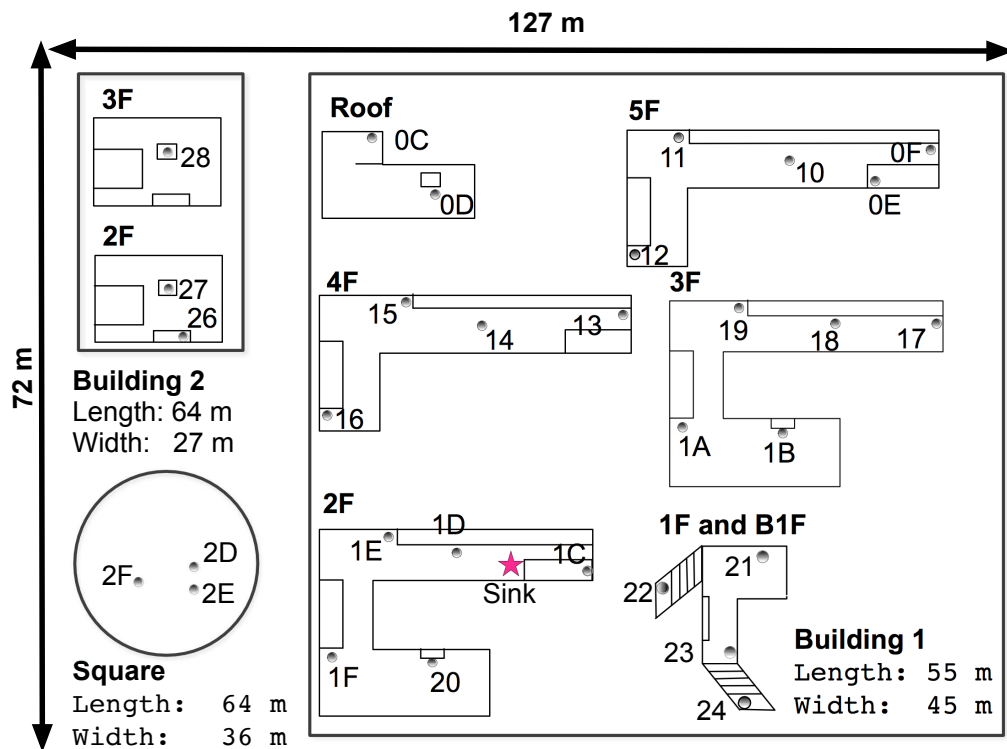
Fig. 4.13 Node deployment in the experiment.

Table 4.3 Parameter space of the experiment.

Parameter	Values
Spreading factor	7 to 12
Tx power	13 dBm
Center frequency	920.6 MHz
Bandwidth	500 kHz
Code rate	4 / 5
Packet length	8 bytes

located in the square. Sufficient indoor coverage is ensured by thoroughly shielding the nodes within a lidless iron box or a cupboard.

4.4.2 Results and discussions

The preparation for SF allocation entailed collecting the connectivity information between any pair of nodes. The specific setup and parameter space are listed in Table 4.3. Fig. 4.14 shows the topology of all nodes using one SF where each link exists with a Packet Reception Rate (PRR) of more than 90 % and each path is the shortest path to the sink node. Fig. 4.14 (a) and (b) present the cases for SF7 and SF12, respectively. As compared to SF7, even though the maximum hop count decreased when using SF12, the connectivity of the nodes increases where a node is able to communicate with additional nodes within one hop. Accordingly, this enabled us to gather the one-hop knowledge of each node for the connectivity check. The proposed algorithm is executed off-line which needs to collect the connectivity information from a static topology. A variation of topology (e.g., mobile nodes) may lead to the necessity of regular update on the connectivity information which consumes the time and energy in practice. The development of a method to conduct fast topology collection in practice is beyond the scope of this paper.

The experiment was designed to evaluate whether parallel transmissions degenerate the overall performance of the network by analyzing the airtime and the PRR. Based on different SF allocation methods, we compare different searching algorithms after using MHE and MAT and execute the algorithm iteratively. Based on the results in Table 4.4, we can compute that BBFS deceases the network airtime by 62.8 % as compared to the network using only SF7. On the other hand, BFS and DFS reduce the airtime by 51.3 % and 60 %, respectively. The result shows that, by conducting parallel transmission in a mesh LoRa network, the achievable airtime of the network is improved $1/(1-0.628) = 2.69$ times as compared to all nodes using single SF7.

In addition, we collected the PRR of the subnets for each SF by adopting a concurrent transmission protocol for data collection in LoRa. Fig. 4.15 shows the PRR of the TSCA as compared with other approaches. The x-axis represents the respective subnets using a specific SF and the y-axis shows the PRR calculated for each subnet. The blue solid lines show the mean PRR and the red dashed lines show the minimal PRR. The results show that the mean PRR of each subnetwork is approximately 90 % when the TSCA is used. The use of multiple SFs to achieve parallel transmission did not result in extensive interference nor did it cause the performance of the entire network to degenerate. Moreover, the
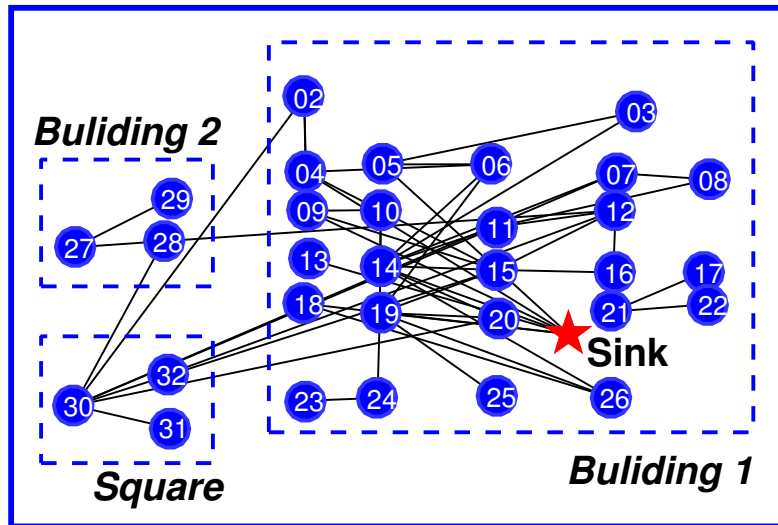
(a) SF7
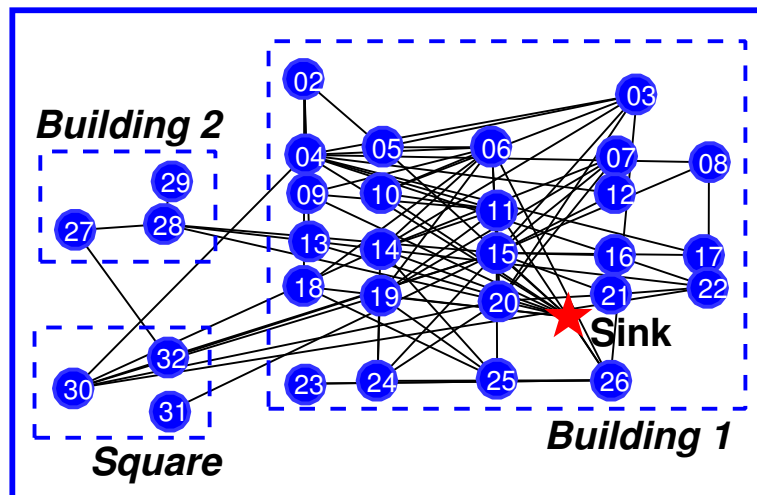
(b) SF12

Fig. 4.14 Topology of the network when using (a) SF7 and (b) SF12, respectively.

largest SF (SF11, SF12) shows the strongest interference resilience whereas SF7 is the most affected by collision.

Table 4.4 Experimental results of SF allocation.

		BBFS	DFS	BFS	Only SF7
SF7	M_7	13	14	17	30
	$H_{max,7}$	6	6	6	7
SF8	M_8	7	4	4	0
	$H_{max,8}$	3	2	2	0
SF9	M_9	4	5	3	0
	$H_{max,9}$	2	3	3	0
SF10	M_{10}	3	3	3	0
	$H_{max,10}$	2	2	2	0
SF11	M_{11}	2	2	2	0
	$H_{max,11}$	2	2	2	0
SF12	M_{12}	1	2	1	0
	$H_{max,12}$	1	2	1	0
Maximum airtime (T)		0.0143	0.0154	0.0187	0.0384
Airtime reduction ratio		62.8 %	60.0 %	51.3 %	N/A
airtime enhancement		2.69	2.50	2.05	N/A

4.5   Summary

In this chapter, we introduce the parallel transmission in a multi-hop CT-LoRa network by exploiting the orthogonality of multiple SFs. We first formulate the SF problem and then analysis the complexity of the problem. Furthermore, we demonstrated that the construction of a more efficient multi-hop LoRa network needs to take SF allocation into account as a matter of priority. Our approach was to develop a tree-based SF clustering algorithm (TSCA) to assign the nodes to several subnets. The algorithm was designed to ensure the connectivity of each subnet, after which the airtime of subnets is balanced by conducting SF airtime estimation with the consideration of the number of nodes, data rates, and the hop count of subnets. The proposed TSCA also uses a bottom-up breadth-first searching algorithm (BBFS) to determine the order in which to extract the nodes from the original network, which uses SF7. We additionally aimed to insert the extracted nodes such that the airtime of the particular subnet was minimized to ensure that the airtime between sub-trees remained balanced. The evaluation confirmed a large performance
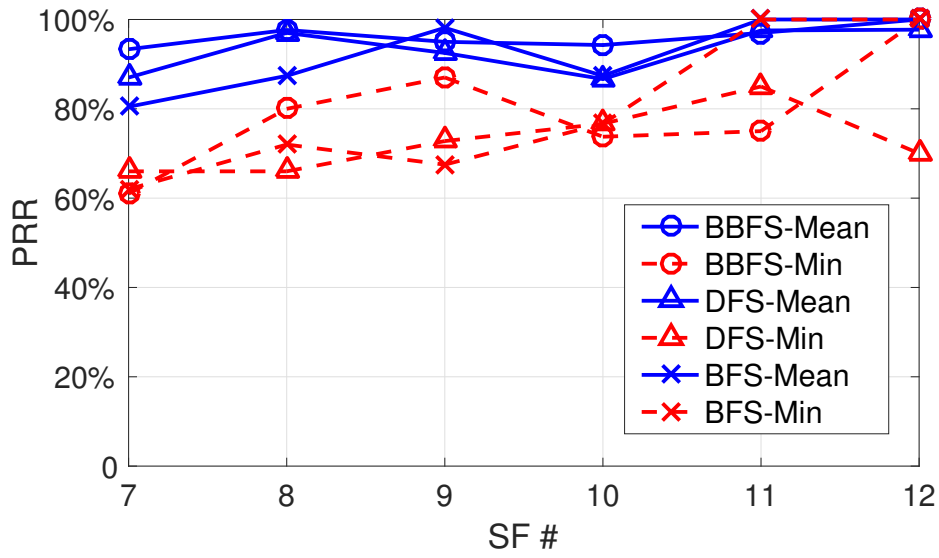
Fig. 4.15 Experimental results for the comparison of different SF allocation methods.

improvement as compared to the SF allocation in a single-hop LoRaWAN network and the tree-based multi-channel assignment approaches in WSN.

Algorithm 2 TSCA Tree-based SF Clustering Algorithm (Continued)

Input: $\Theta_{h,7}$; $\Theta_{h,s\neq 7}$ $\begin{cases} \{root\} & h = 1 \\ \emptyset & h > 1 \end{cases}$; $\Pi_i(n_j)$ and $\Phi_i(n_j)$ set of every node n_j.

Output: $\Theta_{h,s}$

  1: **function** BBFS: NODEEXTRACT($\Theta_{h,7}$)

  2:      // BBFS (default), bottom-up

  3:      **for** $h = H_{max,7}\ : 2$ **do**

  4:         **for** $\forall n_j \in \Theta_{h,7}$ **do**

  5:            $\{n_j\} \leftarrow n_j$

  6:      **return** $\{n_j\}$

  7: **function** CONCHECK($\Theta_{h,7}, n_j$)

  8:      $Checked = 0$

  9:      **if** $(\forall n'_x \in \Phi_7(n_j), n_j\ \subset\ \Pi_7(n'_x))$ **then**

10:         $Checked = 1$

11:      **return** $Checked$

12: **function** NODEASSIGN($\Theta_{h,8\sim 12}, n_j$)

13:      $Agn = 0$

14:      **for** $i = 8\ : 12$ **do**

15:         // TBFS, from top to bottom

16:         **for** $h = 1\ : H_{max,i}$ **do**

17:            **if** $\exists n'_x \subset \Theta_{h,s}, n'_x\ \subset \Pi_i(n_j)$ **then**

18:               $\{i\} \leftarrow i$

19:      // MAT (default), subnet i with the minimal airtime,

20:      $i \leftarrow \min(T_i), i \subset \{i\}$

21:      **return** $Agn = i$

22: **function** TREEMGN($\Theta_{h,s}, n_j, Agn$)

23:      **if** Assigned **then**

24:         $\Theta_{h,Agn} \leftarrow n_j$

25:         $\Theta_{h,7} = \Theta_{h,7} - n_i$

26:      **return** $\Theta_{h,s}$

27: **END**

Algorithm 3 Overriding the Node Extraction Function

Input: $\Theta_{h,7}$;

Output: $\{n_j\}$

 1: **START**

 2: // Overriding the function to 1)BBFS, 2)BFS, 3) DFS

 3: $\{n_j\} \leftarrow$ NODEEXTRACT$(\Theta_{h,7})$

 4: **END**

 5: **function** BFS: NODEEXTRACT$(\Theta_{h,7})$

 6:     // BFS: Breadth-first-searching

 7:     **for** $h = 2 : H_{max,7}$ **do**

 8:         **for** $\forall n_j \in \Theta_{h,7}$ **do**

 9:             $n_j.visited = ture$

10:             $\{n_j\} \leftarrow n_j$

11:     **return** $\{n_j\}$

12: **function** DFS: NODEEXTRACT$(\Theta_{h,7})$

13:     // DFS: Depth-first-searching

14:     init()\{

15:     **for** $h = 2 : H_{max,7}$ **do**

16:         **for** $\forall n_j \in \Theta_{h,7}$ **do**

17:             $n_j.visited = false$

18:             **for** $\forall n_j \in \Theta_{h,7}$ **do**

19:                 DFS$(\Theta_{h,7}, n_j)$ \}

20:     DFS() \{

21:     $n_j.visited = ture$

22:     **for** $\forall n_x \subset \Phi_s(n_i)$ **do**

23:         **if** $n_x.visited == false$ **then**

24:             DFS$(\Theta_{h,7}, n_x)$ \}

25:     **return** $\{n_j\} \leftarrow \{n_j.visited\}$

Chapter 5

Conclusions and Future Works

5.1   Conclusions

In this thesis, we have been striving to further extend the coverage and improve the capacity of LoRa network. To solve the coverage limation problem, we propose to conduct a highly efficient mesh LoRa network by leveraging concurrent transmission (CT) flooding. To further improve the efficiency of mesh CT-LoRa, we propose a spreading-factor-based network cluster algorithm by adopting the multiple access dimension provided multiple almost orthogonal Spreading Factors (SFs) which are the most important factors of LoRa technology. More specifically, we summary our study as follows:

To achieve the goal of constructing an efficient mesh network by leveraging CT, we first analyze the characteristics of LoRa technology and CT protocol from the viewpoint of physical layer, respectively. Next, we verified LoRa receiver performance under CT behavior with each specific SF where we do a full sweep of the well-known effects of same-SF interference (including PO, TO, CFO) which is deterministic in our simulation evaluation. The evaluation shows, with sufficient power offset, CT-LoRa exhibited good performance under packet collision with identical SFs due to the frequency-domain energy spreading effects. Under the identical condition, larger SFs lead to better performance under same-SF interference while performance with smaller SFs was more sensitive to power offset and interference. Also, in practical scenarios, LoRa on each SF can highly possibly benefit from the multi-hop CT flooding as shown in our experimental evaluation.

On the other hand, to evaluate the feasibility of utilizing multiple SFs as a new dimension for multiple access excepting frequency domain and time domain, we have evaluated LoRa receiver performance under the interference with different SFs (Different-SF interference) to verify the orthogonality between each other in which different SIRs are required to transmit the packets successfully using different SFs. Evaluation results show that SFs are not fully orthogonal which leads that the required signal-to-interference ratio (SIR) of using different SFs is different in LoRa. From simulations and real-chip experiments, we confirms although the LoRa receiver has a tolerance in front of co-technology interference, the receiver performance is different as compared to that of using different SF. More specifically, LoRa receiver using the smaller SFs will take a highly possibility affected by the interference with larger SFs, while the receiver using larger SFs show stronger immunity and also have few effects on LoRa receiver performance using smaller SFs.

To further improve the efficiency of CT-LoRa flooding and fully utilizing the multiple access dimension provided by multiple SFs, we show that a more efficient parallel CT-LoRa network can be utilized with a proper SF allocation method.

First, we formulate the SF allocation problem of mesh LoRa network and we analyze the complexity of the optimization problem which is NP-complete. To address SF allocation problem, we proposed a tree-based SF clustering algorithm (TSCA) for realizing parallel CT-LoRa network where we consider a proper SF allocation to balance the airtime of the network with multiple subnets. Specifically, TSCA is designed for fully ensuring the connectivity of the network where all nodes keep using the fastest data rate (SF7) in the original network initially. By constructing the well-connected subnet SF7, the algorithm attempts to remove the nodes to the subnets with larger SFs node-by-node to ensure the connectivity of each subnet while keeping the airtime of subnets in a balanced way. More specifically, to conduct the node allocation into different subnets, a constraint rule is performed to limit the number of nodes in each subtree with the calculation of its capacity which not only includes the data rate but also the mesh topology of each sub-tree. In the initial stage, we first estimate the capacity of each SF by using the maximum achievable hop count on each sub-tree in the condition of all nodes are inserted into the sub-tree. Further, the algorithm is designed such that the constraint rule will update with more iterative cycles when the real hop count of the current topology is determined based on the current topology of each subnet. On the other hand, we consider to reduce the maximum hop count of each sub-tree to further decrease the airtime of the network. In the node extraction process, TSCA adopts the proposed BBFS to try to remove the nodes with the largest hop count in subnet SF7 as much as possible. In the node insertion process, we use TBFS to guarantee the shortest path of the larger SF subnet. Moreover, the removed nodes are inserted into a sub-tree that will have minimal airtime after the insertion to maintain the capacity balance between the sub-trees. Finally, we confirm the algorithm by the evaluation of simulations and experiments. The results show a large performance improvement as compared to the SF allocation as compared to other approaches and no obvious performance degradation when conducting parallel transmission in real practice.

5.2　Future works

In this section, we discuss the research items which still have not been addressed in this thesis and suggest the potential future extensions based on our methodology of realizing mesh efficient CT-LoRa network.

（1）**Potential Extensions for efficient topology collection:** In order to apply TCSA, it is necessary to collect the one-hop topology information between any pair of two nodes using all SFs. During the prior information collection, it's time cost and energy cost for the battery-powered LoRa devices. To address this, a fast link prediction method is required to verify the link quality of the nodes where we have been striving to use a few packets of using smaller SFs to quick predict the D2D link quality of all SFs. Also, this method will benefit other academic approaches when confirming the connectivity of the nodes has been required.

（2）**Potential Extensions for different types of data collection:** To adjust different types of data collection in CT-LoRa, it's necessary to adopt a versatile data transmission scheduler with the consideration of SF allocation mechanism. For example, the data transmission can be event-driven or bursty data with only a few nodes. Probably, to support an emergency event, part of the nodes need to change the location which may also change the SF to allow dynamic SF-allocation-based data collection scheduling.

（3）**Potential Extensions for application-level performance enhancement:** In this study, we focus on the physical layer and network layer characterizes to realize an efficient mesh LoRa network by leveraging CT. On the other hand, from the viewpoint of the users, the higher layer implementation is quite potential to enable QoS-aware service in mesh CT-LoRa network to further enhance the network performance, such as an extension of the internet technology into low-power LoRa devices.

Abbreviations

ACK Acknowledgement

ADR Adaptive data rates

BBFS Bottom-up breadth-first searching alogorithm

BFS Breadth-first-searching alogorithm

BW Bandwidth

BNT Basketball net topology

CDMA Code-division multiple access

CFO Carrier frequency offset

CSS Chirp spreading spectrum

CT Concurrent transmission

CT-LoRa CT-based LoRa network

D2D Device-to-Device

DFS Depth-first-searching algorithm

FFT Fast fourier transform

FSK Frequency-shift keying

H2H Human-to-Human

IFFT Inverse fast fourier transform

LFS Largest first-available SF

MAC Medium access control

MAT Minimal airtime

MHE Maximum-hop estimation

OFDM Orthogonal frequency-division multiplexing

PER Packect error rate

PHY Physical layer

PO Power offset

PRR Packect reception rate

RDS Radio-driven synchronization

SF Spreading factor

SFD The start of frame delimiter

SFS Smallest first-available SF

SHE Single-hop estimation

SIR Signal-to-interference ratio

SINR Signal-to-interference-plus-noise ratio

TBFS Top-down breadth-first searching algorithm

TDMA Time-division multiple access

TMCP Tree-based multichannel protocol

TSCA Tree-based SF clustering alogorithm

TO Timing offset

WSNs Wireless sensor networks

Glossary

ALOHA known as the ALOHA system, the first public demonstration of a wireless data transmittion network developed at the University of Hawaii.

Bluetooth A short range wireless technology based on IEEE 802.15.1 specification.

LPWAN Low-power wide-area network, a type of low power wide area network designed to allow long range wireless communications.

LoRa Short for long range, a spread spectrum modulation technique derived from Chirp Spread Spectrum (CSS) technology.

LoRaWAN A protocol defines the upper layers of LoRa-based networks that has a typical stars of star topology.

LTE Short for Long-Term Evolution, also known as "4G". LTE is a standard for wireless broadband communication developed by the 3GPP (3rd Generation Partnership Project).

LTE-M Short for LTE-MTC, a type of low power wide area network wireless standard developed by 3GPP.

Mesh network A local network using a multi-hop topolgy .

NB-IoT Short for Narrowband Internet of Things, a LPWAN standard developed by 3GPP.

Sigfox A French global network operator that bulids low power wide area networks.

WiFi A family of short range wireless technologies based on the IEEE 802.11 family of standards, and also represents the trademark of the Wi-Fi Alliance.

Zigbee A short range wireless technology based on IEEE 802.15.4 specification.

Acknowledgments

Undertaking this PhD has been a truly life-changing experience for me and I owed my sincere gratitude to many people for their contribution to my PhD study. Without their kind support and guidance, this dissertation would not have been possible.

Foremost, I would like to express my deepest gratitude to my supervisor Professor Hiroyuki Morikawa. Morikawa sensei's immense knowledge, enthusiasm, motivation, and patience have given me more power and spirit for undertaking my study in Morikawa Lab and also my lifetime at The University of Tokyo. Without his persistent guidance and feedback to supervise me well throughout of the research work, this study would not have been achievable. Also, I would like to say thanks to the committee members who spend precious time on examining my dissertation and gave me invaluable comments.

Apart from my supervisor, my deep appreciation goes out to the wireless group members of our Lab: Dr. Yoshiaki Narusue, Dr. Liao Chun-Hao, Dr. Theerat Sakdejayont, Dr. Makoto Suzuki for giving me endless supports, encouragements and sharing insightful suggestions. I also would like to appreciate Mr. Sotaro Ohara and Ms. Atsuko Kawakita for their innumerable technical and administrative supports and say a very big thank you to my dear friends in Morikawa laboratory. They all really mean a lot to me. Those days we work together and fight together with days and nights are hard to forget throughout my life.

Last but not least, I would also like to say my heartfelt thank you to my family and friends who always inspire me with their warm love, continued patience, and support me in every possible way.

朱 桂兵 *Zhu, Guibing*

July 2019

References

[1] "ITU internet reports 2005," International Telecommunication Union, 2005. [Online]. Available: https://www.i-scoop.eu/internet-of-things-guide/

[2] "The Internet of Things (IoT) - essential IoT business guide," i-SCOOP. [Online]. Available: https://www.i-scoop.eu/internet-of-things-guide/

[3] "5G and IoT: the mobile broadband future of IoT," i-SCOOP. [Online]. Available: https://www.i-scoop.eu/internet-of-things-guide/5g-iot/

[4] "第 4 次産業革命における産業構造分析と IoT・AI 等の進展に係る現状及び課題に関する調査研究," 日本国総務省, 2017. [Online]. Available: http://www.soumu.go.jp/johotsusintokei/linkdata/h29_03_houkoku.pdf

[5] Gartner, 2018. [Online]. Available: https://blogs.gartner.com/rene-buest/2018/10/15/

[6] P. Ray, "A survey on Internet of Things architectures," *Journal of King Saud University - Computer and Information Sciences*, vol. 30, no. 3, pp. 291 – 319, 2018. [Online]. Available: http://www.sciencedirect.com/science/article/pii/S1319157816300799

[7] S. Li, L. D. Xu, and S. Zhao, "5G Internet of Things: A survey," *Journal of Industrial Information Integration*, vol. 10, pp. 1 – 9, 2018. [Online]. Available: http://www.sciencedirect.com/science/article/pii/S2452414X18300037

[8] I. Mashal, T. Chung, and O. Alsaryrah, "Toward service recommendation in Internet of Things," in *Proceedings of 2015 Seventh International Conference on Ubiquitous and Future Networks (ICUFN)*, pp. 328–331, July 2015.

[9] A. V. Jerald, S. A. Rabara, and D. P. Bai, "Secure iot architecture for integrated smart services environment," in *Proceedings of 2016 3rd International Conference on Computing for Sustainable Global Development (INDIACom)*, pp. 800–805, March 2016.

[10] "LPWA network technologies and standards: LPWAN wireless IoT guide," iSCOOP. [Online]. Available: https://www.i-scoop.eu/internet-of-things-guide/lpwan/

[11] U. Raza, P. Kulkarni, and M. Sooriyabandara, "Low power wide area networks: An overview," *IEEE Communications Surveys & Tutorials*, vol. 19, no. 2, pp. 855–873, 2017.

[12] M. Centenaro, L. Vangelista, A. Zanella, and M. Zorzi, "Long-range communications in unlicensed bands: The rising stars in the IoT and smart city scenarios," *IEEE Wireless Communications*, vol. 23, no. 5, pp. 60–67, 2016.

[13] C. Buratti, A. Conti, D. Dardari, and R. Verdone, "An overview on wireless sensor networks technology and evolution," *Sensors*, vol. 9, no. 9, pp. 6869–6896, 2009.

[14] "Low Power Wide Area Technology." [Online]. Available: https://www.gemalto.com/m2m/development/innovation-technology/low-power-wide-area-technology

[15] S. Zhu and N. Zhang, "A research about return channel of terrestrial digital based LPWAN," in *Proceedings of 2016 First IEEE International Conference on Computer Communication and the Internet (ICCCI)*, pp. 296–299, Oct. 2016.

[16] J. Petäjäjärvi, K. Mikhaylov, R. Yasmin, and et al., "Evaluation of LoRa LPWAN technology for indoor remote health and wellbeing monitoring," *International Journal of Wireless Information Networks*, vol. 24, no. 2, pp. 153–165, 2017.

[17] C. Pham, "QoS for Long-Range wireless sensors under Duty-Cycle regulations with shared activity time usage," *ACM Transactions on Sensor Networks (TOSN)*, vol. 12, no. 4, pp. 33:1–33:31, Sep. 2016.

[18] D. H. Kim, J. B. Park, J. H. Shin, and J. D. Kim, "Design and implementation of object tracking system based on LoRa," in *Proceedings of 2017 International conference on information networking (ICOIN)*, pp. 463–467, Jan. 2017.

[19] "LoRa Alliance[tm]," LoRa Alliance. [Online]. Available: https://http://www.lora-alliance.org/

[20] N. Sornin and A. Yegin, "LoRaWAN[tm] Specification v1.1," LoRa Aalliance, 2017.

[21] K. H. Ke, Q. W. Liang, G. J. Zeng, J. H. Lin, and H. C. Lee, "A LoRa wireless mesh networking module for campus-scale monitoring: Demo abstract," in *Proceedings of the 14th International Conference on Information Processing in Sensor Networks (IPSN)*, pp. 259–260, 2017.

[22] SEMTECH, "LoRa[tm] modulation basics," May 2015.

[23] F. Ferrari, M. Zimmerling, L. Thiele, and O. Saukh, "Efficient network flooding and time synchronization with Glossy," in *Proceedings of the 10th ACM/IEEE International Conference on Information Processing in Sensor Networks (IPSN)*, pp. 73 –84, Apr. 2011.

[24] "What is LoRa." [Online]. Available: https://www.link-labs.com/blog/what-is-lora

[25] M. Knight and B. Seeber, "Decoding LoRa: Realizing a modern LPWAN with SDR," in *Proceedings of the GNU Radio Conference*, vol. 1, no. 1, Sep. 2016.

[26] T. Petrić, M. Goessens, L. Nuaymi, L. Toutain, and A. Pelov, "Measurements, performance and analysis of LoRa FABIAN, a real-world implementation of LPWAN," in *Proceedings of 2016 IEEE 27th Annual International Symposium on Personal, Indoor, and Mobile Radio Communications (PIMRC)*, pp. 1–7, Sep. 2016.

[27] E. Ruano Lin, *LoRa protocol. Evaluations, Limitations and Practical test.* Universitat Politècnica de Catalunya, May 2016.

[28] K. Mikhaylov, J. Petäjäjärvi, and T. Haenninen, "Analysis of capacity and scalability of the LoRa low power wide area network technology," in *Proceedings of 22th European Wireless Conference*, pp. 1–6, May 2016.

[29] "LoRa: Symbol Generation," 2018. [Online]. Available: https://www.sghoslya.com/p/lora-is-chirp-spread-spectrum.html/

[30] "A technical overwiew of LoRa and LoRaWAN," LoRa Alliance. [Online]. Available: https://lora-alliance.org/resource-hub/what-lorawanr

[31] A. Mahmood, E. G. Sisinni, L. Guntupalli, R. Rondon, S. A. Hassan, and M. Gidlund, "Scalability analysis of a LoRa network under imperfect orthogonality," *IEEE Transactions on Industrial Informatics*, pp. 1–1, 2018.

[32] D.-Y. Kim, S. Kim, H. Hassan, and J. H. Park, "Adaptive data rate control in low power wide area networks for long range IoT services," *Journal of computational science*, vol. 22, pp. 171–178, 2017.

[33] F. Adelantado, X. Vilajosana, P. Tuset-Peiro, B. Martinez, J. Melia-Segui, and T. Watteyne, "Understanding the limits of LoRaWAN," *IEEE Communications Magazine*, vol. 55, no. 9, pp. 34–40, 2017.

[34] B. Reynders, W. Meert, and S. Pollin, "Power and spreading factor control in low power wide area networks," in *Proceedings of 2017 IEEE International Conference on Communications (ICC)*, pp. 1–6, 2017.

[35] B. Reynders, Q. Wang, P. Tuset-Peiro, X. Vilajosana, and S. Pollin, "Improving reliability and scalability of LoRaWANs through lightweight scheduling," *IEEE Internet of Things Journal*, vol. 5, no. 3, pp. 1830–1842, June 2018.

[36] M. Slabicki, G. Premsankar, and M. Di Francesco, "Adaptive configuration of LoRa networks for dense iot deployments," in *Proceedings of 2018 IEEE/IFIP Network Operations and Management Symposium (NOMS)*, pp. 1–9, 2018.

[37] F. Cuomo, M. Campo, A. Caponi, G. Bianchi, G. Rossini, and P. Pisani, "EXPLoRa: Extending the performance of LoRa by suitable spreading factor allocations," in *Proceedings of the 13th International Conference on Wireless and Mobile Computing, Networking and Communications (WiMob)*, pp. 1–8, Oct 2017.

[38] M. N. Ochoa, A. Guizar, M. Maman, and A. Duda, "Evaluating LoRa energy efficiency for adaptive networks: From star to mesh topologies," in *Proceedings of the 13th International Conference on Wireless and Mobile Computing, Networking and Communications (WiMob)*, pp. 1–8, Oct 2017.

[39] K.-H. Ke, Q.-W. Liang, G.-J. Zeng, J.-H. Lin, and H.-C. Lee, "A LoRa wireless mesh networking module for campus-scale monitoring: Demo abstract," in *Proceedings of the 14th International Conference on Information Processing in Sensor Networks (IPSN)*, pp. 259–260, 2017.

[40] F. Wang, D. Li, and Y. Zhao, "Analysis of csma/ca in ieee 802.15. 4," *IET communications*, vol. 5, no. 15, pp. 2187–2195, 2011.

[41] F. Ferrari, M. Zimmerling, L. Mottola, and L. Thiele, "Low-power wireless bus," in *Proceedings of the 10th ACM Conference on Embedded Network Sensor Systems (SenSys)*, pp. 1–14, Nov. 2012.

[42] M. Suzuki, S. Ohara, K. Jinno, C. H. Liao, and H. Morikawa, "Wireless-transparent sensing," in *Proceedings of 2017 International Conference on Embedded Wireless Systems and Networks (EWSN)*, pp. 66–77, Feb. 2017.

[43] K. Leentvaar and J. Flint, "The capture effect in FM receivers," *IEEE Transactions on Communications*, vol. 24, no. 5, pp. 531–539, May 1976.

[44] D. Son, B. Krishnamachari, and J. Heidemann, "Experimental study of concurrent transmission in wireless sensor networks," in *Proceedings of the 4th ACM Conference on Embedded Networked Sensor Systems (SenSys)*, pp. 237–250, Nov. 2006.

[45] C. Gezer, C. Buratti, and R. Verdone, "Capture effect in IEEE 802.15.4 networks: Modeling and experimentation," in *Proceedings of IEEE 5th International Symposium on Wireless Pervasive Computing (ISWPC) 2010*, pp. 204–209, May 2010.

[46] P. Dutta, S. Dawson-Haggerty, Y. Chen, C.-J. M. Liang, and A. Terzis, "Design and evaluation of a versatile and efficient receiver-initiated link layer for low-power wireless," in *Proceedings of the 8th ACM Conference on Embedded Networked Sensor Systems (SenSys)*, pp. 1–14, Nov. 2010.

[47] C. H. Liao, Y. Katsumata, M. Suzuki, and H. Morikawa, "Revisiting the so-called constructive interference in concurrent transmission," in *Proceedings of 2016 IEEE 41st Conference on Local Computer Networks (LCN)*, pp. 280–288, Nov. 2016.

[48] Y. Wu, J. A. Stankovic, T. He, and S. Lin, "Realistic and efficient multi-channel communications in wireless sensor networks," in *Proceedings of IEEE INFOCOM 2008 - The 27th Conference on Computer Communications*, April 2008.

[49] S.-Y. Liew, C.-K. Tan, M.-L. Gan, and H. G. Goh, "A fast, adaptive, and energy-efficient data collection protocol in multi-channel-multi-path wireless sensor networks," *IEEE CIM*, vol. 13, no. 1, pp. 30–40, 2018.

[50] Semtech, "SX1272/73 - 860 mhz to 1020 mhz low power long range transceiver," 2015. [Online]. Available: http://www.semtech.com/images/datasheet/sx1272.pdf

[51] STMicroelectronics, "STM32L151x6/8/B - ultra-low-power 32-bit MCU ARM-based Cortex-M3, 128KB Flash, 16KB SRAM, 4KB EEPROM, LCD, USB, ADC, DAC," 2016.

[52] C. H. Liao, G. Zhu, D. Kuwabara, M. Suzuki, and H. Morikawa, "Multi-hop lora networks enabled by concurrent transmission," *IEEE Access*, vol. 5, pp. 21 430–21 446, 2017.

[53] O. Georgiou and U. Raza, "Low power wide area network analysis: Can LoRa scale?" *IEEE Wireless Communications Letters*, vol. 6, no. 2, pp. 162–165, 2017.

[54] J. Petajajarvi, K. Mikhaylov, A. Roivainen, T. Hanninen, and M. Pettissalo, "On the coverage of LPWANs: range evaluation and channel attenuation model for LoRa technology," in *Proceedings of 2015 14th International Conference on ITS Telecommunications (ITST)*, pp. 55–59. IEEE, 2015.

[55] K. Mikhaylov, J. Petäjäjärvi, and J. Janhunen, "On LoRaWAN scalability: Empirical evaluation of susceptibility to inter-network interference," in *Proceedings of the European Conference on Networking and Communications (EUCNC)*, pp. 1–6. IEEE, 2017.

[56] T. Elshabrawy and J. Robert, "Capacity planning of LoRa networks with joint noise-limited and interference-limited coverage considerations," *IEEE Sensors Journal*, 2019.

[57] I. P. Gent and T. Walsh, "Analysis of heuristics for number partitioning," *Computational Intelligence*, vol. 14, no. 3, pp. 430–451, 1998.

[58] B. Hayes, "Computing science: The easiest hard problem," *American Scientist*, vol. 90, no. 2, pp. 113–117, 2002.

[59] MIT OpenCourseWare, "Design and analysis algorithms," https://ocw.mit.edu/courses/electrical-engineering-and-computer-science/6-046j-design-and-analysis-of-algorithms-spring-2015, 2015.

Publications

Journal

[1] **G. Zhu**, C.-H. Liao, T. Sakdejayont, I.-W. Lai, Y. Narusue, and H. Morikawa, "Improving the Capacity of a Mesh LoRa Network by Spreading-Factor-Based Network Clustering," *IEEE Access*, Feb. 2019, vol.7, pp.21584-21596.

[2] C.-H. Liao, **G. Zhu**, D. Kuwabara, M. Suzuki, and H. Morikawa, "Multi-hop LoRa Networks Enabled by Concurrent Transmission," *IEEE Access*, Sep. 2017, vol.5, pp.21430-21446.

[3] Y. Hokazono, A. Koizuka, **G. Zhu**, M. Suzuki, Y. Narusue, and H. Morikawa, "IoTorch: LED-to-Camera Communication for Smartphones Based on Flash Blinks againstInter-Frame Gaps and Frame Drops," *IEEE Transactions on Mobile Computing*, resubmitted to the Journal.

International Conference

Oral Presentation

[4] **G. Zhu**, C.-H. Liao, M. Suzuki, Y. Narusue, and H. Morikawa, "Evaluation of LoRa Receiver Performance under Co-technology Interference," in *Proceedings of 15th IEEE Annual Consumer Communications Networking Conference (CCNC)*, Jan. 2018, pp. 1-7.

Technical Report

[5] **G. Zhu**, C.-H. Liao, T. Sakdejayont, Y. Narusue, and H. Morikawa, "Improving the Capacity of Mesh LoRa Network by Tree-based Spreading Factor Clustering Algorithm", *IEICE Technical Report on Radio Communication System (RCS)*, vol. 118, no. 101, RCS2018-75, June 2018, pp. 237-242.

[6] **G. Zhu**, C.-H. Liao, M. Suzuki, Y. Narusue, and H. Morikawa, "Investigating the LoRa Receiver Performance under Mutual Interference," *IEICE Technical Report on Radio Communication System (RCS)*, vol. 117, no. 132, RCS2017-110, July 2017, pp. 103-108.

[7] C.-H. Liao, **G. Zhu**, D. Kuwabara, S. Ohara, M. Suzuki, and H. Morikawa, "Evaluating the Sub-GHz LoRa Receiver Performance under Synchronized Packet Collisions," *IEICE Technical Report on Radio Communication System (RCS)*, vol. 117, no. 11, RCS2017-27, Apr. 2016, pp. 143-148.

Domestic Conference

[8] S. Kikuchi, **G. Zhu**, C-H. Liao, T. Sakdejayont, Y. Narusue and H. Morikawa, "An Efficient Data Collection Scheme using Parallel Concurrent Transmission Flooding with Non-arrival Information," *IEICE General Conference*, B-18-16 Mar. 2019. [in Japanese]

[9] S. Sasaki, **G. Zhu**, Y. Narusue, T.-M. Wen, B.-Z. Qiu, C.-H. Liao, T. Sakdejayont, and H. Morikawa, "A Study on Signal Strength Prediction Model and Sensor-location Selecting Method for Low-cost Continuous Radio Spectrum Monitoring System," *IEICE General Conference*, B-18-14 Mar. 2019. [in Japanese]

[10] **G. Zhu**, C.-H. Liao, T. Sakdejayont, Y. Iwai, Y. Narusue and H. Morikawa, "Evaluation of Fast Connectivity Prediction by using RSSI and SNR in LoRa," *IEICE Society Conference*, B-5-94 Sept. 2018.

[11] **G. Zhu**, C.-H. Liao, T. Sakdejayont, Y. Narusue and H. Morikawa, "Improving the Capacity of Multi-hop LoRa Network by Network Clustering," *IEICE Society Conference*, B-18-33 Mar. 2018.

[12] **G. Zhu**, C.-H. Liao, T. Sakdejayont, Y. Narusue, and H. Morikawa "Enabling the Fast Flooding over Multi-hop LoRa Network using SF-pipeline," *IEICE Society Conference*, B-5-91 Sept. 2017.

Patent

[13] 森川 博之, 廖 椿豪, サクデーシャヨン ティラット, 成末 義哲, 朱 桂兵, 鈴木 誠, 大原 壮太郎, "通信装置及びプログラム," 出願予定 , February 2019.

[14] 森川 博之, 廖 椿豪, 鈴木 誠, 大原 壮太郎, 朱 桂兵, "通信装置及びその制御方法," 特許番号: PCT/JP2018/026161, January 2019.